STUDIES ON THE ELECTRICAL PROPERTIES OF THE DORSAL COCHLEAR NUCLEUS CARTWHEEL NEURONS

By

Yuil Kim

A DISSERTATION

Presented to the Neuroscience Graduate Program

and the Oregon Health & Science University

School of Medicine

in partial fulfillment of

the requirements for the degree of

Doctor of Philosophy

March 2009

School of Medicine

Oregon Health & Science University

CERTIFICATE OF APPROVAL

This is to certify that the Ph.D. dissertation of

Yuil Kim

has been approved

Advisor _____

Member _____

Member _____

Member _____

Contents

Acknowledgments

I thank my mentor Dr. Larry Trussell for his guidance, hands-on support, and patience. I thank past and present members of Trussell lab for their support. Especially, thank you to Drs. Gautam Awatramani and Tao Lu for providing generous help when I was a novice in electrophysiology. I would also like to thank Drs. Craig Jahr, Show-Ling Shyng, Gary Westbrook, and John Williams, who were on my thesis and/or defense committee, for their advice and time. Lastly, I thank my family members for their love and support.

ABSTRACT

Cartwheel cells in the dorsal cochlear nucleus (DCN) are glycinergic inhibitory interneurons which form synapses on principal neurons and among themselves. Their activity is characterized by the presence of the complex spike, a brief burst of high-frequency spikes riding on a slow depolarization. The feedforward inhibition mediated by cartwheel cells prominently shapes the response of DCN principal cells to somatosensory input. Therefore, knowledge on how activity of cartwheel cells is regulated is important for input processing in the DCN. I examined two aspects of cartwheel cells, the ionic mechanism of complex spike generation and the glycine reversal potential, using gramicidin perforated-patch recording in a mouse brain slice preparation. Complex spikes require both Ca^{2+} and Na^{+} currents. I monitored the change in spike waveforms elicited by subtype-specific blockers Ca^{2+} channels and Ca^{2+}-activated K^{+} channels. T/R- and L-type Ca^{2+}channels contributed to the slow depolarization of complex spikes, whereas the P/Q-type Ca^{2+} channels reduced the duration of the slow depolarization by coupling to SK channels. Single action potentials repolarized to more negative potential due to the presence of BK channels, which lowered the tendency to fire complex spikes. Thus, the balance between the depolarizing influence of a variety of Ca^{2+} channels and the repolarizing effect of Ca^{2+}-activated K^{+} channels shaped the complex spike and controlled its occurrence.

In a second set of experiments, I examined the factors controlling the activity-dependence of glycine responses in cartwheel cells. Glycine reversal potential (E_{gly}) determines whether the glycine response of the cell is hyperpolarizing or depolarizing. E_{gly} shifted negative, increasing inhibition, after complex spiking or Ca^{2+} spiking, and

this effect was prevented by blocking Ca^{2+} influx. I hypothesized that Ca^{2+}-dependent intracellular acidification led to a negative shift in E_{gly} as a result of a decrease in intracellular HCO_3^- and fall in intracellular Cl^-, the latter via activation of the Na^+-driven Cl^--HCO_3^- exchanger (NDCBE). I used simultaneous measurements of intracellular pH and E_{gly} to examine the relationship between intracellular pH and E_{gly}. Intracellular acidification did occur with spiking activity, and such acidification, as well as the negative E_{gly} shift was sensitive to Ca^{2+} channel block. Intracellular acidification induced with a weak acid in the quiescent state could shift the E_{gly} negative. The intracellular Cl^- concentration, monitored with the Cl^--sensitive dye MQAE, indeed fell after complex spiking. Blocking NDCBE with H_2DIDS or HCO_3^-/CO_2 removal eliminated the negative E_{gly} shift and slowed the recovery from intracellular acidification. These results largely supported the hypothesis. The Ca^{2+}-dependent negative shift in E_{gly} may be a feedback suppression mechanism for excessive complex spiking.

INTRODUCTION

The dorsal cochlear nucleus

The dorsal cochlear nucleus (DCN), where the cartwheel neuron resides, receives excitatory input from the cochlea through the auditory nerve. The DCN in many mammals, excluding primates, has a layered cellular organization consisting of a molecular layer, fusiform cell layer and deep layer (Fig. 1) (Cant, 1992). In addition to the input from the tonotopic array of auditory nerve fibers in the deep layer, the DCN has a second input system similar to the cerebellum, which consists of mossy fibers arising from the medullary somatosensory nuclei, the vestibular afferents as well as higher-order auditory centers (Weedman et al., 1996). Mossy fibers synapse onto granule cells and the granule cell axons form the parallel fibers in the molecular layer. The principal cells of the DCN, which project to the contralateral inferior colliculus, receive both auditory nerve and parallel fiber inputs, and are thus considered to be the sites where the two inputs are integrated in the DCN (Oertel and Young, 2004). The DCN may function to correct spectral sound localization cues for the position of head and external ear. This function has been inferred from several lines of evidence (Young and Davis, 2001): DCN principal cells are sensitive to spectral cues for sound localization; such spectral cues are created by the external ear, movement of which is a strong somatosensory stimuli to the DCN (Kanold and Young, 2001); and cats with lesions of the DCN output tract are unable to position their head toward a test sound (May, 2000).

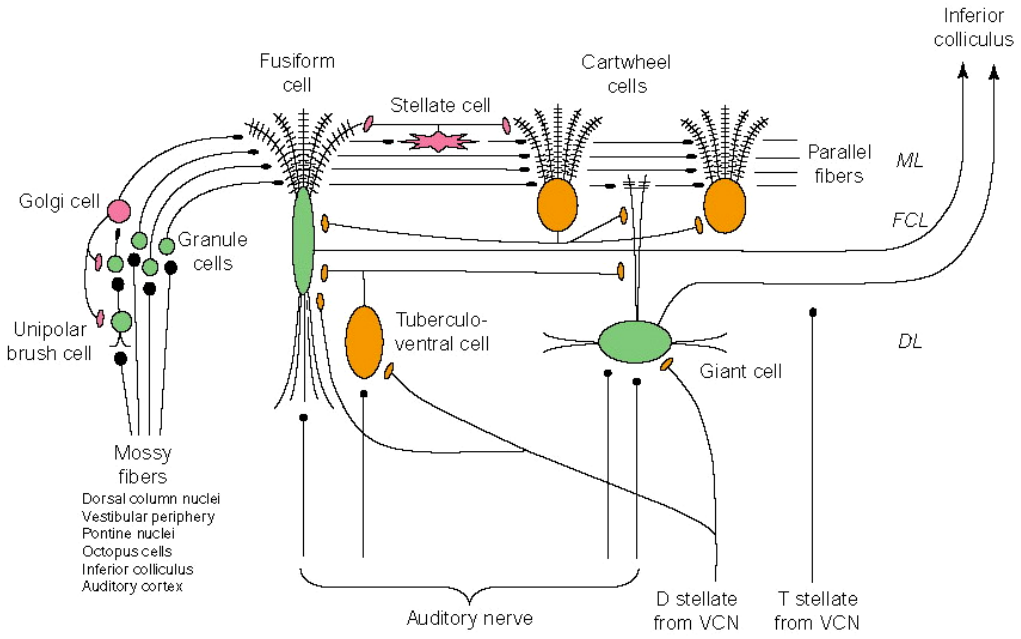

Fig. 1 Circuitry of the DCN. *ML*, molecular layer; *FCL*, fusiform cell layer; *DL*, deep layer. (Oertel and Young, 2004; permission on page 182)

Neurons of the dorsal cochlear nucleus

The fusiform cell is one of two types of principal, glutamatergic neurons of DCN. It has a large elongate or pyramidal soma and bipolar dendrites (Fig. 1). The basal dendrites are contacted by auditory nerve fibers carrying information about a narrow range of sound frequencies, whereas the spiny apical dendrites are contacted by parallel fibers (Oertel and Young, 2004). The giant cell, the other principal neuron, has its large cell body in the deep layer and has not been studied as extensively as the fusiform cell (Zhang and Oertel, 1993b). Fusiform cells are spontaneously active and their responses to the excitatory auditory and parallel fiber input are shaped by feed-forward inhibition from interneurons, such as tuberculoventral cells and cartwheel cells (Zhang and Oertel, 1994; Young and Davis, 2001). The glycinergic tuberculoventral cells in the deep layer

are excited by auditory nerve input (Zhang and Oertel, 1993c). Cartwheel cells, the subject of this thesis, are the most numerous intermediate-size neurons in the molecular and fusiform cell layers (Wouterlood and Mugnaini, 1984; Berrebi and Mugnaini, 1991). They have medium-sized soma and spiny dendrites that are innervated by the excitatory parallel fibers. Cartwheel cells are not contacted by auditory nerve fibers (Brown and Ledwith, 1990; Rubio, 2004), but they show some responses to sound, presumably through parallel fibers that carry auditory mossy fiber input (Parham and Kim, 1995; Davis and Young, 1997; Portfors and Roberts, 2007). Cartwheel cell axons contact fusiform cells and other cartwheel cells (Mugnaini et al., 1987; Berrebi and Mugnaini, 1991). Cartwheel cells are glycinergic and GABAergic, being immuno-positive for glutamate decarboxylase (GAD) and glycine (Osen, 1990). Postsynaptic potentials originating from presynaptic cartwheel cells are blocked largely by a glycine receptor antagonist (strychnine) and to a lesser extent by $GABA_A$ receptor antagonists (Golding and Oertel, 1996; Roberts et al. 2008). Synaptic endings containing both glycine and GABA, presumed to be of cartwheel cells, are present along cell bodies and dendrites of cartwheel cells and fusiform cells. Some of these endings on fusiform cells are on axon initial segments, optimally suited to inhibit action potentials (Rubio, 2004). Stellate cells, another class of interneurons in the DCN molecular layer, are known as small to medium-sized GABAergic cells that are contacted by parallel fibers on their relatively aspiny dendrites (Wouterlood et al., 1984). The targets of stellate axons have not been clearly identified, but the small number of GABAergic boutons on cartwheel and fusiform cells may come from stellate cells (Rubio, 2004).

The complex spike of the cartwheel cell

The electrical activity of cartwheel cells is characterized by a complex spike, a high-frequency burst of action potentials of decreasing amplitude (spikelets) superimposed on depolarizing envelope. Cartwheel cells also produce a simple spike, i.e. single action potential (Zhang and Oertel, 1993a). Ca^{2+} currents may underlie the slow depolarization of complex spikes, whereas spikelets are Na^{+}-dependent, as are the simple spikes (Golding and Oertel, 1997; Molitor and Manis, 2003). In Chapter 1, I investigated which subtype Ca^{2+} channels contributed to generation of the complex spike and whether Ca^{2+}-activated K^{+} channels were involved.

A number of neurons can generate complex spikes, including pyramidal cells of neocortex and hippocampus (Chagnac-Amitai et al., 1990; Kandel and Spencer, 1961), thalamocortical neurons (Deschenes et al. 1982), dorsal root ganglion neurons (White et al., 1989) and cerebellar Purkinje neurons (Schmolesky et al., 2002). The role of complex spikes has been implicated in the induction of synaptic plasticity and in reliable information transfer (Lisman, 1997; Paulsen and Sejnowski, 2000; Ito, 2001). Complex spiking by cartwheel cells has been compared to cerebellar Purkinje cells, with which cartwheel cells share some common features such as spiny dendrites and biochemical markers including calbindin-d28k and PEP-19 (Mugnaini and Morgan, 1987; Berrebi et al., 1990; Berrebi and Mugnaini, 1991). Although complex spikes in Purkinje cells are driven by climbing fiber-mediated postsynaptic potentials, cartwheel cells do not receive climbing fiber input. Instead, complex spikes in cartwheel cells occur spontaneously, can be evoked by a depolarizing current injection, or a depolarizing postsynaptic potential (Golding and Oertel, 1996; Tzounopoulos et al., 2004). For Purkinje cells, activation of

the climbing fiber and complex spikes facilitate the induction of long term depression in parallel fiber synapses (Ito, 2001). This plasticity likely results from the rise in intracellular Ca^{2+} concentration ($[Ca^{2+}]_i$), especially in dendrites, which is associated with the complex spike (Konnerth et al. 1992; Miyakawa et al. 1992; Wang et al. 2000). The complex spike of cartwheel cells also induces an increase in $[Ca^{2+}]_i$ (Molitor and Manis, 2003; Roberts et al, 2008), but its role in synaptic plasticity has not been demonstrated yet. However, in the case of spike timing-dependent plasticity of the parallel fiber-cartwheel cell synapses, either a simple or complex spike is sufficient (Tzounopoulos et al., 2004).

The effect of glycinergic/GABAergic input in cartwheel cells

Although glycine and GABA are generally considered as "inhibitory" neurotransmitters, the action of glycine and GABA may be excitatory in developing neurons or even into mature stage in some neurons (Ben-Ari et al., 2007; Marty and Llano, 2005). For cartwheel cells, there is conflicting evidence whether glycinergic/GABAergic input is inhibitory or excitatory. The reversal potential for glycinergic and GABAergic postsynaptic potentials (PSPs) was ~10 mV more positive than the resting membrane potential in mouse cartwheel cells recorded using potassium acetate-filled microelectrodes (Golding and Oertel, 1996). These authors described the action of glycinergic and GABAergic PSPs as "context-dependent", because PSPs were excitatory at resting membrane potential, but inhibitory during intense firing associated with depolarization. Spontaneous glycinergic and GABAergic PSPs were depolarizing at the resting potential in this study. However, others have reported inhibitory spontaneous

glycinergic or GABAergic PSPs in cartwheel cells. In guinea pig cartwheel cells, spontaneous hyperpolarizing PSPs were observed at the resting potential with potassium acetate-filled microelectrodes (Manis et al., 1994). *In vivo*, iontophoretic application of the $GABA_A$ receptor blocker bicuculline and the glycine receptor blocker strychnine increased the spontaneous and driven spike rate of some presumed cartwheel cells in cat DCN (Davis and Young, 2000). In Chapter 2, I examined glycine responses in cartwheel cells using gramicidin perforated-patch method to resolve the conflicting reports of glycine actions in the DCN.

Intracellular [Cl^-] and [HCO_3^-], the determinants of the glycine/GABA reversal potential

The glycine reversal potential in cartwheel cells in my experiments was variable among different cells and that it fluctuated with activity in single cells (Chapter 2). Because glycine and $GABA_A$ receptors are permeable to Cl^- and HCO_3^-, the reversal potential of glycine or $GABA_A$ receptor-mediated currents (E_{gly} or E_{GABA}) is determined by the concentration gradient of these ions, according to the Goldman-Hodgkin-Katz voltage equation (Bormann et al., 1987; Kaila and Voipio, 1987): $E_{gly/GABA} = (RT/F) \ln(([Cl^-]_i + r\,[HCO_3^-]_i)/([Cl^-]_o + r\,[HCO_3^-]_o))$. The ratio ($r$) of the permeability of HCO_3^- to that of Cl^- for $GABA_A$ and glycine receptors is 0.1 – 0.4 (Bormann et al., 1987; Kaila and Voipio, 1987; Fatima-Shad and Barry, 1993), which indicates that Cl^- is more important in setting $E_{gly/GABA}$ than HCO_3^-. Because extracellular Cl^- concentration is relatively constant (120 – 145 mM in cerebrospinal fluid of mammals; Davson and Segal, 1996), variations in reversal potential of glycine or GABA have been attributed to

variability in $[Cl^-]_i$ (Ben-Ari et al., 2007). Intracellular Cl^- is set by the balance between the influx and efflux mediated by transporters and channels. K^+-Cl^- cotransporters (KCC), Na^+-K^+-Cl^- cotransporters (NKCC), Na^+-independent and Na^+-driven Cl^--HCO_3^- exchangers are present in neurons (Farrant and Kaila, 2007; Romero et al. 2004) including NKCC1 (Plotkin et al. 1997), KCC2 (Kanaka et al. 2001; Payne et al. 1996), AE3 (Hentschke et al. 2006; Kopito et al. 1989) and NDCBE (Chen et al. 2008a; Grichtchenko et al. 2001) (Fig.2).

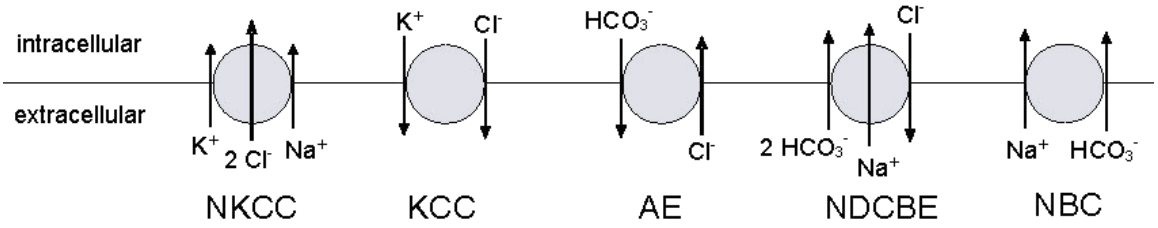

Fig. 2 The stoichiometry and transport directions of Cl^- and HCO_3^- transporters are depicted. NBC, Na^+-HCO_3^- co-transporter.

For cartwheel cells, the expression of these Cl^- transporters is not known, except that KCC2 has been detected in rat DCN (Vale et al. 2005). However, cerebellar Purkinje cells express KCC2 (Kanaka et al. 2001), KCC3 (Pearson et al. 2001), AE3 (Kopito et al. 1989), NDCBE (Chen et al. 2008a; Damkier et al. 2007) as well as Na^+-HCO_3^- cotransporters (Chen et al. 2008b; Damkier et al. 2007; Rickmann et al. 2007). KCC and NKCC use the gradient of K^+ and Na^+ across plasma membrane set by the Na^+-K^+-ATPase (i.e., secondary active transport) to extrude and import Cl^-, respectively. The Na^+-driven Cl^--HCO_3^- exchanger (NDCBE) also uses Na^+ gradient in importing two HCO_3^- along with one Na^+ in exchange for extrusion of one Cl^-. In contrast, the transport

direction of Na^+-independent Cl^--HCO_3^- exchanger (AE) is determined by the equilibrium $[Cl^-]_i/[Cl^-]_o = [HCO_3^-]_i/[HCO_3^-]_o$, i.e., pH gradient-dependent. It moves Cl^- inward at normal intracellular pH (~7.10), but it can work in reverse mode at more acidic intracellular pH (pH_i). Similarly, KCC may reverse to mediate Cl^- uptake under raised extracellular $[K^+]$ (equilibrium at $[Cl^-]_i/[Cl^-]_o = [K^+]_o/[K^+]_i$).

Although HCO_3^- is less permeable than Cl^- through glycine/$GABA_A$ receptors, a change in its concentration gradient can affect E_{gly}/E_{GABA}. The concentration of HCO_3^- in intracellular or extracellular fluid is determined from the equilibrium, $CO_2 + H_2O \leftrightarrow H_2CO_3 \leftrightarrow H^+ + HCO_3^-$ (Roos and Boron, 1981). The hydration of CO_2 to carbonic acid is catalyzed by the carbonic anhydrase, which is found both intra- and extracellularly. Without the enzyme, the reaction takes tens of seconds to equilibrate (Ridderstrale and Wistrand, 1998). Because CO_2 is diffusible across plasma membrane, P_{CO2} is assumed to be equal intra- and extracellularly (45–50 mmHg in cerebrospinal fluid; Davson and Segal, 1996). Assuming the solubility of CO_2 and the dissociation constant of H_2CO_3 are the same intra- and extracellularly, the following establishes: $[HCO_3^-]_i/[HCO_3^-]_o = [H^+]_o/[H^+]_i = 10^{(pHi-pHo)}$ (Roos and Boron, 1981). Therefore, given the extracellular pH and HCO_3^- concentration are constant, decrease or increase in pH_i should decrease or increase $[HCO_3^-]_i$, respectively. Kaila et al (1993) have shown that extracellular application of weak acid or base, presumed to cause intracellular acidification or alkalinization, shifted E_{GABA} negative or positive, respectively. The authors attributed the change in E_{GABA} to the change in $[HCO_3^-]_i$. The resting pH_i of various rodent neurons is 6.90–7.30 ± 0.05–0.30 pH units (mean ± S.D.; Leniger et al. 2004; Ou-yang et al. 1993; Pocock and Richards 1992; Schwiening and Boron 1994). Thus the range of the resting

pH_i within single class of neurons suggests that heterogeneity in resting $[HCO_3^-]_i$ could contribute to heterogeneity in resting $E_{gly/GABA}$, as I show in cartwheel cells in Chapter 2.

Intracellular acidification occurring with depolarization or spiking activity

The pH_i can decrease when neurons are depolarized or fire action potentials (Ballanyi and Kaila, 1998; Chesler, 2003). In a number of these studies, acidification was inhibited by Ca^{2+} channel blockers, supporting the idea that the pH_i decrease depends on a rise in intracellular Ca^{2+} (e.g. Ahmed and Connor 1980; Meech and Thomas, 1987, Meyer et al., 2000; Trapp et al. 1996a). The generation of metabolic acids also has been proposed as the cause of acidification (Zhan et al., 1998). I show in Chapter 2 that the activity-dependent intracellular acidification occurred in cartwheel cells, and that such acidification was Ca^{2+}-dependent. Several mechanisms for a Ca^{2+}-dependent pH_i decrease have been suggested: 1) displacement of H^+ by Ca^{2+} from intracellular binding sites; 2) mitochondrial Ca^{2+} uptake which releases H^+ to cytoplasm; 3) Ca^{2+}-H^+ ATPase-mediated translocation of cytoplasmic Ca^{2+} to extracellular space or endoplasmic reticulum; and 4) elevation in metabolic acid or CO_2 production due to Ca^{2+}-induced stimulation of metabolism (Ballanyi and Kaila, 1998; Chesler, 2003). Among these, the contribution of the plasma membrane Ca^{2+}-H^+ ATPase (PMCA) to depolarization-induced acid loading was first demonstrated by Schwiening et al. (1993) in snail neurons: intracellular injection of vanadate, an inhibitor of ATPases, inhibited both the Ca^{2+} clearance and the extracellular alkalinization associated with intracellular uptake of H^+. PMCA inhibitors also caused partial or complete inhibition of depolarization-induced acidification in rat hippocampal neurons (Trapp et al., 1996b) and cultured rat cerebellar

granule cells (Wu et al., 1999; Vale-Gonzalez et al., 2006). Schwiening and Thomas (1998), however, warned that discriminating between the above four mechanisms is difficult because blocking one process, e.g. PMCA, increases $[Ca^{2+}]_i$, which then could recruit other secondary processes.

Activity-dependent changes in glycine/GABA reversal potential

There have been three reported postsynaptic mechanisms of "activity-induced" changes in glycinergic or GABAergic synaptic responses. Depolarizing shifts in E_{GABA} can result from prolonged high-frequency stimulation of GABAergic inputs (Thompson and Gahwiler, 1989; Staley et al., 1995, Lamsa and Taira, 2003). The proposed mechanism of hyperpolarizing to depolarizing GABAergic PSPs in these studies was the collapse of transmembrane Cl^- gradient and domination by HCO_3^- current of the GABA-activated conductance. The second category attributes the change in the polarity of glycinergic/GABAergic responses to fluctuations in membrane potential associated with spiking activity assuming that $E_{gly/GABA}$ is close to the membrane potential and rather constant. For example, Chavas and Marty (2003) reported on the variable effect of GABA on cerebellar basket cells and Golding and Oertel (1996) proposed a "context-dependent" action of glycine in cartwheel cells. Finally, it has been suggested that $E_{gly/GABA}$ shifts arise from alteration in $[Cl^-]_i$ due to changes in the activity or number of Cl^- transporters after a period of spiking (Woodin et al., 2003; Fiumelli et al., 2005; Brumback and Staley, 2008). The shift in E_{GABA} were long-lasting (>30 min) in these studies, whereas the changes in the above two categories were transient. Woodin et al. (2003) and Fiumelli et al. (2005) in hippocampal neurons showed that the activity-

induced positive shift in E_{GABA} required intracellular Ca^{2+} rise, which led to the down-regulation of KCC2. In contrast, Brumback and Staley argued that the activity-dependent positive shift in E_{GABA} in neonatal hippocampal neurons was due to a change in the set-point for NKCC. Another report of long-lasting activity- and Ca^{2+}-dependent shift in E_{GABA} concerns subthalamic neurons, but the underlying mechanism has not been examined (Wang et al. 2006). I probed the mechanism of activity-dependent negative shifts in E_{gly} in cartwheel cells in Chapter 2 based on the hypothesis that activity-induced intracellular acidification lowered $[HCO_3^-]_i$ and/or caused $[Cl^-]_i$ to decrease via activation of NDCBE.

Course of Thesis

I studied mouse cartwheel cells in brainstem slices with gramicidin perforated-patch recording to avoid the complications of whole-cell recording and to preserve intracellular Cl^-. In Chapter 1, I examined the mechanism of complex spike generation using blockers of various ion channels to gain insight into the regulation of complex spiking. In Chapter 2, I examined the effect of glycine on spontaneous activity along with measurements of E_{gly}. I also probed the mechanism of activity-dependent shift in E_{gly} by simultaneously monitoring intracellular pH, E_{gly} and intracellular Cl^-.

Chapter 1

Ion channels generating complex spikes in cartwheel cells of the dorsal cochlear nucleus.

Yuil Kim[1] and Laurence O. Trussell[2]

[1] Neuroscience Graduate Program

Oregon Health & Science University

Portland OR 97239

[2] Oregon Hearing Research Center/ Vollum Institute

3181 SW Sam Jackson Park Road, Mail Code L-335A
Portland, OR 97239

Number of Figures: 11 **Number of Tables**: 1

Number of Supplemental Figures: 4

Acknowledgments: This work was supported by NIH grant R37NS28901. Thanks to Dr. Donata Oertel for comments on the manuscript.

ABSTRACT

Cartwheel cells are glycinergic interneurons that modify somatosensory input to the dorsal cochlear nucleus. They are characterized by firing of mixtures of both simple and complex action potentials. To understand what ion channels determine the generation of these two types of spike waveforms, we recorded from cartwheel cells using the gramicidin perforated patch technique in brain slices of mouse dorsal cochlear nuclues and applied channel-selective blockers. Complex spikes were distinguished by whether they arose directly from a negative membrane potential or later during a long depolarization. Ca^{2+} channels and Ca^{2+}-dependent K^+ channels were major determinants of complex spikes. Onset complex spikes required T-type and possibly R-type Ca^{2+} channels, and were shaped by BK and SK K^+ channels. Complex spikes arising later in a depolarization were dependent on P/Q- and L-type Ca^{2+} channels, as well as BK and SK channels. BK channels also contributed to fast repolarization of simple spikes. Simple spikes featured an afterdepolarization that is probably the trigger for complex spiking and is shaped by T/R-type Ca^{2+} and SK channels. Fast spikes were dependent on Na^+ channels; a large persistent Na^+ current may provide a depolarizing drive for spontaneous activity in cartwheel cells. Thus the diverse electrical behavior of cartwheel cells is determined by the interaction of a wide variety of ion channels, with a prominent role played by Ca^{2+}.

INTRODUCTION

The dorsal cochlear nucleus (DCN) is a cerebellum-like component of the mammalian auditory system that may play a role in sound localization (Oertel and Young

2004; Young and Davis 2001). Auditory nerve fibers terminate on dendrites of giant cells and fusiform cells in the DCN deep layer, and their input is modified by various interneurons within the cochlear nucleus (Nelken and Young 1994; Zhang and Oertel 1993b, 1994, 1993c). The fusiform cells of the DCN also receive excitation through a system of granule cells and their associated parallel fibers in the DCN molecular layer. Some of the fibers that drive the granule cell, originate in medullary somatosensory nuclei and may convey ear and head position. Indeed, one proposed function of the DCN has been that it contributes to orienting toward specific sounds by integrating auditory, somatosensory and vestibular input (Kanold and Young 2001; May 2000; Oertel and Young 2004; Young and Davis 2001). Cartwheel cells (CWCs) are inhibitory interneurons that receive parallel fiber input and form synapses on fusiform cells, and among themselves, in the molecular and fusiform cell layer of the DCN (Berrebi and Mugnaini 1991; Mugnaini et al. 1987). The output of DCN principal neurons *in vivo* or *in vitro* has been characterized by inhibition of background spontaneous activity, and it is believed that CWCs play an important role in this process, being spontaneously active and capable of providing powerful feed-forward inhibition of parallel fiber input (Young and Davis 2001; Zhang and Oertel 1994). However, *in vivo* recordings have been made in immobilized animals where many of the somatosensory and vestibular inputs to granule cells are not activated, making the physiological activity of the molecular layer poorly understood.

CWCs are unique in the cochlear nucleus for their ability to generate complex spikes (Manis et al. 1994; Zhang and Oertel 1993a). Complex spikes, also called "bursts", consist of brief (< 100 ms), clusters of high-frequency (> 100 Hz) action

potentials superimposed on an underlying slow depolarization, and are seen in several neuronal cell types (Athanassiadis et al. 2005; Brumberg et al. 2000; Chagnac-Amitai et al. 1990; Deschenes et al. 1982; Jung et al. 2001; Kandel and Spencer 1961; Niespodziany and Poulain 1995; Schmolesky et al. 2002). The slow underlying depolarization of CWC complex spikes is believed to be Ca^{2+}-dependent, whereas the fast action potentials riding on the slow wave are Na^{+}-dependent, as are single action potentials (the "simple spike") in these same cells (Golding and Oertel 1997). The terms "complex spike" and "simple spike" imply electrophysiological similarity of the CWCs to the cerebellar Purkinje cells, and are in keeping with other studies highlighting morphological, genetic, and molecular parallels between these two cell types (Berrebi et al. 1990; Berrebi and Mugnaini 1991; Mugnaini and Morgan 1987). However, several features that differentiate these cell types suggest that a more careful investigation of CWC firing properties is needed. For example, Purkinje cells fire complex spikes only in response to climbing fiber activity; this activity is believed to play a key role in induction of synaptic plasticity at climbing fiber and parallel fiber synapses (Hansel and Linden 2000; Ito 2001; Konnerth et al. 1992). By contrast, CWCs may fire complex spikes spontaneously or in response to glutamatergic parallel fibers or glycinergic inputs from other CWCs (Golding and Oertel 1996; Tzounopoulos et al. 2004; Zhang and Oertel 1993a). Thus, the computational meaning of complex spikes may be different in the two cell types. We therefore have investigated the channel types underlying firing of complex and simple spikes, and what conditions promote each mode of firing, in slices of mouse DCN. Our results identify the role of multiple Ca^{2+} channels and Ca^{2+}-dependent K^{+} channels as well as Na^{+} currents in promoting and shaping the complex spike.

METHODS

Slice preparation, recording and analysis of data

Brain stem slices containing the DCN were prepared from ICR mice aged 16–23 days (Harlan, Indianapolis, IN). Mice were anesthetized with isoflurane and then decapitated in accord with the regulations of the Institutional Animal Care and Use Committee of Oregon Health and Science University. Subsequently, a block of brain stem was isolated and horizontal slices of 210-μm thickness were cut with a vibrating slicer (VT1000S, Leica, Deerfield, IL). Dissection and slicing were done in a warm (~ 30 °C) solution, which was composed of (in mM) 130 NaCl, 3 KCl, 1.2 KH_2PO_4, 2.4 $CaCl_2$, 1.3 $MgSO_4$, 20 $NaHCO_3$, 3 HEPES and 10 glucose, and was saturated with 95% O_2/5% CO_2. The chamber containing DCN slices were incubated at 34.5°C for the first hour and left at room temperature thereafter. For recording, a slice was transferred to the recording chamber on the stage of Olympus BX51WI microscope, and DCN cells were visualized with infrared differential interference contrast videomicroscopy. The bathing solution for recording was the same as that used for dissection and was perfused at 2–3 ml/min to the recording chamber by a peristaltic pump (Minipulse 3, Gilson, Middleton, WI). The temperature of the solution at the recording chamber was maintained at 33°C by a heating water jacket around perfusion tubing or by an in-line heating device.

Medium-sized cells in the molecular and fusiform cell layers of DCN were identified as CWCs if they showed complex spikes spontaneously or on injection of depolarizing current. The majority of data presented in this study were obtained with gramicidin perforated-patch recording (Kyrozis and Reichling 1995; Rhee et al. 1994) unless otherwise specified. The pipette solution for perforated patch recording consisted

of (in mM) 140 KCl, 10 NaCl and 10 HEPES (pH adjusted to 7.25 with KOH), and gramicidin was added just before use at a final concentration of 10–40 μg/ml from a stock solution of 10–30 mg/ml DMSO. The tip of the recording pipette was filled with the same solution but without gramicidin. For examination of the effect of increased intracellular Ca^{2+} buffering, conventional whole-cell recording was employed: a standard internal solution containing (in mM) 113 K-gluconate, 4.5 $MgCl_2$, 14 trisphosphocreatine, 9 HEPES, 0.1 EGTA, 4 Na-ATP and 0.3 Tris-GTP (pH adjusted to 7.3 with KOH), was modified to have higher EGTA at 5 mM or to include 20 mM BAPTA (tetrapotassium salt) in place of equimolar K-gluconate. Patch pipettes for recording electrodes of 2–6 MΩ resistances were prepared by pulling thick-walled filamented borosilicate glass capillaries (1B120F-4, World Precision Instruments, Sarasota, FL), and wrapped with Parafilm along one third of length from the tip to reduce capacitance. The liquid junction potentials measured (according to Neher 1992) and then corrected (for the reference junction, with JPCalc(Barry 1994)) were 2.8, 16 and 13.7 mV for the 140 mM KCl-based, 5 mM EGTA-containing and 20 mM BAPTA-containing pipette solutions, respectively; the values for latter two solutions were subtracted from the voltage data obtained with each solution off-line.

Recordings were made with a BVC-700A (Dagan, Minneapolis MN) or MultiClamp 700B amplifier (Molecular Devices, Sunnyvale, CA) in conjunction with pClamp 9.2 software (Molecular Devices). Data were digitized with Digidata 1322A (Molecular Devices) at 20 kHz (current-clamp) or 10 kHz (voltage-clamp) and low-pass filtered at 10 kHz (current-clamp) or 3 kHz (voltage-clamp). Pipette capacitance was compensated in all current-clamp recordings. For perforated-patch recording, after the

electrode had formed a seal (> 1GΩ) on the cell membrane in voltage-clamp, the progression of perforation (reduction in series resistance, R_s) was monitored in current-clamp by periodic bridge balancing and by observing the growth in amplitudes of spontaneous fast spikes (see *terminology*). Within 40 min of forming a seal, the R_s dropped to 20–40 MΩ; cells in which the R_s did not go below 40 MΩ were excluded from analysis. Occasionally, the perforated patch spontaneously ruptured, thus establishing whole-cell configuration. There were several signs of patch rupture when the recording pipette contained the 140 mM KCl-based solution in the preceding text, listed in the order of occurrence: an abrupt positive shift in voltage trace by 7–10 mV accompanied with an increase in amplitude of fast spikes (due to R_s reduction; Supplemental Fig 1Bi), very large depolarizing glycinergic/GABAergic postsynaptic potentials when the corresponding synaptic blockers were not present, and changes in pattern and waveforms of spikes characteristic of whole-cell recording with a KCl-based internal solution (Supplemental Fig 1Bii). In some cases, the V_m shift occurred slowly, obscuring detection of patch rupture, but the striking effects of dialysis with KCl eventually confirmed the rupture. Extracellular recordings were done in voltage-clamp mode (V_H = 0 mV) with a bath solution-filled recording pipette loosely attached to a cell.

Data were analyzed with Clampfit (pClamp 9.2) and Microsoft Excel. The membrane potential (V_m) between spikes of spontaneously active CWCs often fluctuated over a broad (~ 20 mV) range (see RESULTS). When there were not such fluctuations in basal V_m, an approximate level of interspike trough potentials, V_{trough}, (Fig 1Ei) was used as a representative value of V_m. The thresholds of fast spikes were defined by the potential at the inflection point of the rising phase of the spike waveform (Fig 1Ab,

arrows). For the repolarizing phase of a fast spike, the most negative V_m before the afterdepolarization, which may be a consequence of the fast afterhyperpolarization (fAHP), was measured and termed pFR (potential of fast spike repolarization; Fig 1Ab, arrowheads). The half-width of a fast spike was measured at the mid-point between the threshold and the peak of the spike. For comparison of spike waveform parameters between different conditions in one cell, the initial spikes in response to step current injections of a given amount were selected to obtain measurements, unless otherwise specified. The threshold and pFR of spontaneous simple spikes were measured for some cells for inter-cellular comparison. For cells firing simple spikes with stable V_{trough}, the threshold and pFR were measured from randomly selected spikes. However, for some cells in which the basal V_m during trains of simple spikes fluctuated (e.g., control trace in Fig 9Aii), spikes sitting on the most negative deflections of basal V_m were chosen for measurement of the two parameters.

For analyzing some drugs' effect on the frequency and duration of spontaneous complex spikes, data obtained by extracellular recording were included. The frequency of spontaneous complex spikes was measured by counting complex spikes in a 25-s period. The duration of complex spikes was quantified by summing interspikelet intervals. The "interspikelet" intervals of an extracellular complex spike were measured between negative peaks, as extracellular spikes/spikelets are biphasic. The extracellular spike seen in voltage-clamp mode is considered the sum of the capacitative and ionic current caused by the intracellular action potential (Fenwick et al, 1982). The waveform of our extracellular spikes generally resembled that of the first derivative of the intracellular fast spike; the extracellular interspikelet interval is similar to the interval

between the points of maximum rise slope of two adjacent intracellular spikelets. If all the spikelets are uniform in waveform, the extracellular interspikelet interval should be the same as the intracellular ones. For a typical complex spike in which the successive spikelets are smaller in amplitude and slower rising, the extracellular interspikelet interval is likely to be shorter than the intracellularly recorded interspikelet interval, at least for later appearing, small spikelets. Thus, the sum of interspikelet intervals of an extracellular complex spike may be a slight underestimate of that of the underlying intracellular complex spike. To document changes in the shape of Ca^{2+} spikes, rough indices of amplitude and decay time, the (maximum, if multi-peaked) peak-to-trough amplitude and the (last, if multi-peaked) peak-to-trough duration, respectively, were used. These were measured and averaged, for each control and drug condition, from all HTSs or LTSs (see Results for definition) evoked during 1–2 runs of an incremental (100 – 700 pA) current step protocol given from a V_m more negative than –75 mV. Voltage-clamp mode was used to measure steady-state currents (Fig 3B). The pipette and whole-cell capacitance were partially compensated but the R_s was not. Statistical presentation of data were given as means ± S.D., and the difference between two groups of data were tested using two-tailed *t*-test (paired or unpaired) at the 0.05 level of significance.

Drug application

All the pharmacological agents were applied by bath perfusion. Blockers of fast glutamatergic, GABAergic and glycinergic transmission (20 μM 6,7-dinitroquinoxaline-2,3-dione (DNQX), 100 μM 2-amino-5-phosphonovaleric acid (APV), 10 μM SR95531 and 0.5 μM strychnine) were added to the bath solution after an initial

examination of spiking properties unless otherwise specified. Drugs were obtained from Sigma-Aldrich (St Louis, MO) with the exception of SR95531 (Tocris Cookson, Ellisville, MO), tetrodotoxin (TTX), ω-conotoxin-GVIA, iberiotoxin, apamin (Alomone labs, Jerusalem, Israel), ω-agatoxin-TK, ω-agatoxin-IVA and ω-conotoxin-MVIIC (Peptide International, Louisville, KY). When applying peptide toxins, 0.5 mg/ml cytochrome C (for agatoxins, conotoxins), or 0.1 mg/ml bovine serum albumin (BSA, for iberiotoxin) was included in the drug perfusate to reduce nonspecific binding, and control traces were obtained in the presence of cytochrome C or BSA alone before drug application began. Agatoxins, conotoxins and iberiotoxin were perfused for at least 15 min using recirculation. When $CdCl_2$ or $NiCl_2$ was used, KH_2PO_4 in the bathing solution was replaced with KCl to prevent precipitation.

Terminology

Fast action potentials riding on the slow depolarization of a complex-spike waveform became slower and smaller as they arose from more depolarized membrane potentials (Manis et al. 1994). However, the initial fast spikes could have similar thresholds and amplitude to simple spikes. We used the term “spikelets” to refer specifically to the spikes comprising a complex spike, and “fast spikes” to indicate both simple spikes and initial spikelets of complex spikes. Figure 12 diagrams several types of spike discussed here.

Requirement for perforated-patch recording and consideration of voltage offsets

Whole-cell recording with the standard K-gluconate solution was generally avoided because of the following changes which developed within 15 minutes from the moment of patch break-through in CWCs: V_m became hyperpolarized resulting in loss of spontaneous activity, later, complex spikes would occur more frequently and at a lower stimulus level in response to step depolarizations, and fast spikes repolarized less, the pFR becoming depolarized by 3.2 ± 3.4 mV (n = 24). These changes progressed more slowly when using recording pipettes of smaller bore, and therefore must be related to the dialysis of cytoplasmic constituents. Changing the major anion of the internal solution to methylsulfate or methanesulfonate did not prevent time-dependent changes. On the other hand, with gramicidin perforated-patch recording, spontaneous spike activity was maintained, although slight depolarization of V_m, as apparent from increase in spiking frequency, was often seen during early periods of recording. Most importantly, the increase with time in complex spiking on routine step current protocols did not occur, as it did with whole-cell recording. Supplemental Fig 1A illustrates changes in spike properties of a cell that had been recorded initially in perforated-patch mode and then in whole-cell mode with the K-gluconate based solution after rupture of patch.

A sudden ~ 8 mV jump in V_m and corresponding shift in spike parameters (threshold, pFR) were observed when the perforated patch ruptured during recordings with the 140 mM KCl-based internal solution. This shift in potential might suggest that a junction potential existed across the gramicidin perforated patch between the pipette solution and the cytoplasm, such that the potential at the recording electrode had been more negative than the true V_m; alternatively, it may be that a Donnan potential

developed on patch rupture (Horn and Marty 1988). Similar positive V_m shifts at patch rupture during gramicidin recording have been reported and considerations for correction of the recorded V_m by adding the magnitude of shift have been addressed (Atherton and Bevan 2005; Brockhaus and Ballanyi 1998; Hallworth et al. 2003). In our recordings, however, the initial 8 mV upward shift in V_m later appeared to sag back toward the original potential (Supplemental Fig 1Bi); during the 20-s period after rupture, peaks of fast spikes gradually declined in spiking cells, and in silent cells the V_m settled to a final level 3–5 mV more depolarized than the potential before the sudden jump. This led us to wonder what correction should be applied to the recorded V_m, if any. We have found that when gramicidin perforated patch recordings were done with a pipette solution composed of (in mM) 140 K-gluconate, 1 $MgCl_2$ and 10 HEPES, no shift of V_m was noticeable at patch rupture; this indicates that there may be no junction potential between this solution and the cytoplasm. To estimate the potential difference between the 140 KCl solution and the cytoplasm, we employed dual perforated-patch recording on single cells with the 140 K-gluconate solution in one recording pipette and the 140 KCl solution in the other. The difference in V_m read-out between the two recording electrodes was 14.7 ± 1.3 mV (n = 10), and when the patch under the K-gluconate pipette was ruptured to form a whole-cell configuration, the potential difference did not change. The mean value, 14.7 mV, was corrected for liquid junction potentials of each solution (13.3 and 2.8 mV, respectively) to become 4.2 mV, which is the estimated potential difference across the perforated-patch between the 140 KCl solution and the cytoplasm. Because the offsets to be considered for the V_m recorded with 140 KCl solution were similar in magnitude and

of opposite direction (–2.8 for liquid junction potential, +4.2 mV for the patch potential) leaving 1.4 mV, we opted not to apply any correction.

RESULTS

Spontaneous spiking activity in CWC

CWCs were identified as medium-sized neurons located in the molecular and fusiform cell layers of the DCN that fired complex spikes in response to depolarizing current injection. Of the 335 CWCs recorded with gramicidin perforated-patch method and not previously exposed to pharmacological agents, 33.7 % (n = 113) were silent and the rest, 76.3 % (n = 222), were spontaneously spiking. Silent cells had a mean resting potential of –82.3 ± 2.7 mV (range –76 ~ –88 mV; n = 113). Among spontaneously active cells, a range of spiking patterns was observed with respect to the tendency to fire complex spikes: 72.1 % (n = 160) showed only simple spikes ("all-simple-spiking"), whereas the others (27.9 %, n = 62) showed different frequencies of complex spikes along with simple spikes ("complex-spiking"). Another characteristic feature of CWCs was a slow fluctuation or oscillation in the basal profile of V_m. The V_m excluding spikes (base V_m) coursed between levels close to and far from the spike thresholds, generating periods of spiking interposed with deep hyperpolarized periods of silence (Fig 1A). Such fluctuation in base V_m was seen in most complex-spiking cells and in 24.5 % of all-simple-spiking cells (together, 44.8% of spontaneously spiking cells). The remainder of all-simple-spiking cells maintained relatively stable base V_m while firing quasi-regularly at 10−30 Hz (Fig 1Ei) or irregularly at a lower frequency. Silent CWCs were heterogeneous with respect to their tendency to fire complex spikes or exhibit fluctuating

base V_m behavior when made to spike with small depolarizing holding currents. Elimination of spontaneous synaptic potentials by applying a cocktail of blockers of ionotropic glutamate, $GABA_A$, and glycine receptors did not eliminate spontaneous spike activity of CWCs, suggesting that CWCs' spiking characteristics—complex spikes and slow V_m fluctuation—are intrinsically determined.

Variety of complex spikes

In this section, we will describe at some length the appearance and variety of complex spikes, as these detailed characteristics helped make clear what factors promote complex versus simple spiking. We noticed that spontaneous complex spikes of individual CWCs were often not uniform: some were distinct while others appeared to blend with neighboring simple spikes, especially on the rising phase of their underlying depolarization, which made the beginning of such complex spikes unclear. However, these are all recognized as complex spikes based on a core motif in their waveform, including the terminal part in the rising phase where the slope was steepest and the presence of two to three spikelets having intervals of < 4 ms. We used the term "prompt" spike to refer to a distinct form of the complex spike, which is separated from a previous spike by at least 30 ms and has an initially fast rise consisting of three to four spikelets at intervals < 6 ms (Figs 1Aa, and 12). The less distinct complex spikes, which appeared to follow directly from one or more simple spikes having 7–25-ms interspike intervals, were termed "delayed" spikes (Figs 1Ab,c,d, and 12). Spontaneous complex spikes were often preceded by a hyperpolarization. Typically, in a given cell, the prompt complex spike occurred after a long (> 100 ms) hyperpolarized phase of slow V_m oscillation, and the

delayed spike after a short hyperpolarization (Fig 1Ai). However, some cells showed only delayed complex spikes even after prolonged hyperpolarizations (Fig 1Aii). Spontaneous complex spikes occurring in the middle or end of a prolonged spiking phase without a clearly preceding hyperpolarization were also observed in some cells. It was also possible to recognize prompt and delayed complex spikes in extracellular recordings (Fig 1B; n = 65 cells) (Tzounopoulos et al. 2004). To summarize, we distinguished two main classes of spontaneous complex spike: prompt spikes arising quickly from a preceding hyperpolarization, and delayed spikes, arising soon after simple spike activity.

The repolarizing phase of a complex spike was steeper when there were more spikelets, as shown from comparison of prompt complex spikes with random variation in spikelet number observed in same cells (Fig 1C). Sometimes the extra spikelet(s) was much slower than the preceding ones ("slow spikelet") and appeared to occur from the repolarizing phase of the underlying slow depolarization (Fig 1C, 3rd pair). These data suggest that current activated during spikelets drive repolarization of the complex spike; in a later section we show that part of this current is due to SK K^+ channels.

The ability to fire complex spikes on depolarizing current injection distinguished all-simple-spiking or silent CWCs from other neurons in the DCN (Fig 1E). Most CWCs, when given incremental depolarizing current steps (Δ20–25 pA, 200–300 ms) from a quiescent state near –80 mV (with hyperpolarizing bias current for spontaneously active cells), fired only simple spikes as their first active response (Fig 2Ai). With increasing step depolarizations, they generated complex spikes, of which we distinguished two types based on their thresholds. Typically, one complex spike appeared first at onset of the depolarizing step followed by simple spikes throughout (the

"onset" spike). Then with larger depolarizations, additional complex spikes arose after the onset spike, interspersed with simple spikes, and are termed "late" spikes. Late complex spikes became more frequent as depolarization increased (Fig 2Ai). Occasional deviations from this pattern included, for example, cases in which the cells first gave rise to late complex spikes (as in Fig 6Ai, top), and then with more current generated the onset spike. In some cells, the initial spike response to depolarizing steps was one or more complex spikes with or without following simple spikes (Fig 2Aii). Stronger depolarizations made the next responses follow the more typical pattern. The onset spike for these cells occurred immediately on the stimulus regardless of the magnitude of stimuli, but for other cells, the onset spike appeared delayed when first seen at the threshold stimulus, and the delay decreased on increasing stimuli (Fig 2Ai). To examine the dependence of complex spikes on the preceding potential, onset spikes were triggered with a two-step current protocol (Fig 2Bi). As the conditioning V_m was gradually made more positive than –80 mV, the onset spike became delayed and eventually could not be triggered. The level of V_m above which an onset spike (limited to those arising within 40 ms) could not be evoked with this protocol varied between –70 and –65 mV across different cells (Fig 2Bii). A transient depolarization at the onset of a current step was often observed at stimulus levels subthreshold to the appearance of a delayed onset complex spike (Fig 2Ai 80 pA trace) or at failure of an onset spike (Fig 2Bi right bottom).

Afterdepolarization as a trigger for complex spikes.

The waveform of CWC simple spikes had a characteristic bump-like afterdepolarization (ADP) following the end of repolarization (Fig 1Ab) (Manis et al.

1994; Zhang and Oertel 1993a). When the first spikelet of a prompt complex spike and an isolated simple spike having the same threshold belonging to the same cell were superimposed, the waveforms appeared indistinguishable, except that the pFR of the former tended to be slightly (~ 1.5 mV) less negative than that of the latter. Considering this similarity and that the simple spike's ADP peaks within 3–6 ms of the peak of the spike, it seemed possible that the prompt complex spike starts from a simple spike having a larger ADP, such that the ADP triggers the second spikelet and the rest of a complex-spike waveform, the core motif. In the same manner, the delayed complex spike might arise where a simple spike's ADP is not depolarized enough to give rise to a fast spike at its peak, but enough that another simple spike arises on its decay phase, and so on, until the threshold for the core burst is reached on a spike's ADP (Fig 1A, b–d). Examples in which successive ADPs accumulate but decay without reaching such threshold are seen in the beginning of the fourth spike cluster in Fig. 1Aii and the 80-pA response in Fig. 2Ai. Is there a systematic relationship between the threshold for a fast spike, the peak of the ADP, and the probability of firing complex spikes? Spontaneous simple spikes' thresholds and pFRs were measured for subsets of complex spiking and all-simple-spiking CWCs (Table 1). The pFR was measured as an indirect index of the basal ADP level of simple spikes, because the ADP itself appeared to vary in amplitude in some cells (Supplemental Fig 2). The mean pFR and the mean difference between pFR and threshold of spontaneous simple spikes were found to be significantly different between all-simple-spiking cells and complex-spiking cells ($p < 0.001$ for both), such that spontaneous complex spikes were not seen in cells in which the fAHP brought the membrane potential farther from threshold.

To explore this relationship further, we evoked single spikes with a short (< 1.5 ms) current pulse while a bias current was maintained to keep the cell silent (at V_m ~ –80 mV) before and after the spike. Although the pFR and the amplitude of ADP (the difference between the base V_m and the peak of ADP) of spikes evoked by short pulses were variable among CWCs (Fig 1D), the pFR was more negative (by 2.5 ± 1.2 mV, n = 28, paired *t*-test, $p < 0.001$), and the bump of the ADP was less apparent for spikes evoked by short pulses than for spontaneous spikes. In cells with more negative pFRs, a slow afterhyperpolarization reaching negative to –80 mV could be observed (12 of 115 cells examined with short pulses; Fig 1Dii). Short pulses elicited only simple spikes in most CWCs, including about two thirds (20 of 29) of the spontaneously complex-spiking cells tested, but they could also elicit complex spikes (Figs 1Di and 11E, left) from some prompt complex-spiking cells and from silent cells. These features will be used in the following sections to explore the effect of selective channel blockers.

Effect of Na^+ channel block.

Application of the voltage-dependent Na^+ channel blocker TTX (0.5 μM) eliminated fast action potentials. TTX did not affect the resting potential of silent cells, but in spiking cells the V_m in TTX ranged between –75 and –50 mV. For all-simple-spiking cells that fired quasi-regularly without base V_m oscillation, the V_m in TTX was less negative than the interspike trough potential (V_{trough}) before TTX by 10 ± 5.6 mV (n = 20). Depolarizing current evoked slow spikes in a pattern reminiscent of complex spikes (109 of 109 cells given TTX; Fig 3A). Typically, a lone slow spike could be observed at the onset of a step depolarization, and then with larger depolarizing steps,

more slow spikes appeared (Fig 4Ai). The slow spike at onset of depolarization appeared graded in amplitude with the amount of current injected, whereas the later occurring ones were all-or-none. The threshold current for the late slow spikes was 293 ± 83 pA (n = 21, V_m held at – 80 mV), and this was 112 ± 91 pA more than that required for the late complex spikes before TTX application in the same cell. A more detailed study of slow spikes is presented in later sections of the RESULTS.

CWCs have a persistent Na^+ current. When stepping to potentials less negative to –70 mV from a holding potential of –80 mV, a persistent inward current was observed that was blocked by TTX (Fig 3Bi). Accordingly, a negative slope conductance region existed in the steady-state current-voltage (I-V) plot of CWCs, which started between –70 and –75 mV extending to about –55 mV where the plot terminated due to limitation in voltage control (Fig 3Bii). The I-V plots varied in their vertical position with respect to the 0-current axis. For many silent cells, the plot crossed 0-current axis once at their resting potential with the negative slope region located above the 0-current axis. On the other hand, the entire plot lay below the 0-current axis for many spontaneously spiking cells. The current at the crest of I-V plot was –14 ± 21 pA (n = 52) for spiking cells and 78 ± 51 pA (n = 32) for silent cells (*t*-test, $p < 0.001$). TTX eliminated, or in some silent cells reduced the negative slope region (Fig 3B). The difference currents obtained by subtracting the currents in the presence of TTX from those in its absence, show that the persistent Na^+ current activated near –75 mV, and reached –139 ± 31 pA (n = 15) at –55 mV. In current clamp, the V_m was unstable above –75 mV, and drifted in the depolarizing direction until cycles of fast spikes were generated. It is likely that this drift

arose from activation of persistent Na^+ current. Similar observations were made with sharp electrode recordings (Hirsch and Oertel 1988).

Effect of general Ca^{2+} channel block and properties of the slow spikes.

Ca^{2+} currents are believed to contribute to the underlying depolarization of complex spikes (Golding and Oertel 1997). We thus examined how the removal of regenerative Ca^{2+} currents with Cd^{2+} or by replacing Ca^{2+} with Mg^{2+} affected firing. As Cd^{2+} (200 μM, n = 3; 100 μM, n = 2) entered the recording chamber, there was a transient period of enhanced complex spiking in all CWCs (Fig 5A, middle). After a longer exposure to Cd^{2+}, cells fired broadened simple spikes at high rates and in long clusters. Eventually only a two-spikelet pair remained at the onset of a step depolarization (Fig 5A, bottom) or at the beginning of spontaneous, simple spike clusters. The simple spikes in Cd^{2+} appeared broadened more toward their base, and comparison of the spike width at 40 % of amplitude yielded a more significant result than that of the half-width (40%-width, 0.45 ± 0.07 vs. 0.64 ± 0.17 ms, n = 5, paired *t*-test, p = 0.021; half-width, p = 0.047). Cd^{2+} also caused a hyperpolarization of V_m by less than 10 mV but this was not studied further. Removal of external Ca^{2+} (replaced with Mg^{2+}, n = 3) also abolished complex spikes and broadened the base of simple spikes (40%-width 0.52 ± 0.06 vs. 0.63 ± 0.08 ms, paired *t*-test, p = 0.01). However, in the absence of Ca^{2+}, CWCs eventually became depolarized and were unable to fire more than a few spikes even with a hyperpolarizing holding current.

In the presence of TTX, the slow spike triggered at the onset of a depolarizing step only occurred when the preceding potential was more negative than ~ – 65 mV (Fig

4B), suggesting that the onset spike had a lower threshold than later slow spikes (see also Fig 4Ai). The slow spike at the onset will be referred to as the low-threshold spike (LTS), and the later ones, the high-threshold spike (HTS). Expecting that these TTX-insensitive slow spikes were mediated by Ca^{2+}, Cd^{2+} was added (50 μM, n = 2; 200 μM, n = 4; 500 μM, n = 3). HTSs, but not LTS, were abolished by Cd^{2+} at all the concentrations tried (n = 9; Fig 5Bi). The low-threshold nature and the relative resistance to Cd^{2+} suggest that T-type Ca^{2+} channels mediate LTS (Ertel 2004). Ni^{2+}, a more efficient blocker of T-type Ca^{2+} channels, was therefore applied at 500 μM plus 100 μM Cd^{2+} (n = 1), or alone at 500 μM (n = 1; Fig 5Bii), or at 1 mM (n = 1). Under these conditions, HTSs were eliminated and the maximum peak-to-trough amplitude of the LTS evoked with a series of hyperpolarizing presteps (as in Fig 4B) was reduced by 73, 63 and 87%, respectively. Removal of external Ca^{2+} also eliminated all slow spikes in TTX (n = 3). The differences in threshold and in sensitivity to Cd^{2+} and Ni^{2} indicate that the LTS and HTS were Ca^{2+} spikes that were mediated by different subtypes of Ca^{2+} channels. The forms of Ca^{2+} spikes were not as stereotypical as those of Na^{+} spikes; the amplitude and width of HTS or LTS varied within a CWC depending on the V_m from which spikes were evoked and on the amount of current injected. HTSs were more frequent and larger when evoked from a more depolarized V_m, and multi-peaked broader forms could be seen in some CWCs with threshold current injection (Fig 4A). The magnitude of depolarizing current steps just sufficient to elicit HTS or LTS and the maximum amplitude of these spikes differed among CWCs, as did the onset and late complex spikes in control solutions. Moreover, the amplitude of the LTS varied between cells, and could be quite small (Fig 10Bi).

To determine whether Ca^{2+} channels shape the ADP and fAHP, spikes evoked with short pulses of current were recorded in the presence of 100 μM Cd^{2+} plus 500 μM Ni^{2+} (Fig 5C; n = 8). The short pulse-evoked fast spikes broadened toward the base of the spike (width at – 40 mV, roughly just below half-amplitude level, 0.52 ± 0.06 vs. 1.16 ± 0.38 ms, n = 8, paired *t*-test, p = 0.001) and repolarized to less negative potentials. The changes in repolarization suggested involvement of Ca^{2+}-mediated outward currents. To identify the subtype channels underlying these effects, further experiments were conducted with specific blockers of Ca^{2+} channel and Ca^{2+}-activated K^+ channel subtypes.

Effect of intracellular Ca^{2+} buffering.

To test the possibility that Ca^{2+}-activated K^+ conductances served as repolarizing currents, intracellular Ca^{2+} was buffered using whole-cell recording with an EGTA- or BAPTA-containing pipette solutions. As mentioned in METHODS, whole-cell recording, with 0.1 mM EGTA, led to hyperpolarization, increased complex spiking, and a small depolarizing shift in pFR. Raising the EGTA to 5 mM or including 20 mM BAPTA caused progressive changes in spike waveforms far larger than those seen with 0.1 mM EGTA.

In recordings using 5 mM EGTA in the patch pipette, the pFR became less negative by 8.1 ± 1.4 mV after 15 min of dialysis (n = 6). Moreover, complex spikes occurred more readily with depolarizing current injection and had a broader appearance and several slow spikelets (Fig 6Ai). The half-width of fast spikes after 15 min was 0.45 ± 0.03 ms (n = 6), which was not significantly longer than that measured from 6 whole-cell recordings with an internal solution containing 0.1 mM EGTA (0.42 ± 0.04 ms, *t*-test,

p = 0.16). In the presence of TTX, 5 mM EGTA, caused the HTSs to become prolonged and to acquire multiple peaks (n = 3; Fig 6Aii). The LTS did not noticeably change, except that an HTS often appeared to occur on top of the LTS (Fig 6Aii). The effect of a faster Ca^{2+} buffer, BAPTA, at 20 mM, was also examined. Complex spikes broadened in less than 1 min after patch break-through (Fig 6Bi, top), and then a marked loss of fAHP ensued. Simple spikes disappeared leaving only complex spikes consisting of a half-repolarizing fast spike and many slow spikelets (Fig 6Bi, middle) (n = 7). Eventually the pFR became very depolarized (by 41.3 ± 4.3 mV after > 15 min; n = 7), and the complex spike waveform became narrower, appearing more like a broadened simple spike with inflections in its repolarizing phase (Fig 6Bi, bottom, initial 2 spikes; half-width 1.22 ± 0.53 ms, n = 7). In the presence of TTX, a similar broadening-narrowing sequence in waveforms of HTSs was observed as BAPTA diffused intracellularly (Fig 6Bii; n = 3).

Effect of BK and SK channel block.

Because blocking Ca^{2+} channels or buffering intracellular Ca^{2+} slowed spike repolarization, we turned to selective blockers of Ca^{2+}-activated K^+ channels, using iberiotoxin for the large-conductance Ca^{2+}-activated K^+ (BK) channel and apamin for the small-conductance Ca^{2+}-activated K^+ (SK) channel. Incubation in iberiotoxin (100 nM) led to spontaneous firing of complex spikes in all-simple-spiking cells (n = 6). In two cells that were silent and gave only simple spikes at rheobase (i.e., the smallest suprathreshold depolarizations), iberiotoxin also led to firing of complex spikes. Iberiotoxin generally increased firing of complex spikes (Fig 7A) but the degree of increase was quite variable; among five spontaneously complex-spiking cells monitored

with intra-or extracellular recording, the increase in spiking was 0, 116, 154, 390, and 536% (paired *t*-test, n = 5, p = 0.10). Along with this enhancement of complex spiking was a reduction in the fAHP (pFR depolarized by 13.9 ± 4.8 mV, n = 9; Figs 7Ai, inset, and 7B) and increase in the half-width of fast spikes (0.42 ± 0.08 vs. 0.49 ± 0.11 ms, n = 9, paired *t*-test, p = 0.007). The less negative pFR in iberiotoxin was accompanied by a shortening of the first interspikelet interval for the one cell that had spontaneous, prompt, complex spikes (Fig 7Ai inset) and conversion of delayed onset complex spikes to prompt ones for other cells (Fig 7Aiii); prompt complex spikes appeared in spontaneous or evoked activity of cells that did not display such complex spikes in control conditions. The decrease in the first interspikelet interval for spontaneous prompt complex spikes, when jointly assessed with measurements from four extracellularly recorded complex-spiking cells, all of which displayed prompt complex spikes in control conditions (e.g., Fig 7Aii), was significant (4.0 ± 0.5 vs. 1.8 ± 0.2 ms, paired *t*-test, n = 5, p < 0.001). The reduced fAHP and boosted complex spiking in iberiotoxin was also observed for spikes evoked by short pulses (n = 3). The three tested cells generated only simple spikes in control conditions; two of these became able to fire complex spikes robustly (Fig 7B). In the presence of TTX, iberiotoxin increased the amplitudes of Ca^{2+} spikes (Fig 7C, n = 7). The peak-to-trough amplitude of HTSs increased by 51 ± 17 % (from 17.8 ± 4.4 mV, paired *t*-test, n = 7, p < 0.001), whereas the peak-to-trough time did not change (9.9 ± 2.0 vs. 10.0 ± 1.7 ms, paired *t*-test, n = 7, p = 0.8). For the LTS, four of the seven cells showed an increase in the peak-to-trough amplitude (by 70 ± 6 %, paired *t*-test, p = 0.014). Among the other three cells that had no or barely noticeable LTS, two gained a

clear LTS in iberiotoxin. Thus, BK channels played a key role in determining the shape of fast spikes and the likelihood of generating complex spikes.

Blockade of SK channels using apamin (100 nM, n = 7, or 50 nM, n = 9), also increased the tendency to fire complex spikes. Four of the five all-simple-spiking cells as well as complex-spiking cells (n = 5) started to fire broad, prompt or short-delay (preceded by just one simple spike with the interval <10 ms) complex spikes, isolated or clustered with more complex spikes and few interposing simple spikes (Fig 8A). For the five complex-spiking cells and one extracellularly recorded complex-spiking cell, the frequency of spontaneous complex spikes increased in apamin (0.9 ± 0.8 vs. 2.7 ± 1.4 Hz, 15 – 1440 % increase, n = 6, paired *t*-test, p = 0.015). Silent cells' firing at rheobase also became predominantly complex spiking in apamin (n = 7 of 8 cells). The usual initial response to step current injections, either all simple spiking or an onset complex spike followed by simple spikes, became replaced in apamin with all complex spiking, whereas responses to larger current injections were also dominated by complex spikes (Fig 8B). For the cell shown in Fig. 8B, a transitional effect of apamin as the drug washed in was also recorded (Supplemental Fig 3A): the train of simple spikes following the onset spike depolarized more steeply, giving rise to late complex spikes at a higher frequency than in control. Thus, apamin appeared to impair CWCs' ability to fire simple spikes with a stable V_{trough}.

We measured interspikelet intervals of spontaneous complex spikes and plotted these for successive spikes in the waveform. To monitor spikes of uniform shape, we only included those spikes preceded by 150 ms of silence; this was done for six cells including one extracellular recording. Figure 8C shows two sets of such plots for two

cells, the second one (ii) extracellularly recorded. Both cells in control conditions had delayed complex spikes, starting with an interspikelet/spike interval > 5 ms, and the first interval varied rather widely (7.6 ± 4.2 (n = 18) and 15.0 ± 3.6 ms (n = 73), for Fig 8C, i and ii). In apamin, both cells showed marked decrease in the duration and variability of the first interspikelet interval (3.8 ± 0.2 (n = 25) and 5.2 ± 0.9 (n = 92) ms, for i and ii), so that the complex spikes in apamin were prompt or of short-delay. These changes in the first interspikelet interval in apamin occurred in all of the five complex-spiking cells and one extracellularly recorded cell (n = 6; Δduration, –4.5 ± 3.5 ms, paired *t*-test; p = 0.025; F-test, p < 0.001 for every cell). When short pulse-evoked complex spikes were examined (n = 4, 2 of complex-spiking cells and 2 silent cells) the first interspikelet interval was also found significantly decreased by apamin (Fig 8Dii; Δ –0.9 ± 0.5 ms, paired *t*-test, p = 0.041). Compared with the effects of BK channel block, which also include the shortening of first interspikelet interval, the pFR and the half-width of fast spikes were not affected by apamin (Fig 8D, i-iv; ΔpFR of short pulse evoked spikes, –0.1 ± 0.5 mV, n = 16, paired *t*-test, p = 0.23). However, the slope of the first interspikelet interval appeared steeper in apamin, and this may have led to a shortening of the interval (Fig 8D, i and ii). The complex spikes in apamin appeared prolonged with more spikelets but repolarized to a lesser extent (Fig 8D, i and ii). To measure complex spikes' duration, we summed the interspikelet intervals of each complex spike preceded by > 150 ms of silent period, beginning from the first interval ≤ 5 ms to exclude the long intervals before the abrupt rise of underlying slow depolarization in delayed complex spikes. The sum of interspikelet intervals thus obtained from spontaneous complex spikes was compared between control and apamin-treated conditions. For the five complex-spiking cells and

one extracellularly recorded cell, the complex spike duration increased from 6.6 ± 1.1 ms in control to 17.6 ± 8.8 ms in apamin (n = 6, 50 – 470 % increase, paired *t*-test, p = 0.034), along with the change in the number of spikelets (number of included intervals + 1) from 3.3 ± 0.5 in control to 6.7 ± 2.8 in apamin (n = 6, 40 – 360 % increase, paired *t*-test, p = 0.045).

In 9 of 16 cells treated with apamin, short pulses that initially evoked simple spikes continued to do so in apamin although their spontaneous activity or response to longer step depolarizations became predominantly complex spiking. However, the simple spikes triggered by short current pulses in the presence of apamin revealed a larger, or more slowly-decaying, ADP compared with that in control conditions. The corresponding depolarizing shifts of V_m at 10 ms from the peak of the averaged evoked spikes were significant (Fig 8Dv; Δ 4.7 ± 3.5 mV, n = 9, paired *t*-test, p = 0.004). For Ca^{2+} spikes in TTX, apamin caused a general enhancement of HTSs, including broadened appearance with more peaks, larger amplitude and higher frequency compared with those evoked by same current injection in control conditions. However, the HTS in apamin had a slowed repolarization and afterhyperpolarization (Fig 8E; peak-to-trough time, 12.3 ± 1.8 vs. 17.5 ± 3.5 ms, n = 6, paired *t*-test, p = 0.004; peak-to-peak amplitude, 17.6 ± 3.8 vs. 20.7 ± 3.9 mV, n = 6, paired *t*-test, p = 0.026). The LTS did not appear changed in apamin. Thus, SK channels determine the duration of complex spikes and likelihood of complex spikes, possibly by regulating the duration and size of the ADP.

Given the effects of blocking SK and BK channels on spike waveforms, the results of buffering intracellular Ca^{2+} with EGTA and BAPTA were revisited. Although complications of whole-cell recording were necessarily superimposed, 5 mM EGTA

appeared to inhibit partially BK channels, because it reduced the fAHP only moderately, whereas the signs of SK channel block, broadening of complex spikes and the HTS, were more obvious. This suggests that BK channels may lie in close proximity to Ca^{2+} channels and the slow buffering by EGTA affects the Ca^{2+} concentration near the BK channels only little. BAPTA (20 mM), on the other hand, caused a far greater loss in fast spike repolarization than iberiotoxin. It is unclear whether this was due to incomplete block of BK channels by iberiotoxin, as the sensitivity of BK channels to iberiotoxin may vary with subunit composition (Meera et al. 2000), or due to consequences of whole-cell dialysis or extremely low intracellular Ca^{2+}. It is also possible that the eventual narrowing of complex spikes with 20 mM BAPTA may not be related to the block of BK and SK channels because multi-spikelet waveforms persisted during the combined application of apamin and iberiotoxin (extracellular recording, n = 3; not shown).

Specific block of subtype Ca^{2+} channels:

I. N-type

Application of ω-conotoxin-GVIA (1–3 μM), which specifically blocks N-type channels had no effect on either the firing pattern or on the shape of spikes (n = 2 without TTX, n = 3 with TTX).

II. P/Q-type

The presence of P/Q type Ca^{2+} channels was probed with ω-agatoxin-TK, ω-agatoxin-IVA or ω-conotoxin-MVIIC. ω-agatoxin-TK (100–200 nM; n = 16), ω-agatoxin-IVA (200 nM; n = 1) and ω-conotoxin-MVIIC (2–3 μM; n = 5) each caused

increased complex spiking. Thirteen all-simple-spiking cells as well as 2 complex-spiking cells started to fire clusters of complex spikes and higher frequency simple spikes in the presence of these toxins (Fig 9A). The frequency of spontaneous complex spikes for the two complex-spiking cells and three extracellularly recorded complex-spiking cells was increased in P/Q channel blockers (0.8 ± 0.6 vs. 1.9 ± 0.8 Hz, n = 5, paired *t*-test, p = 0.043). The spontaneous complex spikes in the presence of P/Q channel blockers were often broader with more spikelets than those in control conditions (Fig 9Aii). Plots of interspikelet intervals versus their duration were generated and analyzed as with apamin-treated cells (Fig 9B). The duration of spontaneous complex spikes for one of the two complex-spiking cells and three extracellularly recorded cells, increased from 4.4 ± 0.9 ms to 10.0 ± 1.2 ms in P/Q channel blockers (n = 4; paired *t*-test, p = 0.011). The number of spikelets included was 2.7 ± 0.5 in control and 3.8 ± 1.2 in the drug (n = 4, paired *t*-test, p = 0.083). The duration of the first interspikelet interval, unlike with apamin, did not decrease (Δ 3.9 ± 5.0 ms, n = 4, paired *t*-test, p = 0.22). The one complex-spiking cell not included in the preceding text fired only two-spikelet complex spikes after >150 ms of hyperpolarized periods in control condition, and continued to do so in P/Q channel blocker but with increased occurrence of delayed complex spikes following the two-spikelet one. For this cell, the interspikelet interval of the two-spikelet complex spikes increased from 4.7 ± 0.6 (n =23) to 5.5 ± 0.9 ms (n = 20; p = 0.002). In the response to depolarizing current pulses, P/Q channel blockers caused faster trains of simple spikes, such that the maximum frequency of simple spike train not giving rise to a late complex spike during a 325-ms current step was increased (78 ± 30 vs. 115 ± 55 Hz, n = 15, paired *t*-test, p = 0.001). Also, the late complex spikes appeared

at a lower current levels in the presence of P/Q channel blockers (140 ± 78 vs. 37 ± 33 pA, n = 12, paired *t*-test, $p < 0.001$) suggesting that the excitability of CWCs had increased (Fig 9C and Supplemental Fig 3C). The late complex spikes were broadened, while the onset spike did not appear so (Fig 9C and Supplemental Fig 3C). The lowering of the threshold for complex spikes by P/Q channel blockers was reminiscent of the effects of apamin (Supplemental Fig 3, A and B vs. C), suggesting that the Ca^{2+} influx through P/Q-type Ca^{2+} channels serves to activate SK channels. However, differences between the effect of P/Q blockers and that of apamin were noted in short pulse-evoked spikes, in induced complex spikes, and in Ca^{2+} spikes. P/Q blockers caused the pFR of short pulse-evoked spikes to become less negative by 1.8 ± 1.4 mV (n = 11, paired *t*-test, $p = 0.002$), whereas apamin did not affect the pFR. The less negative pFR led to a more depolarized ADP (Fig 9D), and 1 of the 10 cells that under control conditions responded to short pulses with only simple spikes became able to fire complex spikes. In one cell the averaged pFR of spikes evoked by short pulses did not change in the presence of P/Q channel blockers; in this cell the amplitude and decay of the ADP also were unaffected by P/Q channel blockers. All-simple-spiking cells were induced to fire spontaneous complex spikes along with slow V_m oscillations by both the SK and P/Q-type Ca^{2+} channel blockers. A difference in these cases between the block of these two channels was that the complex spike occurring after a hyperpolarized phase was prompt or just briefly delayed when SK channels were blocked, but only delayed when P/Q channels were blocked (Figs 8B, left traces vs. 9Ai or Supplemental Fig 3, B vs. C).

The shapes of Ca^{2+} spikes recorded in the presence of TTX were also affected by P/Q channel blockers (Fig 9E). ω-Agatoxin-TK changed the waveform of HTSs

without affecting the LTS; HTSs became broader with slowed repolarization and afterhyperpolarization (peak-to-trough time, 10.8 ± 2.6 vs. 15.9 ± 3.1 ms, n = 7, paired *t*-test, p = 0.005), and reduced peak-to-trough amplitude (15.1 ± 2.3 vs. 12.1 ± 2.5 mV, n = 7, paired *t*-test, p < 0.001). Compared with the effect of SK channel block on HTSs, P/Q block caused the peaks of HTSs to become less distinct or attenuated.

III. L-type

Block of L-type Ca^{2+} channels with the dihydropyridine, nifedipine, (2–10 μM; n = 14) did not cause notable changes in firing patterns of eight spontaneously spiking cells except for slightly depolarizing the base V_m. Six all-simple-spiking cells fired at higher (Δ 2–10 Hz) frequencies. The pFR and ADP of spikes evoked by short current pulses were unchanged by the presence of nifedipine (ΔpFR 0.3 ± 0.6 mV, n = 6; paired *t*-test, p = 0.26). However, in responses to longer depolarizing current pulses half (7 of 14) of the cells became devoid of the late complex spikes, leaving only an onset complex spike followed by a simple spike train (Fig 10A). In the other half of the cells, nifedipine slightly or moderately depressed the late complex spikes (Fig 10C, top 2 traces). Increasing the concentration of nifedipine (up to 20 μM) did not further attenuate the late complex spikes for these cells. In many cells treated with nifedipine, accommodation of fast spikes and development of a plateau depolarization occurred during responses to current steps of 0.5–0.7 nA, whereas in control solutions, currents in excess of 0.7 nA would be required for a comparable response. This plateau depolarization may result from inhibition of voltage-dependent K^+ channels, which has been reported for dihydropyridines including nifedipine (Fagni et al. 1994; Grissmer et al. 1994).

We then examined the effect of nifedipine on Ca^{2+} spikes in TTX (n = 19). As with the onset complex spike, the LTS was not affected by nifedipine. By contrast, HTSs were eliminated or largely depressed when evoked by current steps from a relatively hyperpolarized V_m (more negative than ~ –70 mV) in nifedipine (Fig 10Bi). However, at depolarized holding potentials, from which evoked HTSs are inherently more robust (Fig 4A), slower regenerative events ranging in appearance from distinct spikes to small (< 5 mV peak-to-peak) irregular oscillations could be seen in nifedipine across different cells. These nifedipine-resistant regenerative events or spikes were found to be abolished by 200 nM ω-agatoxin-TK when the drug was added along with nifedipine and TTX to cells that showed relatively distinct events (peak-to-peak amplitude > 5 mV) (n = 6; Fig 10Bii). We then examined how P/Q blockers affect nifedipine-resistant late complex spikes. One all-simple-spiking cell and one silent cell (Fig 10C), both of which showed late complex spikes in responses to injection of depolarizing current pulses in nifedipine, developed spike clusters during spontaneous and evoked activity, respectively, when ω-agatoxin-TK (100–200 nM) was added, as often seen with P/Q blockers applied alone (Fig 9A). The spike clusters in these cases, however, often included a plateau depolarization that sometimes required hyperpolarizing current injection to reinstate spike activity (Fig 10C, bottom 2 traces). For these two cells, TTX was added subsequently and absence of regenerative events was confirmed. In these cells and five other cells for which P/Q blockers were applied first followed by addition of nifedipine, late complex spikes could no longer be seen in response to current steps, replaced with plateau depolarizations. Thus, these data indicate that both P/Q- and L-type channels may be required for late complex spikes during a long depolarizing stimulus.

IV. Role of Low-voltage activated Ca^{2+} channels in generation of complex spikes.

Several lines of evidence suggesting the presence of a low-threshold inactivating conductance and its contribution to complex spiking in CWCs have been presented in this study so far: 1) The LTS, a presumptive T-type Ca^{2+} spike, could be observed in the presence of TTX in many CWCs. 2) The onset complex spike evoked by step depolarizations depended on a previous hyperpolarized V_m (more negative to ~ –65 mV). And 3) In the context of the spontaneous slow V_m oscillation, complex spikes were more frequently observed after hyperpolarized periods. Another line of evidence in the same context was found when the amplitude of a clearly distinguishable LTS was compared retrospectively between complex-spiking and all-simple-spiking cells. The maximum peak-to-trough amplitude was significantly larger in the complex-spiking cells than in all-simple-spiking cells (12.8 ± 5.2 (n = 22) vs. 8.4 ± 3.3 mV (n =41), $p < 0.001$). Mibefradil has been shown to block T-type and some forms of R-type Ca^{2+} channel more effectively than other Ca^{2+} channel subtypes (Martin et al. 2000; Bezprozvanny and Tsien 1995). Mibefradil, in the presence of TTX, reduced the maximum peak-to-trough amplitude of LTSs (protocol as in Fig 4B) by 76, 82 and 53% for three cells (at 10, 3 and 3 μM respectively) without an apparent change in the shape of HTSs (Fig 11C). Spontaneous or evoked spiking was monitored with 1.5–3 μM mibefradil to reduce mibefradil's effects on ion channels other than the Ca^{2+} channels (Bezprozvanny and Tsien 1995; Eller et al. 2000). We have observed that mibefradil caused small depolarization of V_m when used in the presence of TTX, and indeed increases in firing frequency were noted in six all-simple-spiking cells in mibefradil. In five complex spiking cells and two silent cells, all of which showed prompt complex spikes in their

spontaneous or induced activity in control conditions, the prompt spikes were lost in mibefradil (Fig 11A). Where prompt complex spikes preferentially occurred in the context of slow V_m oscillation in control conditions, delayed complex spikes or simple spikes became prominent. In three cells that also fired complex spikes in the middle of spiking phases of slow V_m oscillation, such complex spikes persisted but with longer trains of preceding simple spikes in mibefradil (Fig 11Aii and Supplemental Fig 4). Similarly, in responses to current pulses, late complex spikes did not appear different but the onset complex spikes were variably affected. Among 21 cells treated with mibefradil, 10 cells, including 5 of the 6 all-simple-spiking cells, stopped firing complex spikes at the onset of depolarizations.

T-type and/or R-type Ca^{2+} channels may contribute to the ADP in CWC. In some cells it was clear that ADPs were larger for simple spikes at the beginning of a spike cluster that terminated a period of hyperpolarization (Supplemental Fig 2). Spikes evoked by short pulses were inspected for changes in the pFR and ADP caused by mibefradil (3 μM), and the result is plotted in Fig. 11D for 14 cells. Nine cells fired only simple spikes, one cell fired both complex and simple spikes (Fig 11E), and four cells fired only complex spikes. In the 10 cells that had simple spike responses in control conditions, the peak potential of ADP became more negative by mibefradil (ΔADP peak 2.4 ± 3.3 mV, n = 10, paired *t*-test, p = 0.047). For the four cells that responded to short pulses with complex spikes, two failed to fire complex spikes in mibefradil, but the other two continued to generate three-spikelet complex spikes which had longer first interspikelet intervals than those of control complex spikes (from 3.0 to 3.9, from 2.2 to

2.9 ms, respectively). For pFR, a small but significant negative shift was observed in mibefradil (ΔpFR –1.1 ± 1.1 mV, n = 14, paired *t*-test, $p < 0.001$).

There was a confounding factor in the action of mibefradil on spike activity, aside from the V_m depolarization, which could be controlled with injection of a negative bias current. Mibefradil caused fast spike thresholds to increase by 1.4 ± 0.9 mV (at 1.5 μM, n = 4) or 2.9 ± 0.9 mV (at 3 μM, n = 8). A higher threshold for fast spikes would be expected to decrease the efficiency of generating a complex spike from a simple spike's ADP. We therefore applied TTX at 10 nM to block Na^+ channels partially so that fast spikes would persist with elevated thresholds. Spontaneous fast spikes became smaller in amplitude and their thresholds were raised by more than 10 mV in 10 nM TTX. Spikes evoked by short pulses in 10 nM TTX were smaller in amplitude and required larger currents than in control conditions (Fig 11F) but neither pFR nor the ADP peak level was changed significantly (ΔADP peak 0.2 ± 1.5 mV, n = 5, p = 0.74; ΔpFR 0.0 ± 0.6 mV, n = 6, p = 0.84; paired *t*-test for both). One of the cells that fired three-spikelet complex spikes on depolarization with short pulses in control conditions, fired complex spikes with two-spikelets in 10 nM TTX, with the interspikelet interval longer than the first interspikelet interval of control complex spikes (not shown). Under voltage-clamp, a reduction in the persistent inward current was observed with 10 nM TTX (n = 2, by 36 and 56 pA, which were 40 and 36% of the mean 500 nM-TTX-sensitive, persistent current). Thus, although mibefradil's depression of prompt or onset complex spikes can arise partly from an elevation of fast spike threshold, the lack of 10 nM TTX's effect on ADP of isolated spikes evoked from a hyperpolarized V_m suggests that mibefradil's primary action on complex spike suppression may be block of a low-voltage activated

Ca^{2+} current that contributes to the ADP. We suggest therefore that such channels facilitate complex spike generation after hyperpolarized periods by enhancing the ADP.

DISCUSSION

Ionic mechanisms underlying spike waveforms

Blocking all Ca^{2+} conductances in CWCs suppressed complex spikes while increasing excitability and weakening simple spike repolarization. Buffering of intracellular Ca^{2+} also markedly affected spike shape. We explored the basis of these effects by selectively blocking subtypes of Ca^{2+} channels and Ca^{2+}-dependent K^+ channels. Our results are summarized in Fig. 12. The repolarization of the fast Na^+ spike requires BK channels in addition to voltage-dependent K^+ channels. BK channels presumably contribute more toward the late part of the spike because BK block, as well as general block of Ca^{2+} channels, made pFR less negative and broadened the base of the spike. The source of Ca^{2+} for BK channels is probably mainly from R-type Ca^{2+} channels and in small part from the P/Q-type channels, because among the subtype-specific blockers we have used, only P/Q-type blockers reduced pFR. On the other hand, mibefradil, which blocks T-type and some forms of R-type channels, caused a small negative shift of pFR along with a decrease in ADP for spikes evoked from hyperpolarized V_m. This suggests that the low-voltage activated Ca^{2+} current, when available, provides depolarization at the end of a fast spike, which adds to the ADP. The ADP of a simple spike decays to the trough level between spikes; this can be viewed a second afterhyperpolarization (Manis et al. 1994; Zhang and Oertel 1993a). The SK channel may participate in this process, as block of this channel made the trajectory of

single evoked spikes' ADP less negative, and caused interspike intervals to progressively depolarize during a train of simple spikes. The major supply of Ca^{2+} for SK channels during interspike intervals at depolarized V_m is probably from the P/Q-type Ca^{2+} channel, as P/Q-type blockers caused similar depolarization of interspike intervals. For single spikes evoked from a hyperpolarized V_m, SK channel activation during ADP decay may occur by the Ca^{2+} influx through the T- or R-type channel (White et al. 1989; Metz et al. 2005).

Figure 12 shows a prompt onset spike and a late spike evoked from a hyperpolarized V_m by a current step. The LTS and HTS are thought to share their Ca^{2+} conductance with the onset and late complex spike, respectively, so the different susceptibility of these Ca^{2+} spikes were taken into account in deducing the conductance underlying different complex spikes. The onset complex spike, which is a low-threshold response, was delayed at just-suprathreshold current injection in many all-simple-spiking cells, and became prompt with larger current injection. The onset spike, whether delayed or not, was unaffected in the presence of N-, L- or P/Q-type Ca^{2+} channel blocker alone or L- and P/Q-type blockers together. However, mibefradil at concentrations exerting partial block of T- or R-type channels eliminated or attenuated the onset spike. Considering that the LTS is mediated by the T-type Ca^{2+} channel, given its resistance to Cd^{2+}, the T-type current may be essential in generating the onset complex spike. The T-type Ca^{2+} current was probably active at the end of a single spike evoked by a short pulse from a hyperpolarized V_m because mibefradil also attenuated the ADP. The transient subthreshold depolarization seen before the rise of a delayed onset spike (Fig 2Ai 80 pA trace) with a long depolarizing current pulse, may then be caused by directly evoked T-

type current or summated spike aftercurrent. It remains unclear whether T-type channels alone mediate the full spectrum of onset spikes, from delayed to prompt, or whether a higher-threshold Ca^{2+} current, the R-type, adds to the depolarization from T-type current to drive the steep upslope of the underlying envelope (the core motif). This distinction is further obscured as mibefradil has been reported to block the R-type current from expressed $Ca_v2.3$ channels or in cerebellar granule cells with a potency lower than or comparable to that for the T-type (Bezprozvanny and Tsien 1995; Jimenez et al. 2000; Randall and Tsien 1997). The observation that only a vestigial onset complex spike could be seen in Cd^{2+}, supports a role for R-type current.

For the late complex spike, L-type and P/Q-type Ca^{2+} currents together may provide the underlying depolarization, with a larger contribution from the L-type current. Blockade of L-type channels eliminated late complex spikes in half of the cases, and blocking the L- and P/Q-type channels together abolished all high-threshold regenerative events in TTX. It was not clear however whether, after blocking these channels in the absence of TTX, the late complex spike was suppressed or just prevented by an overwhelming plateau depolarization. If one was to view the disappearance of the HTSs as well as late complex spikes in L-plus-P/Q-blockers as mere depolarization block, the alternative interpretation could be that the L-type Ca^{2+} current's role was largely in providing the slow depolarizing course of V_m leading to the steep rise of the late complex spike or the HTS. In this view, the HTS could be mediated mainly by an R-type Ca^{2+} current with small contribution of L- and P/Q-type current; however, the R-type current in this role would have to be of higher-threshold than the L-type current and not affected by mibefradil. The SK channel is believed to contribute to the termination of the

underlying slow depolarization of complex spikes, as apamin broadened most complex spikes. The fact that block of the P/Q-type Ca^{2+} current caused similar broadening of complex spikes indicates that this current flows during complex spikes and activates the SK channel. The apparently unaffected duration of onset complex spikes during block of P/Q-type Ca^{2+} or SK channel may be due to the presence of a voltage-dependent K^{+} current activated at the onset of a current step.

This discussion has so far focused on evoked onset and late complex spikes with obvious low- and high-threshold characteristics. In spontaneous activity, prompt or short-delay complex spikes preceded by clear hyperpolarized periods were suppressed in mibefradil and thus are considered to share the same ionic mechanism with the onset spike. On the other hand, the equivalent of late complex spikes in spontaneous activity, delayed spikes that are preceded by longer than 100 ms of depolarized (V_{trough} less negative than –70 mV) activity, were rare, so we could not examine the effect of blockers on them. However, spontaneous delayed spikes of intermediate characteristics, with a hyperpolarization ending 50–100 ms before the complex spike (like some in Fig 11Aii control), were not uncommon, and when treated with mibefradil these complex spikes became less frequent. Two possible interpretations are that these intermediate delayed complex spikes are also mediated by T- or T- plus R-type Ca^{2+} current but were not completely blocked by low concentrations of mibefradil, or that spontaneous complex spikes are not only generated by either low- or high-threshold Ca^{2+} currents, but rather that the two types of Ca^{2+} current can cooperate to generate complex spikes.

Why do some CWC not show spontaneous complex spikes? The increased tendency for complex spiking was found with those blockers that, in single evoked spikes,

reduced fAHP (BK blocker) or increased ADP (SK blocker), whereas one that reduced ADP (T-type blocker) decreased complex spikes. These, along with the finding that spontaneously complex-spiking cells had less fAHP in their simple spikes than did all-simple-spiking cells, suggest that more depolarized ADPs facilitate the generation of complex spikes in CWCs, as suggested for other "bursting" neurons in different brain areas (Brumberg et al. 2000; Franceschetti et al. 1995; Jung et al. 2001; Metz et al. 2005; Nishimura et al. 2001; White et al. 1989; Wong and Prince 1981; Yue et al. 2005; Yue and Yaari 2004). Different balances of spike aftercurrents that regulate ADP size, BK and SK versus T/R-type Ca^{2+} current, across different CWCs can be one reason for the variable propensity for complex spiking. Another factor can be the difference in the ability to fire with slow V_m oscillation, the mechanism of which may involve an interaction of subthreshold conductances (Del Negro et al. 2002; Williams et al. 1997; Wilson 2005). Almost all complex-spiking cells we have observed showed intermittent hyperpolarizations after which a complex spike was often recognized. Similar to CWCs in this relationship of slow V_m oscillation and low-threshold complex spike are the thalamocortical neurons and thalamic reticular neurons, although in these neurons the T-type Ca^{2+} spike is the primary event that sustain the bursts (Crunelli et al. 2005; McCormick and Bal 1997). Still other possibilities include a difference in dendritic membrane contributions, such arises from variation in the size or number of dendrites (Chagnac-Amitai et al. 1990; Mainen and Sejnowski 1996; Mason and Larkman 1990), provided that dendritic electrogenesis contributes to complex spike generation. In neocortical and hippocampal pyramidal cells, simultaneous dendritic and somatic recordings, as well as computer models, have shown that dendritic depolarization by

electrotonically or actively propagated somatic action potential contributes to the somatic ADP, which can trigger a burst when boosted by a more depolarizing event in the dendrite, such as a Ca^{2+} spike and/or excitatory postsynaptic potential (Golding et al. 1999; Larkum et al. 1999; Mainen and Sejnowski 1996; Traub et al. 1991; Williams and Stuart 1999).

Persistent Na^+ current and its contribution to firing

A persistent Na^+ current was apparent in CWC as a TTX-sensitive, negative slope conductance in steady-state I-V plots. This current was manifest in current-clamp mode as a depolarizing trend in V_m starting at around –75 mV. The occasional non-decaying subthreshold responses from which a fast spike would arise (e.g., Fig 11F, control trace) and additional firing of fast spikes during decay of a depolarized ADP (Fig 5C) may reflect the V_m being amplified to a critical range by persistent Na^+ current (Hirsch and Oertel 1988). Thus, it is expected that without persistent Na^+ current, the rheobase for silent cells would be larger, and conversely, spiking cells would require less hyperpolarizing current to be quieted. The persistent Na^+ current may contribute to ongoing spike discharge by providing a depolarizing ramp before the fast upstroke of each spike (Fig 12). Indeed it has been shown in a variety of neurons that TTX-sensitive currents flow during interspike intervals in studies employing action potential waveforms as voltage commands (Do and Bean 2003; Raman and Bean 1999; Taddese and Bean 2002). Taddese and Bean (2002) have suggested that the persistent Na^+ current is generated from the same Na^+ channel responsible for the transient Na^+ current and so that all neurons that fire Na^+ spikes have the "intrinsic drive" to repetitive discharge, resulting

in spontaneous firing as long as the current is not counteracted by a resting K^+ conductance. For CWCs, the presence of subthreshold conductances active below the threshold of the persistent Na^+ current is suggested by variation in our I-V plots: although the persistent Na^+ current showed a similar activation range across cells, silent cells had their I-V curve shifted up, whereas in spiking cells, it was shifted down. The inward rectifier K^+ current and hyperpolarization-activated cation current (I_h) are present in CWCs, and inhibition of each led to depolarization or hyperpolarization of the V_m, respectively (Kim and Trussell, unpublished observations). The balance of these conductances along with any leak conductance may be important in determining the level of activity for CWCs.

Comparison with the Purkinje cell

It is of interest to compare the ionic mechanism of complex spiking in CWC with that of cerebellar Purkinje cells, as these are often considered to be molecularly and functionally related cell types (Berrebi et al. 1990; Berrebi and Mugnaini 1991; Mugnaini and Morgan 1987). We identified a number of differences on comparing Purkinje cell spikes from the literature or recorded by us with those of CWCs. For example, simple spikes of Purkinje cell are narrower in half-width (~ 0.25 vs. 0.4 ms of CWCs), repolarize faster, and do not show an ADP comparable to that of CWCs (Kim and Trussell, unpublished observations; Manis et al. 1994). The fast repolarization of the Purkinje cell simple spike, attributable to the expression of Kv3 channels, enables tonic high-frequency (> 40 Hz) firing (Akemann and Knopfel 2006; Martina et al. 2003; McKay and Turner 2004), which CWCs cannot reliably do without giving rise to late complex spikes.

The inability of CWC to emit long periods of regular activity suggests a different role in information processing when compared with Purkinje cells. With strong current injection, or even spontaneously in some cells, Purkinje cells discharge mixed bursts of Na^+ and Ca^{2+} spikes ("Ca^{2+}-Na^+ burst"), similar to the generation of late complex spikes in CWCs; moreover, both cells produce Ca^{2+} spikes in TTX that occur in similar patterns to their respective burst events, the Ca^{2+}-Na^+ burst or late complex spikes (Llinas and Sugimori 1980; Womack and Khodakhah 2002; McKay and Turner 2004). However, Ca^{2+} spikes of Purkinje cells are mediated by the P-type channel, and unlike in CWCs, the low-threshold Ca^{2+} spike has been rarely seen in somatic recordings except in immature cells and in cultured cells (Cavelier and Bossu 2003; Llinas et al. 1989; McKay and Turner 2005; Watanabe et al. 1998) even though the T-type current could be isolated at the soma (Isope and Murphy 2005; McDonough and Bean 1998). The fast rising CWC complex spike (the prompt spike) and Purkinje cell complex spike seem comparable at first glance. One notable difference was that, with Purkinje cells, the second spikelet, arising from a depolarized level, was often the smallest in the entire waveform (Khaliq and Raman 2005). By contrast, in CWC spikes, the last (i.e., the 3rd or 4th) spikelet was the shortest; in this respect, the CWC complex spikes may appear more like those of hippocampal or neocortical pyramidal cells (Manis et al. 1994; Khaliq and Raman 2005). The shape of the underlying depolarization is likely to be responsible for this difference: a fast rising synaptic potential in Purkinje cells versus a more gradual depolarization triggered from the ADP of the first spikelet in CWCs. This difference may bear on the frequency of information transferred to the axon. Indeed, the propagation of complex spikes down the axon has been reported to be correlated with the spikelet amplitude with

the shortest one propagating least well (Khaliq and Raman 2005; Monsivais et al. 2005). Thus, it is expected that the initial two to three spikelets of a CWC complex spike would be more reliably transmitted than those of Purkinje cell complex spikes down the axon; these would appear as the multi-peaked high-frequency postsynaptic potentials that are seen in target cells of CWCs (Golding and Oertel 1997; Tzounopoulos et al. 2004). Therefore, although the CWC and Purkinje cell, share many molecular markers and similar electrophysiological hallmarks, they may utilize a different balance of ion channels, and this difference could bear on the meaning of their spike output.

- -

Table 1. Simple spike threshold, pFR and the difference between them (mean ± SD).

	n	Threshold (mV)	pFR (mV)	Threshold – pFR (mV)
Complex-spiking cells	52	–60.0 ± 3.8	–65.9 ± 3.3	5.9 ± 2.8
All-simple-spiking cells	135	–60.1 ± 3.2	–68.9 ± 3.7 *	8.8 ± 2.8 *
Total	187	–60.1 ± 3.4	–68.0 ± 3.8	8.0 ± 3.1

*, $p<0.001$

Figure 1. Basic properties of CWC spikes and spontaneous spike patterns.

A, examples of spontaneous activity with complex spikes from two different cells: one with frequent prompt complex spikes, *i*, and the other with delayed complex spikes, *ii*. Complex spikes are marked with *asterisks*. On the right of *i* and *ii* are complex spikes on expanded time base: 3rd (*a*) and 5th (*b*) complex spike for *i*, and 1st (*c*) and 3rd (*d*) one for *ii*. The threshold (*arrow*), pFR (the end point of repolarization, *arrowhead*), and the ADP (afterdepolarization, *dot*) are indicated for two fast spikes in *d*. **B**, an example of extracellularly recorded complex-spiking activity with expanded views below. Empty circles indicate prompt complex spikes, and filled circles, delayed complex spikes. **C**, spontaneous variation in spikelet number showed that complex spikes repolarize more deeply when there were more spikelets. Overlaid pairs are from three different cells. **D**, examples of spikes triggered with a short pulse protocol. Four traces are superimposed. *i*, random triggering of either a complex spike or a simple spike with a large ADP. *ii*, an extreme example with a minimal ADP associated with a slow afterhyperpolarization. The lower-most gray trace in *i* and the gray trace in *ii* are passive responses. Bias current: −55 pA for *i*, −35 pA for *ii*. **E***i*, an example of spontaneous activity with only simple spikes. Dashed line indicates the level of interspike trough potential, V_{trough}. **E***ii*, the same cell as in D*i* revealed complex spikes on depolarizing current injection.

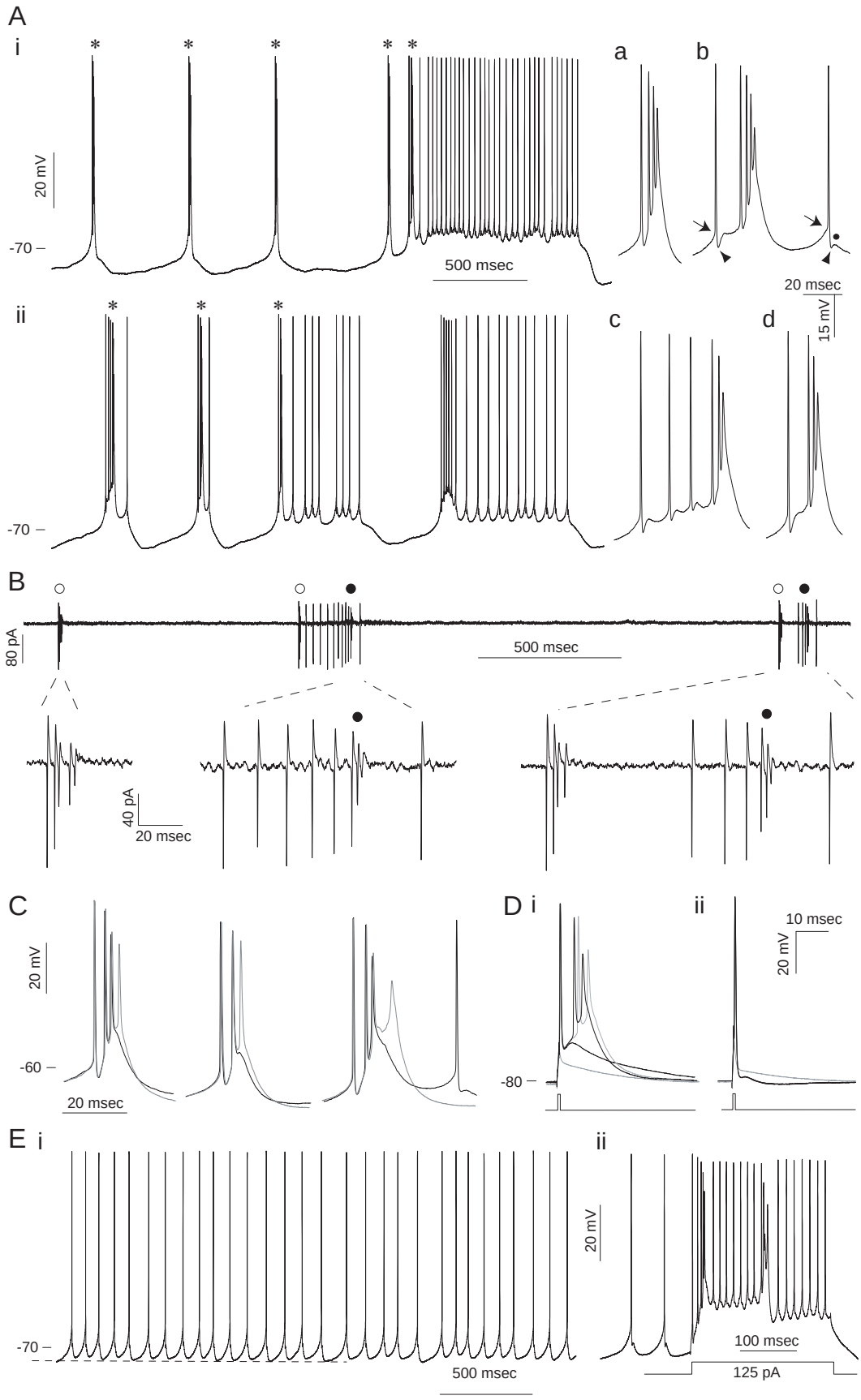
A
i
a
b
20 mV
-70
500 msec
20 msec
ii
c
d
15 mV
-70
B
80 pA
500 msec
40 pA
20 msec
C
20 mV
-60
20 msec
D i
ii
10 msec
20 mV
-80
E i
ii
20 mV
-70
500 msec
100 msec
125 pA

Figure 1

Figure 2. Complex spikes evoked with depolarizing current steps.

A*i*, typically as larger currents were injected, the sequence of responses was all simple spikes, an onset complex spike followed by simple spikes, and onset and one or more late spikes. **A***ii*, a spontaneously complex-spiking cell initially responded with a series of complex spikes, then followed the typical pattern as in A*i*. –55 pA bias current was present for A*ii*. **B*i***, the onset spike became delayed and disappeared as the pre-step V_m depolarized. A different cell from those in A*i*. **B***ii*, a plot showing the presence/absence of an onset complex spike versus the V_m during the conditioning current step in **B*i*** for 15 cells.

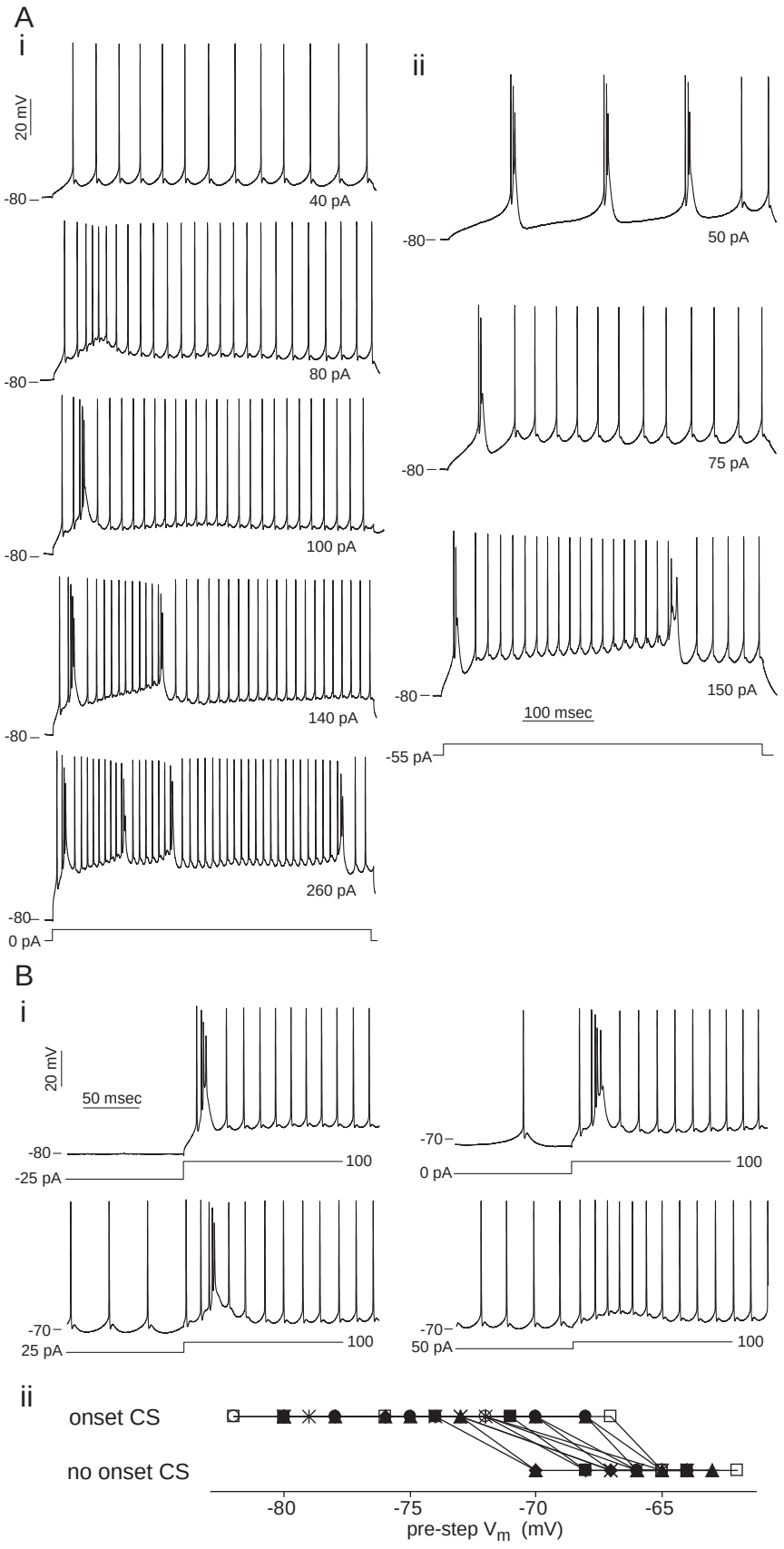
A
i
20 mV
-80
40 pA
80 pA
100 pA
140 pA
260 pA
0 pA
ii
50 pA
75 pA
150 pA
100 msec
-55 pA
B
i
20 mV
50 msec
-80
-25 pA
100
-70
0 pA
25 pA
50 pA
ii
onset CS
no onset CS
-80
-75
-70
-65
pre-step V_m (mV)

Figure 2

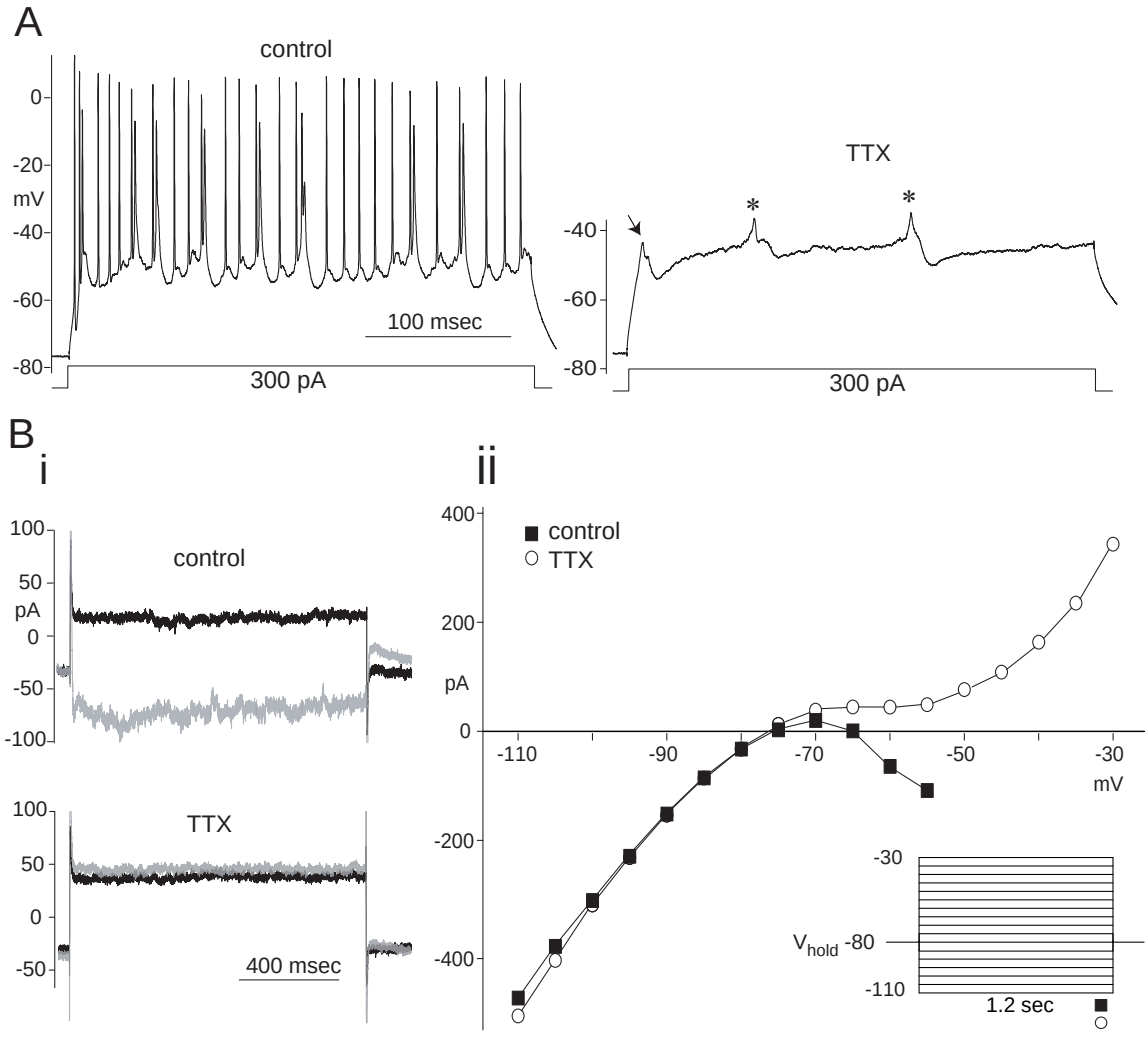

Figure 3. Effect of voltage-sensitive Na^+ channel block.
A, loss of fast spikes and appearance of slow spikes in TTX (0.5 μM). Arrow, the onset slow spike, asterisks, late slow spikes. B, persistent TTX-sensitive conductance shown in voltage-clamp mode from another cell. i, responses to steps to -70 mV (black) and -60 mV (gray) from a holding potential of -80 mV in control and in TTX. ii, steady state IV plot of the same cell. Note the TTX-sensitive negative slope conductance region. Inset, protocol used for i and ii. Synaptic blockers were not present in A.

Figure 4. Characteristics of slow spikes in TTX, 0.5 μM.

A, the responses to depolarizing current steps at two different base V_m: ~ –80 mV, A*i*, and ~ –60 mV, A*ii*. **A***i*, an onset slow spike appeared alone first, *bottom*, and then more spikes followed with larger depolarizing steps, *middle* and *top*. **A***ii*, when current steps were given from a depolarized V_m (with + 50 pA bias current) in the same cell, the onset spike was lost, but the late slow spikes rose more frequently and were larger in amplitude compared to those evoked from a hyperpolarized V_m, A*i*. **A***iii*, a plot summarizing the frequency of evoked late slow spikes ("HTSs"; by a 325-ms 400 pA or 600 pA injection) for six cells held at two different ranges of V_m (– 75 ~ –80 mV, *white*, – 60 ~ –64 mV, *black*). Error bar, one standard deviation. The difference in number of HTSs between 400 pA and 600 pA at each holding potential was significant (both, $p < 0.05$, paired *t*-test), as well as the difference between two holding potentials at each injected current (both, $p < 0.005$, paired *t*-test). **B***i*, inactivation of the onset slow spike ("LTS") with depolarization of pre-step (conditioning) V_m in a different cell. The *left*, *middle*, and *top right* traces are the response to a current injection protocol shown *right bottom*. B*ii*, a plot of normalized peak-to-trough amplitude of the LTS (evoked with the protocol in B*i*) vs. pre-step V_m for nine cells.

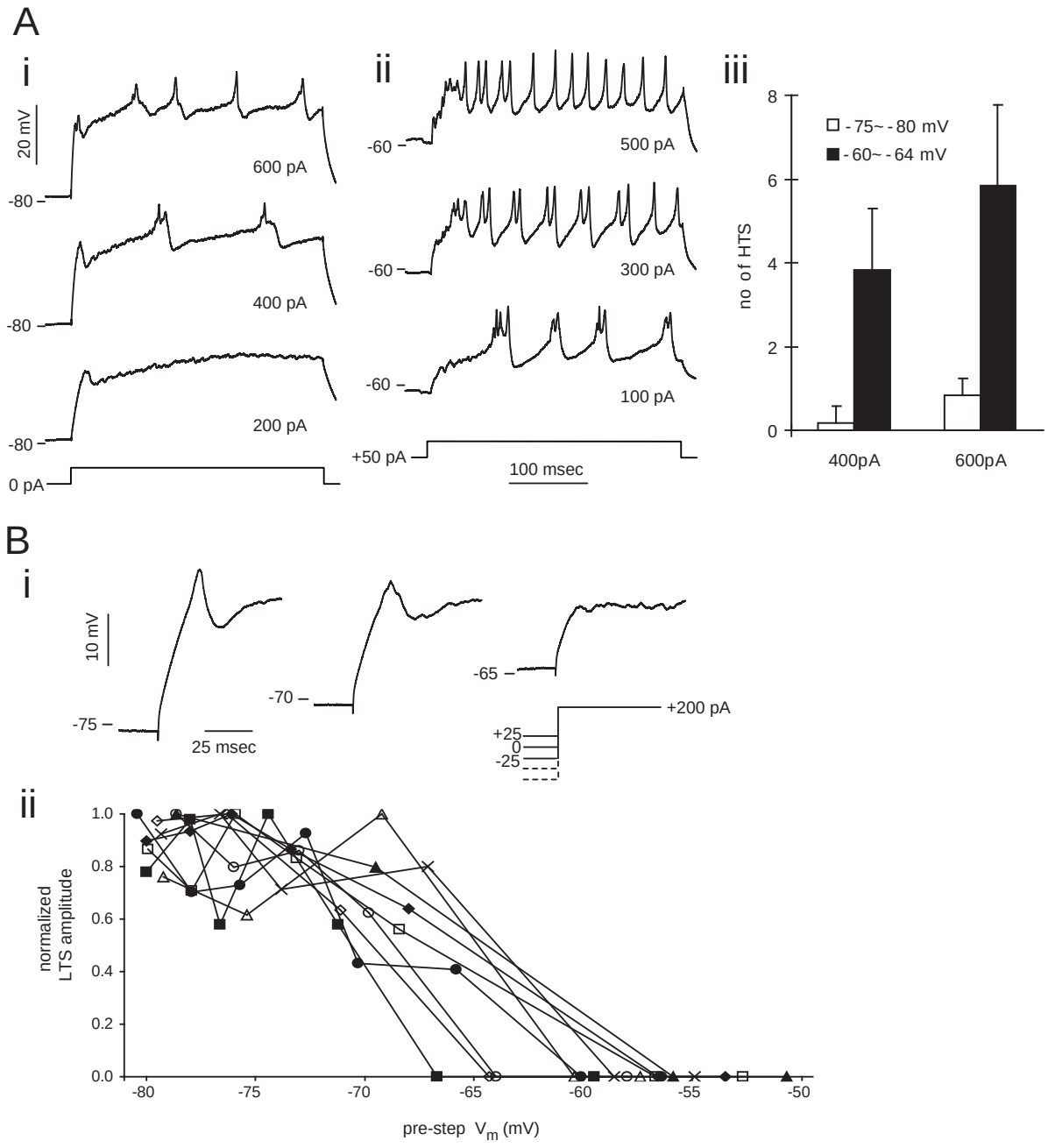
A
i
20 mV
600 pA
-80
400 pA
-80
200 pA
-80
0 pA
ii
-60
500 pA
-60
300 pA
-60
100 pA
+50 pA
100 msec
iii
- 75~ - 80 mV
- 60~ - 64 mV
no of HTS
8
6
4
2
0
400pA
600pA
B
i
10 mV
-75
25 msec
-70
-65
+200 pA
+25
0
-25
ii
normalized LTS amplitude
1.0
0.8
0.6
0.4
0.2
0.0
-80
-75
-70
-65
-60
-55
-50
pre-step V_m (mV)

Figure 4

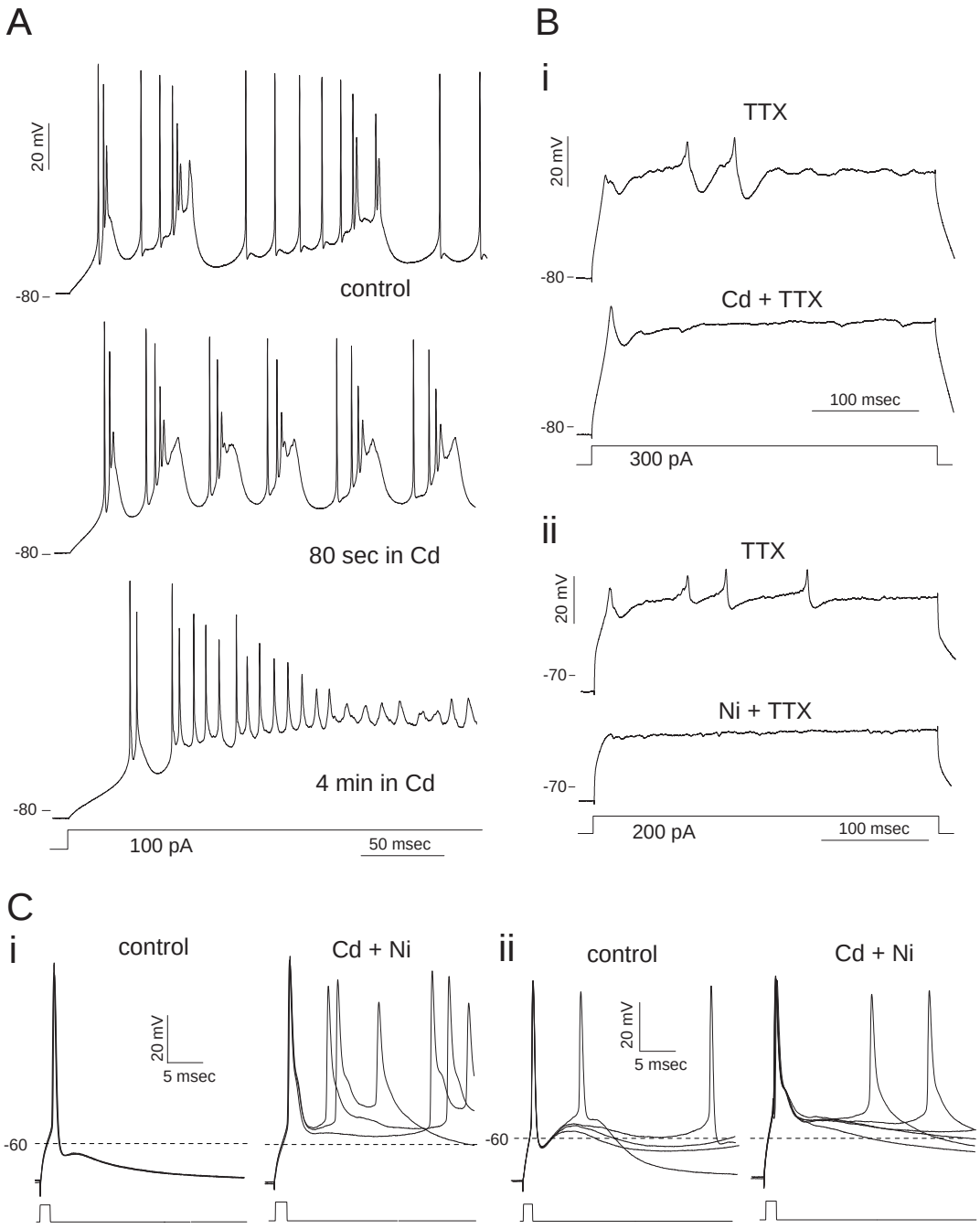

Figure 5. Effect of general Ca^{2+} channel block.
A, complex spikes evoked with depolarizing current injection transiently became enhanced during wash-in of 200 μM Cd^{2+} (middle). Eventually only an attenuated form of complex spike could be seen at the onset (bottom). B, the slow spikes in TTX, 0.5 μM, were Ca^{2+} spikes. i, 200 μM Cd^{2+} blocked only the HTS. ii, in a different cell, 500 μM Ni^{2+} suppressed both the LTS and the HTS. A -90 pA bias current was maintained for the bottom trace with Ni^{2+}. C, changes in the waveform of fast spikes evoked with brief pulses. Shown are superimposed traces from two different cells, i and ii, in control and in 100 μM Cd^{2+} plus 500 μM Ni^{2+}.

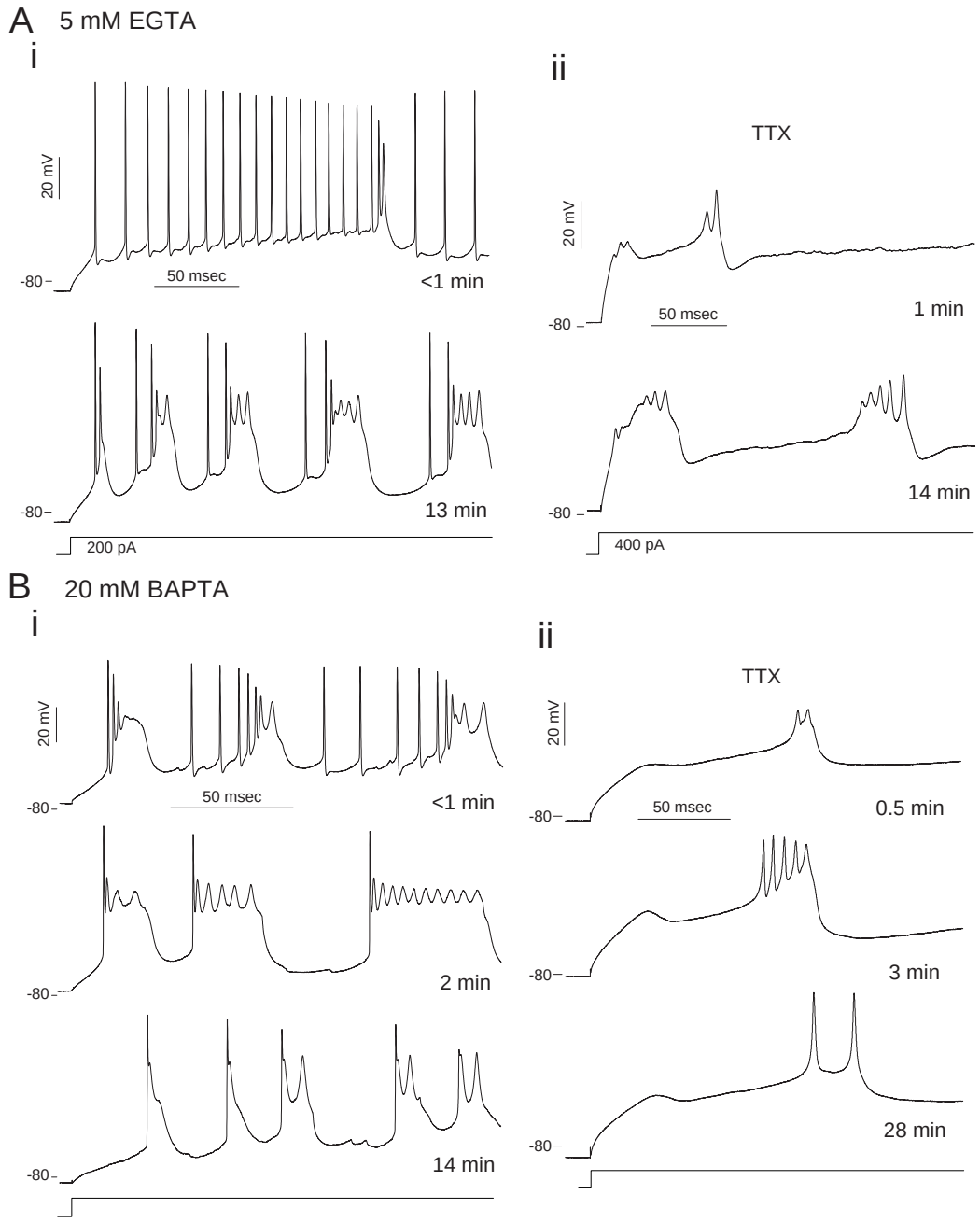

Figure 6. Effect of intracellular Ca2+ buffering examined with whole-cell recording. A, 5 mM EGTA and B, 20 mM BAPTA in pipette solution. Ai and Bi, changes in the complex spike waveform with time from the moment of break-in. Aii and Bii, in different cells, the Ca^{2+} spike (in 0.5 μM TTX) also changed shape with time. Current injected, 175, 200, 300 pA for Bi and 300, 300, 500 pA for Bii in top to bottom order. Synaptic blockers were not present in Bi.

Figure 7. Effect of BK channel block with iberiotoxin (ibtx), 100 nM.

A*i*, increased frequency of complex spikes during spontaneous activity in iberiotoxin compared to the control condition. Inset, depolarized pFR (*arrow*) and shorter interspikelet intervals of complex spikes in ibtx (*red*) were shown by superimposing indicated spikes on the left. **A***ii*, an extracellular recording of a complex-spiking cell. Two prompt complex spikes along with simple spikes are shown in the control trace, while in ibtx all spikes are complex spikes. Inset, indicated complex spikes shown in expanded scales to reveal a decrease in the first interspikelet interval by ibtx. **A***iii*, less negative pFR and facilitation of complex spiking by ibtx shown in current step responses. Note change from a delayed complex spike to two prompt spikes at onset. **B**, Using short stimulus pulses, complex spikes were triggered in ibtx in a cell for which only simple spikes were seen in control solution. Three traces are superimposed for each condition. 50 pA bias current in both conditions. **C**, ibtx enlarged the amplitudes of both the LTS and HTSs in TTX, 0.5 μM. Traces in A, B, and C are from five different cells.

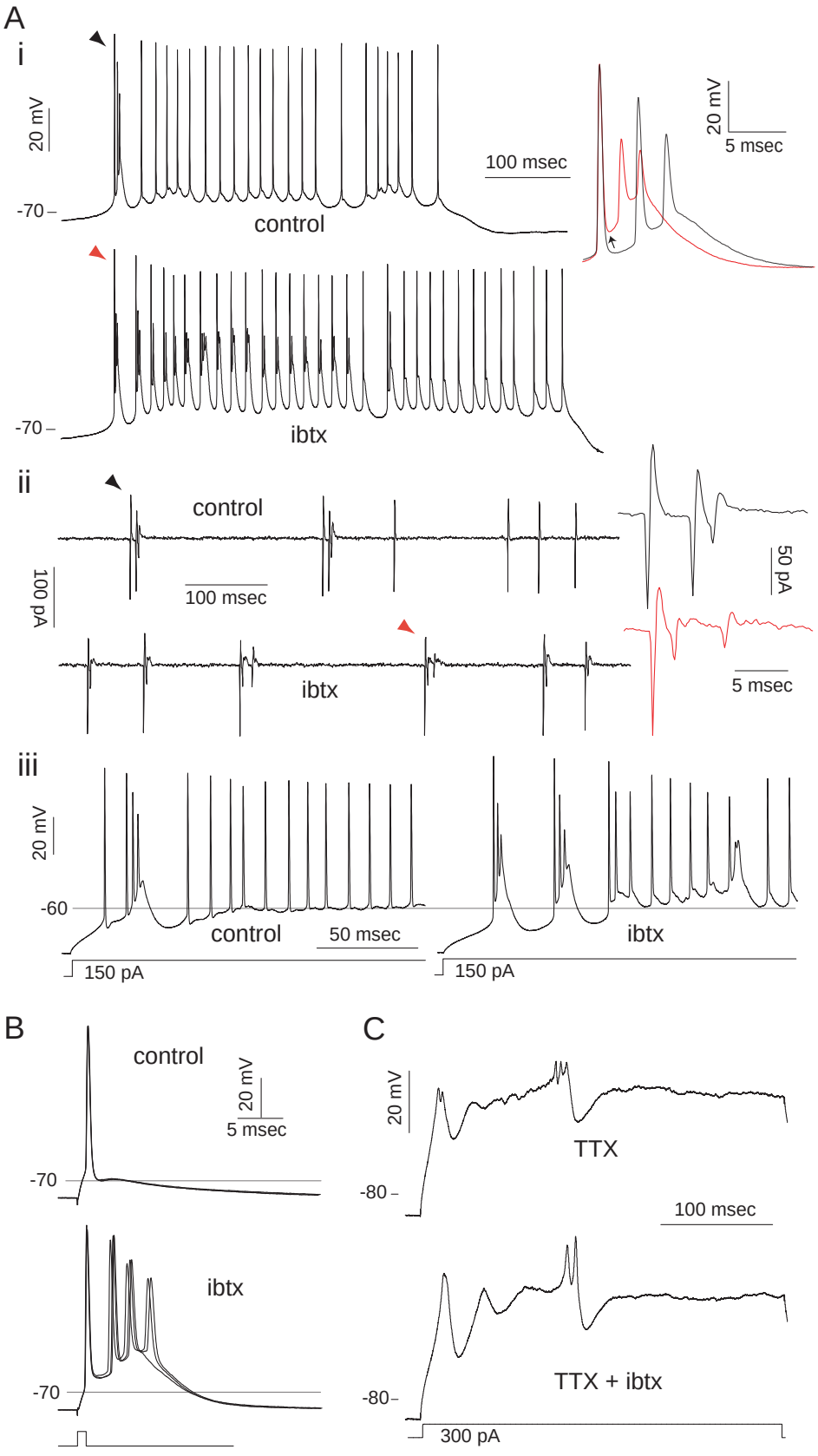
A
i
20 mV
-70
control
100 msec
20 mV
5 msec
-70
ibtx
ii
control
100 pA
100 msec
50 pA
ibtx
5 msec
iii
20 mV
-60
control
50 msec
150 pA
ibtx
150 pA
B
control
20 mV
5 msec
-70
ibtx
-70
C
20 mV
TTX
-80
100 msec
TTX + ibtx
-80
300 pA

Figure 7

Figure 8. Effect of SK channel block.

A, spontaneous activity converted to clusters of complex spikes by100 nM apamin (apm). **B**, responses to step current injections. Stable train of simple spikes could no longer be seen in apm, 50 nM, and broad complex spikes in series occurred. −80 pA bias current for both. **C**, plots of n^{th} interspikelet interval versus its duration for complex spikes that are preceded by > 150 ms of silent period: *i*, the same cell as in A, *ii*, an extracellularly recorded cell. Number of plotted complex spikes: 18, 25, 73 and 92 from left to right. Note the decrease in the duration and variability of the first interval in apm in both cells. In *ii*, an example of extracellular spikes is shown for each condition. The control complex spikes in *ii* can be seen to consist of two groups of delayed complex spikes, one starting with one simple spike ('short-delay') and the other with two simple spikes. **D,** overlaid complex or simple spikes in control (black) and apm (red). **D***i*, complex spikes indicated by arrowheads in A. Note the complex spike in apm is longer in duration but repolarizes less than the one in control conditions. This was also observed in short pulse-evoked complex spikes from a different cell, **D***ii*. Bias, –10 pA in both conditions. **D***iii*, an example of a cell that converted, on short pulses, from a simple spike-responder to a complex spike-responder by apm. Bias, –105 pA in both conditions. **D***iv*, enhanced ADP for short pulse-evoked simple spikes by apm. Each superimposed trace is truncated averaged waveform from one representative cell. Bias: −95 (control), −85 pA (apm). **D***v*, a plot showing depolarizing shifts in the V_m at 10 ms from the peak of the evoked spike (*vertical dashed line* in D*iv*) in 9 cells. **E**, changes in HTSs in TTX, 0.5 μM, by apm, 100 nM, shown for two different cells, *i* and *ii*. HTSs were broadened with more peaks (*) and slower repolarization (*arrows*). The cell on the right had a pre-step V_m of –75 mV.

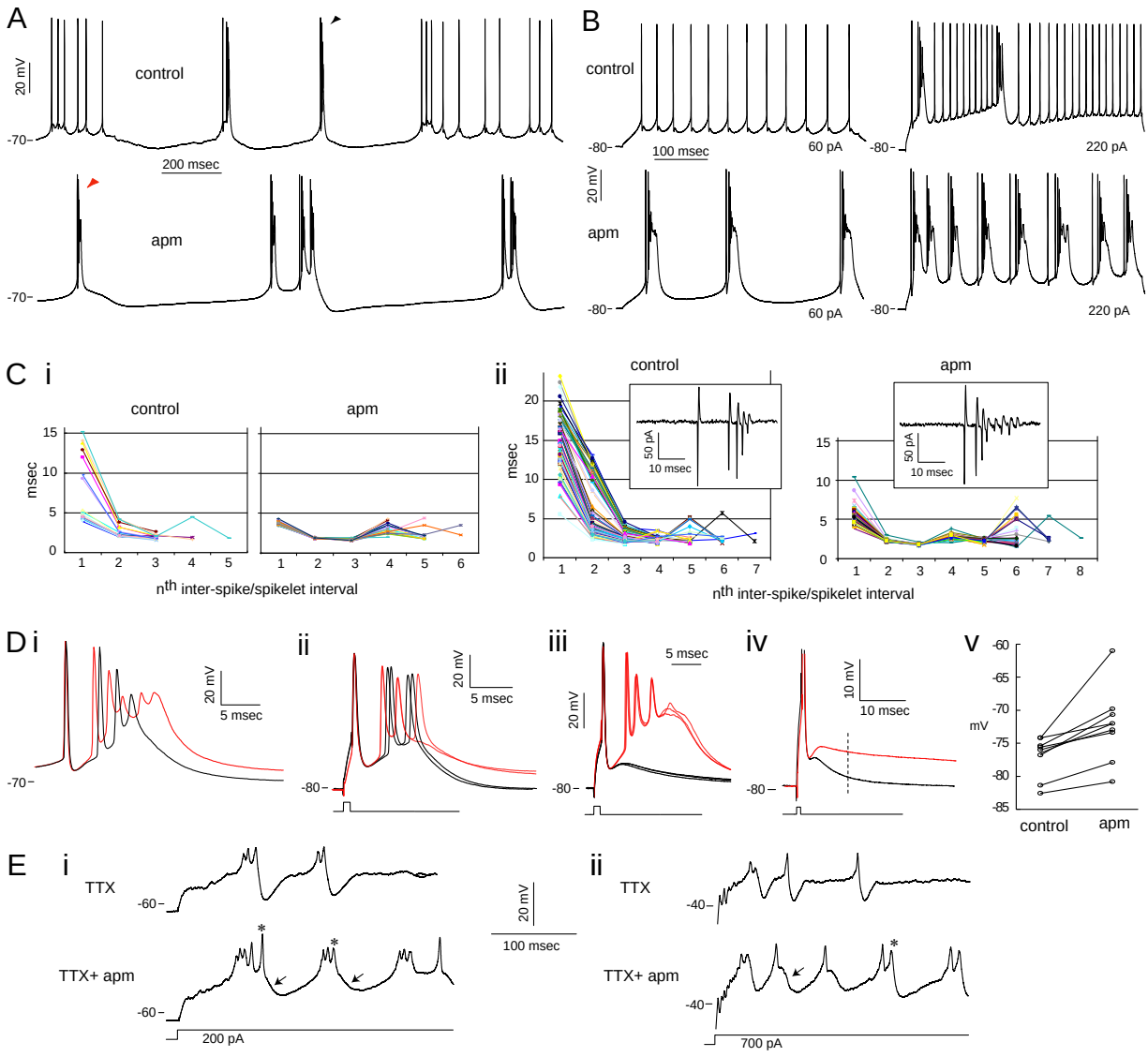
A
control
20 mV
-70
200 msec
apm
-70
B
control
-80
100 msec
60 pA
-80
220 pA
20 mV
apm
-80
60 pA
-80
220 pA
C i
control
apm
msec
nth inter-spike/spikelet interval
ii
control
apm
50 pA
10 msec
msec
nth inter-spike/spikelet interval
D i
20 mV
5 msec
-70
ii
20 mV
5 msec
-80
iii
5 msec
20 mV
-80
iv
10 mV
10 msec
-80
v
mV
control
apm
E i
TTX
-60
TTX+ apm
-60
200 pA
20 mV
100 msec
ii
TTX
-40
TTX+ apm
-40
700 pA

Figure 8

Figure 9. Effect of P/Q-type Ca^{2+} channel block with ω-agatoxin-TK (agtx). **A**, change in spontaneous activity induced with agtx, 100 nM. A*i*, an all-simple-spiking cell developed clusters of simple and complex spikes. A*ii*, a complex-spiking cell fired more complex spikes with more spikelets. Fast spikes are larger in amplitude in the agtx trace because of greater perforation by gramicidin with time. *Insets*, expansion of spikes under asterisks. Calibration, 10 mV and 10 ms. **B**, plots of interspikelet interval versus its duration for complex spikes preceded by > 150 ms of silent period. Two extracellularly recorded cells, *i* and *ii*. Number of plotted complex spikes: 61 for both conditions, *i*, and 41, 50 for control and agtx, *ii*. The number of spikelets and the duration of complex spikes increased in agtx for each cell. An example of spike waveform in control and agtx is shown for *ii*. Calibration, 50 pA and 10 ms. **C**, increase in excitability in the presence of agtx, 100 nM, as shown by increased tendency to fire complex spikes and more depolarized base V_m during a 100 pA step. Note the broader late complex spikes in agtx. A different cell from those in *panel A*. Bias currents were 23(control) and 34 pA (agtx). **D**, small depolarizing shifts of pFR in agtx, 100 nM, as observed from short pulse-evoked spikes. Three superimposed traces of truncated spikes are shown for each condition for two different cells, *i* and *ii*. Bias currents: –25, –20, 23, 23 pA from left to right. **E**, superimposed Ca^{2+} spikes in 0.5 μM TTX (*black*) and in TTX plus 200 nM agtx (*red*) from three different cells. agtx caused the HTS to become broader with reduced afterhyperpolarization and less distinct peaks. The LTS (*asterisks*), was not affected. Spikes were evoked with a 400 pA (left, middle) or 500 pA (right) current steps and the pre-step V_m was –65, –71 and –74 mV from left to right.

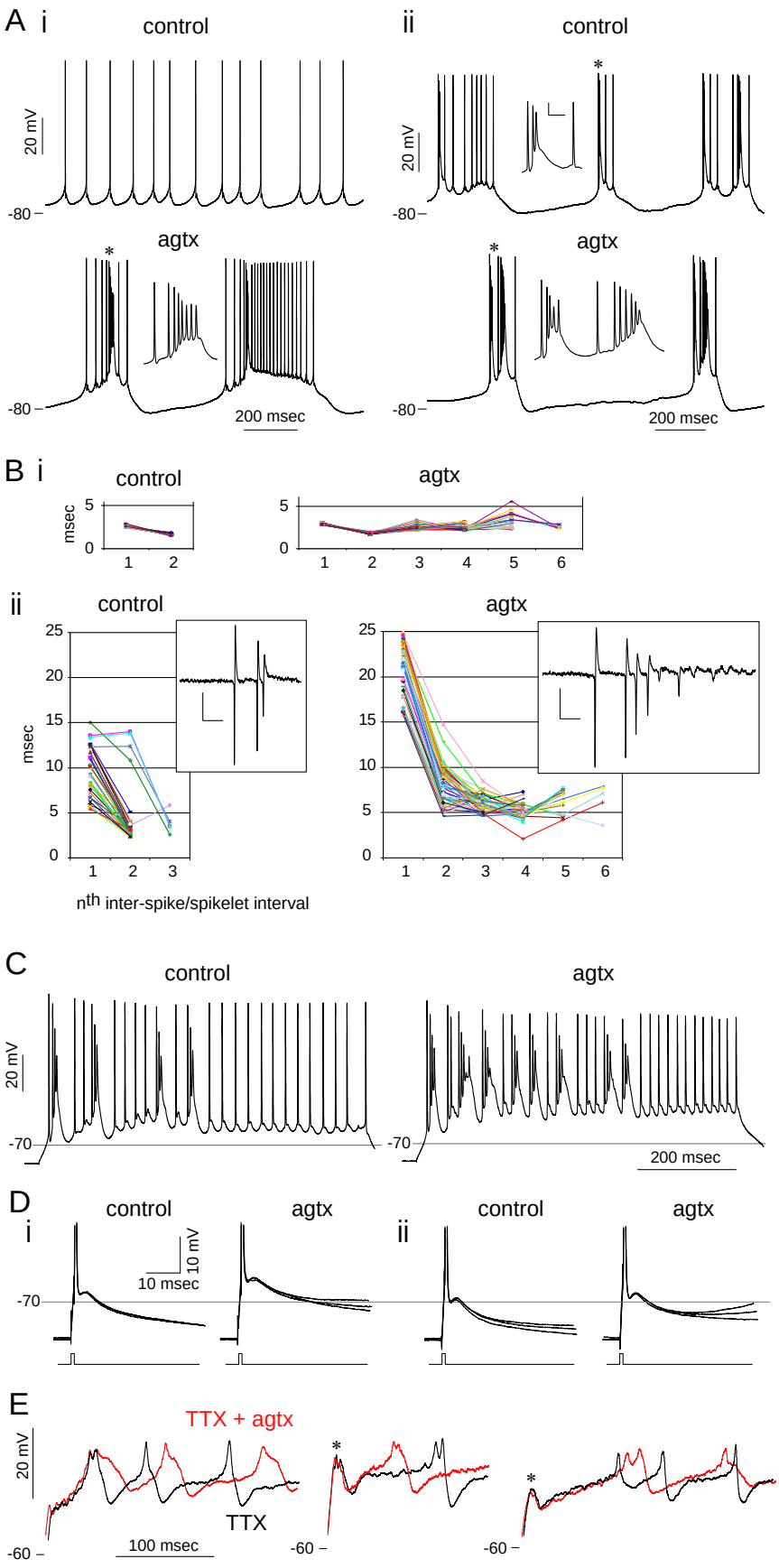
A i
control
20 mV
-80
agtx
200 msec
ii
control
agtx
B i
control
agtx
msec
ii
control
agtx
msec
nth inter-spike/spikelet interval
C
control
agtx
20 mV
-70
200 msec
D
i
control
agtx
10 mV
10 msec
-70
ii
control
agtx
E
TTX + agtx
TTX
20 mV
100 msec
-60

Figure 9

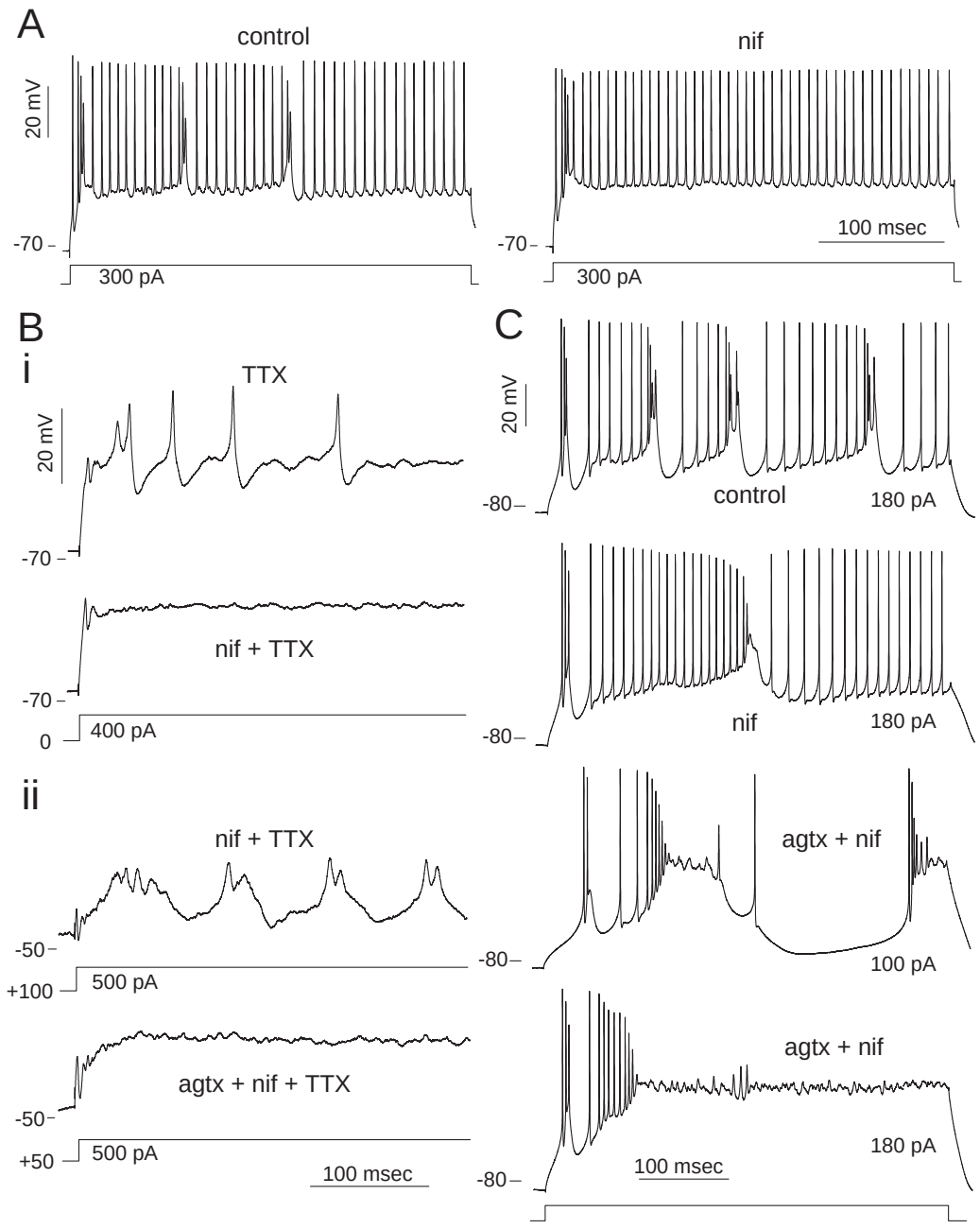

Figure 10. Effect of L-type Ca2+ channel block.
A, an example of late complex spike suppression by nifedipine (nif), 2 μM. B, In TTX, 0.5 μM, HTSs evoked by depolarization from resting potential were eliminated by 10 μM nif. Bii, in the same cell, current step from a depolarized holding potential revealed nif-resistant spikes, which were abolished after subsequent addition of ω-agatoxin-TK (agtx), 200 nM. C, addition of agtx, 200 nM, in addition to nif, 5 μM, (bottom two) made nif-resistant late complex spikes (second from top) disappear instead caused broad plateau depolarizations. Bias currents: 0, -25, -40, -40 pA from top to bottom. A, B and C represent three different cells. Synaptic blockers were not present in A.

Figure 11. Effect of T-type Ca^{2+} channel block with mibefradil (mib).

A, prompt complex spikes (*asterisk*) disappeared in 1.5 μM mib. *i*, a spontaneously complex-spiking cell, *ii*, a silent cell spiking by sustained +100 pA injection. Note in *ii* that short-delay complex spikes (*rectangle*) are also lost. **B**, attenuation of the onset complex spike with slowed rising phase and intact late complex spikes in mib, 3 μM. Bias currents: –45 (control) and –50 pA (mib). **C**, the LTS, asterisk, in 0.5 μM TTX, was inhibited selectively by mib, 3 μM. **D**, changes in the V_m at the peak of ADP (ADP peak) and pFR of short pulse-evoked spikes in mib. *Red symbols*, cells that showed complex spike responses in control condition. **E**, cell 4 in D that had a large ADP and occasionally fired complex spikes with short pulses became unable to do so after its ADP had become smaller in mib, 3 μM. Four traces are overlaid for each condition. –15 pA bias currents for traces in mib. **F**, for comparison, an example of effect of 10 nM TTX on short pulse-evoked spikes is shown. 10 nM TTX did not affect the ADP amplitude or the pFR, but the partial inhibition of Na^+ conductance was evident from the smaller amplitude of evoked spikes and the larger pulse current required to evoke spikes. Four spike traces and one passive response (*gray*) are superimposed for each condition. –20 pA bias currents for both conditions. A*i*, A*ii*, B, C, E and F represent six different cells.

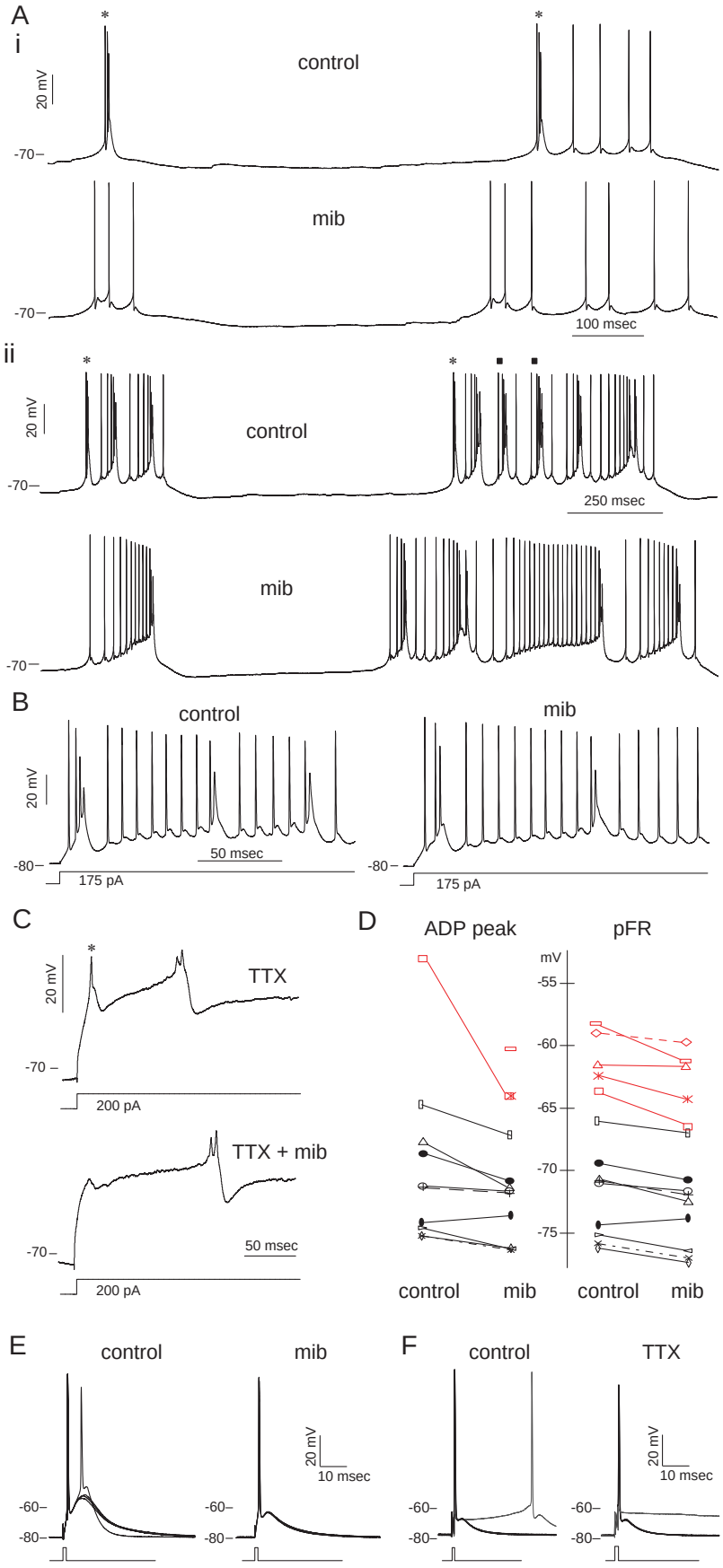
A
i
control
20 mV
-70
mib
-70
100 msec
ii
control
20 mV
-70
250 msec
mib
-70
B
control
mib
20 mV
50 msec
-80
175 pA
-80
175 pA
C
TTX
20 mV
-70
200 pA
TTX + mib
-70
50 msec
200 pA
D
ADP peak
pFR
mV
-55
-60
-65
-70
-75
control
mib
control
mib
E
control
mib
20 mV
10 msec
-60
-80
-60
-80
F
control
TTX
20 mV
10 msec
-60
-80
-60
-80

Figure 11

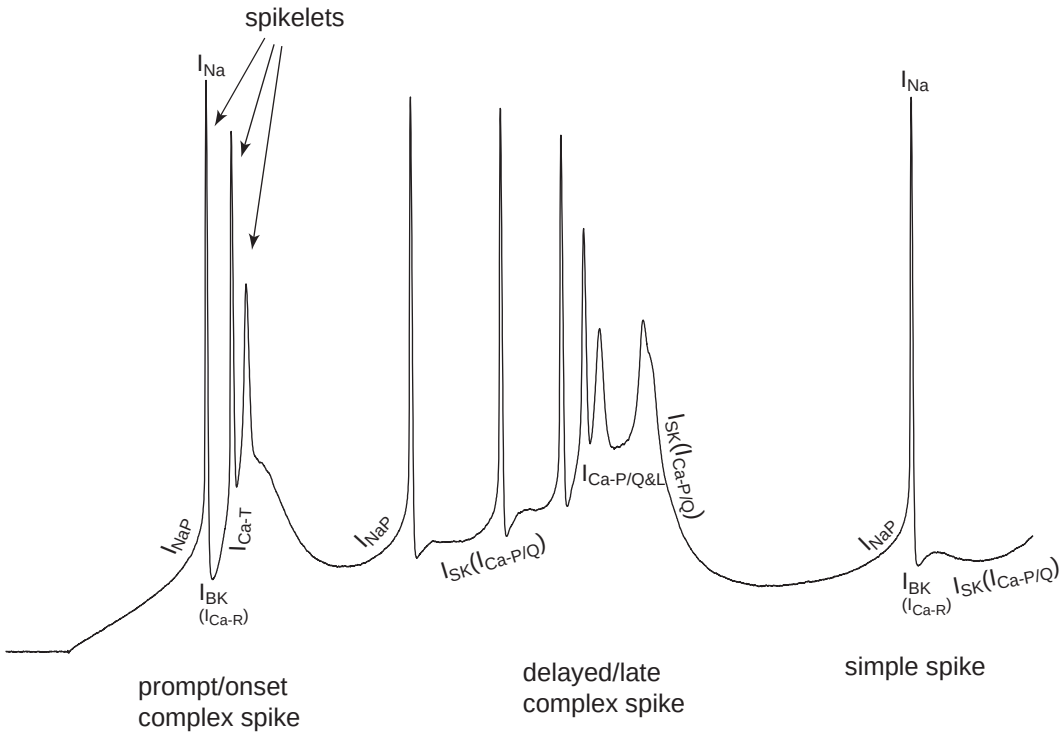

Figure 12. A model for contribution of ionic conductances during the onset and late complex spikes.

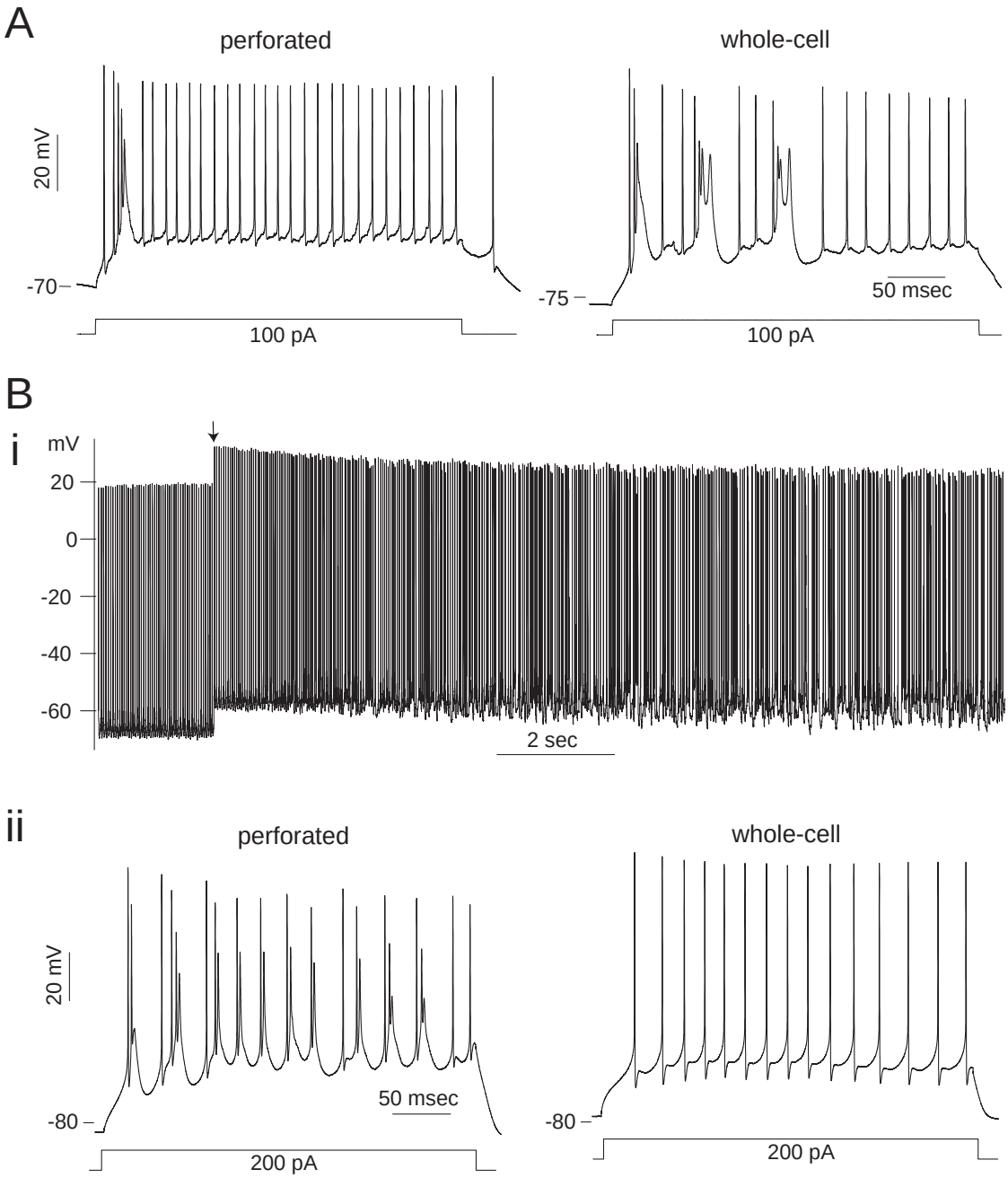

Supplemental Figure 1. Perforated-patch to whole-cell conversion.
A, K-gluconate based solution in recording pipette. V_m became hyperpolarized and complex spikes appeared more frequently with depolarization after patch rupture (right). B, 140 mM KCl in recording pipette. i, a long sweep of spontaneous all-simple-spiking activity showing the ~ 8 mV jump (arrow) in V_m at patch rupture and the following slow sag in V_m. ii, Loss of complex spikes and deepened pFR of simple spikes were characteristic of whole-cell recording with 140 mM KCl solution, as shown for a silent cell's response to depolarizing current injection before (left) and after (right) patch rupture. Synaptic blockers were not present for traces in A and Bi.

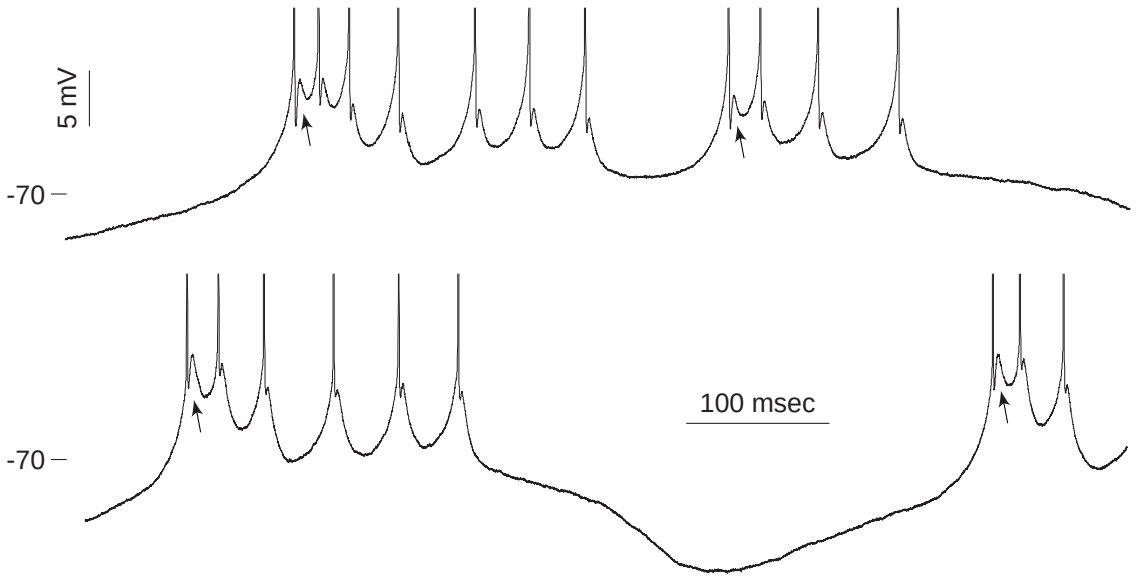

Supplemental Figure 2. Variation in ADP amplitude of spontaneous simple spikes. The two traces are from different cells both of which were complex spiking. Tendency for larger ADPs (arrows) for simple spikes preceded by a hyperpolarization was observed in some complex-spiking cells. Spikes are truncated.

Supplemental Figure 3. Effects of apamin (apm) or ω-agatoxin-TK (agtx) on responses to depolarizing current steps.

A, the same cell as shown in Fig 8B. During wash-in of 50 nM apm, bottom row, excitability was increased, as evident from elevated firing of complex spikes at a given level of depolarizing current; later during incubation all-complex spiking developed (Fig 8B bottom row). Bias currents: –80 (control) and –95 pA (apm). **B**, an example of atypical effects of apm. This cell fired high-frequency simple spikes as well as increased number of complex spikes that were not broadened. Note the response in apm at low level current, 75 pA, is high-frequency firing followed by a hyperpolarization. –10 pA bias current for traces in apm. **C**, Effect of agtx, 200 nM. Note resemblance of agtx effects to those of apm shown in A and B.

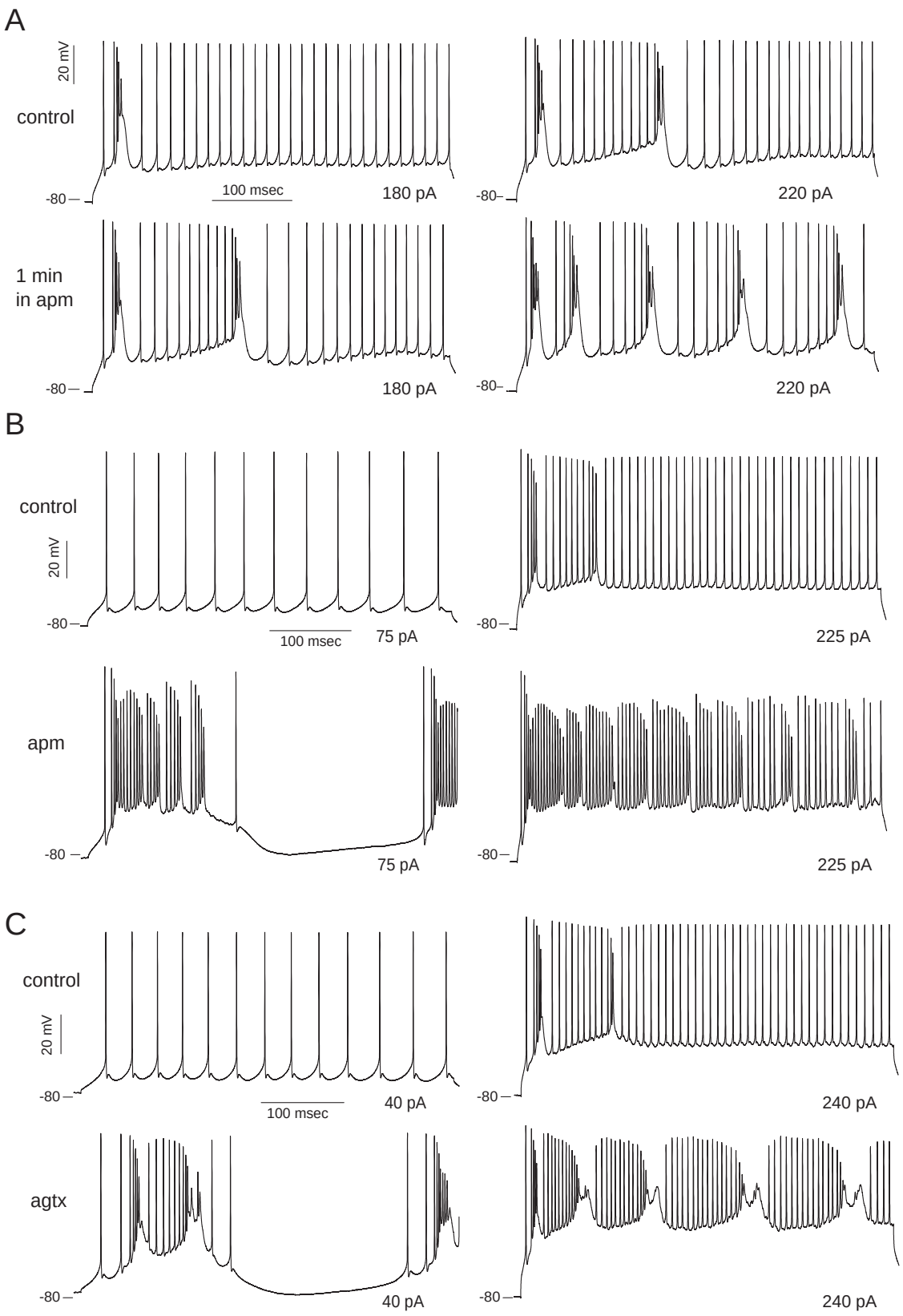

Supplemental Figure 3

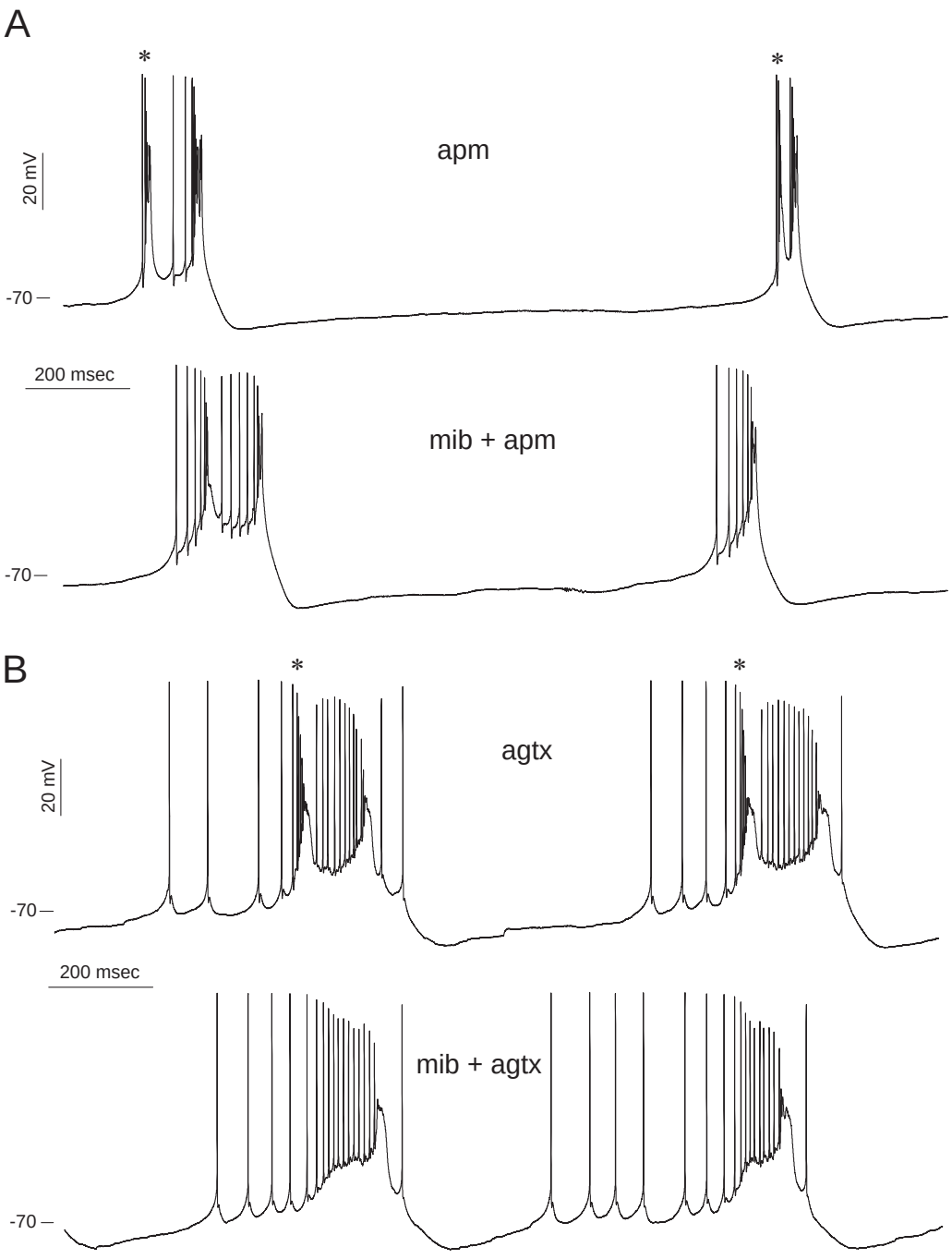

Supplemental Figure 4. More examples of selective suppression of complex spikes by mibefradil (mib). A, control condition in apamin (apm), 100 nM. B, control condition in ω-agatoxin-IVA, 200 nM. Complex spikes marked with asterisks were lost by addition of mibefradil 3 μM(A) and 2 μM(B). The threshold of fast spikes were raised by 4 mV(A), and 2 mV(B) in mibefradil.

Chapter 2

Ca^{2+} and pH dependent negative shift in the glycine reversal potential in complex spiking interneurons.

Yuil Kim[1] and Laurence O. Trussell[2]

[1] Neuroscience Graduate Program

Oregon Health & Science University

Portland OR 97239

[2] Oregon Hearing Research Center/ Vollum Institute

3181 SW Sam Jackson Park Road, Mail Code L-335A
Portland, OR 97239

Number of Figures: 8 **Number of Tables**: 2

Number of Supplemental Figures: 3

ABSTRACT

Cartwheel cells are glycinergic auditory interneurons which fire Na^+ and Ca^{2+} dependent spike bursts, the complex spike, and synapse on both pyramidal cells and one another. Using gramicidin perforated-patch recording, we found that prolonged complex spike or Ca^{2+} spike activity led to a negative shift in the reversal potential for glycine enhancing glycine's inhibitory effect. In combination with ion imaging, we found that electrical activity triggered a rise in intracellular Ca^{2+} and H^+ levels; the Ca^{2+} dependent acidification led to a drop in intracellular Cl^- through bicarbonate-Cl^- exchange. This tendency for a negative shift in E_{gly} opposes that for a positive shift triggered by passive Cl^- redistribution during depolarizations. Thus, a Ca^{2+} dependent mechanism serves to maintain or enhance the strength of inhibition in the face of increased excitatory activity.

INTRODUCTION

Glycinergic and GABAergic synapses are conventionally viewed as inhibitory synapses. Nevertheless, while many produce characteristic hyperpolarizing postsynaptic potentials, it has long been known that glycinergic or GABAergic inputs can be depolarizing, exerting shunting inhibition or even excitation in developing or mature neurons (Ben-Ari et al. 2007; Marty and Llano 2005). The variable, depolarizing or hyperpolarizing, effect of glycine or GABA in the nervous system arises from two characteristics. First, there is a broad range of reported reversal potentials for glycine or GABA-mediated currents or potentials (E_{gly} or $E_{GABA(A)}$) (e.g. –85 mV in cerebellar Purkinje cells (Chavas and Marty 2003), –37 mV in a class of adult hypothalamic neuron (DeFazio et al. 2002)). Second, E_{gly} or E_{GABA} is generally close to the resting membrane

potential, so that the variation in the resting potential can switch the polarity of glycine or GABA effect (Marty and Llano 2005). Glycine and $GABA_A$ receptor channels are permeable to Cl^- and, to a lesser extent, HCO_3^- (Bormann et al. 1987; Kaila and Voipio 1987). The heterogeneity of E_{gly} and E_{GABA} among different types or stages of neurons has thus been attributed to the difference in intracellular Cl^- level, assuming that the intracellular HCO_3^- concentration, which is determined by the intracellular pH, is similar across different cells. Cl^- imaging studies have shown that the intracellular Cl^- concentration ($[Cl^-]_i$) is correspondingly high in some neurons and sensory cells that are known to have depolarized E_{GABA} (Duebel et al. 2006; Rocha-Gonzalez et al. 2008), and that decreases in $[Cl^-]_i$ occur in single types of neurons during the period of development in which the E_{GABA} is known to shift negative (Berglund et al. 2006; Kuner and Augustine 2000).

Neuronal Cl^- levels are potentially regulated by cation-Cl^- cotransporters, KCC2 and NKCC1, and Na^+-independent and Na^+-driven Cl^--HCO_3^- exchangers as well as Cl^- channels (Farrant and Kaila 2007). Therefore steady-state $E_{gly/GABA}$ is dependent on the relative activity of Cl^- extrusion and accumulation mechanisms. An example of such control is the increase in KCC2 expression during the period of developmental negative shift in E_{GABA} in hippocampal and neocortical neurons (Rivera et al. 1999; Yamada et al. 2004), and the presence of NKCC1 with a lack of KCC2 in some neurons having depolarized E_{GABA} (DeFazio et al. 2002; Kim and Chung 2007). However, the $E_{gly/GABA}$ in single neurons may be plastic as well, as suggested by the change in $E_{gly/GABA}$ due to passive redistribution of Cl^- through Cl^- channels (Billups and Attwell 2002; Ehrlich et al. 1999) or prolonged opening of $GABA_A$ receptors (Kaila and Voipio 1987; Staley et al.

1995). Activity-dependent long-lasting positive shifts in E_{GABA} have been described, which may involve modulation of KCC2 or NKCC1 (Brumback and Staley 2008; Fiumelli et al. 2005). Interestingly, although the Cl^--HCO_3^- exchangers have been identified in neurons (Brett et al. 2002; Grichtchenko et al. 2001; Kopito et al. 1989; Schwiening and Boron 1994), their role in regulating $[Cl^-]_i$ or $E_{gly/GABA}$ has received little attention (see Gulacsi et al. 2003), perhaps due to the general assumption that the intracellular pH, which determines the driving force for HCO_3^-, is stable.

The cartwheel cell (CWC) is a glycinergic interneuron in the dorsal cochlear nucleus (DCN) that integrates auditory and non-auditory input (reviewed in Oertel and Young 2004). CWCs form synapses among themselves and with the principal cells of DCN (Berrebi and Mugnaini 1991; Wouterlood and Mugnaini 1984), and it has been shown that CWCs mediate strong feed-forward inhibition of principal cells upon somatosensory stimulation (Davis and Young 1997). The electrical signature of CWCs is the complex spike, a burst of fast spikes with Ca^{2+}-dependent underlying slow depolarization, which occurs spontaneously or on depolarization (Golding and Oertel 1996; Kim and Trussell 2007; Manis et al. 1994; Zhang and Oertel 1993a). Golding and Oertel (1996) have reported using microelectrode recording in mouse DCN slices that the glycinergic and GABAergic input in CWCs were weakly excitatory; however, inhibitory glycine/GABA effect in CWCs has also been described (Davis and Young 2000; Manis et al. 1994). In the present study, we investigated on the nature of glycinergic input in CWCs by recording with gramicidin perforated-patch method (Rhee et al. 1994) in mouse DCN slices. We found that the complex spike activity triggered a negative shift in E_{gly}. This shift occurred as a result of a Ca^{2+}-dependent acidification of the neurons and a

consequent decrease in $[Cl^-]_i$ or $[HCO_3^-]_i$, most likely involving the activity of Na^+-driven Cl^--HCO_3^- exchange. To our knowledge, this is the first demonstration that the anion exchanger, working against physiological intracellular acid load, can control the glycinergic/GABAergic reversal potential.

METHODS

Slice preparation and recording

Brainstem slices containing the DCN were prepared from ICR mice aged 17–27 days (Harlan, Indianapolis, IN). Mice were anesthetized with isoflurane and then decapitated in accord with the regulations of the Institutional Animal Care and Use Committee of Oregon Health and Science University. Subsequently, a block of brainstem was isolated and horizontal slices of 200-μm thickness were cut with a vibrating slicer (VT1200S, Leica, Deerfield, IL). Dissection and slicing were done in a warm (~ 30 °C) solution saturated with 95% O_2/5% CO_2 and composed of (in mM): 1) 129 NaCl, 3 KCl, 1.2 KH_2PO_4, 2.4 $CaCl_2$, 1.3 $MgSO_4$, 20 $NaHCO_3$, 3 HEPES, 10 glucose ("ACSF") or 2) 73 sucrose, 81 NaCl, 3 KCl, 1.2 NaH_2PO_4, 1 $CaCl_2$, 0.7 $MgCl_2$, 1.3 $MgSO_4$, 0.5 ascorbic acid, 25 $NaHCO_3$, 3 HEPES, 10 glucose. The latter solution was used in about half of dissections. The slices were kept in ACSF at 34.5°C for the first hour and then left at room temperature.

ACSF was the standard bathing medium for recordings, except for the following. For inducing intracellular acidification, modified ACSFs were used, in which NaCl was reduce by 20 mM and equiosmolar amount (~22 mM, "20 mM" in Results) of either Na-methanesulfonate ($NaCH_3O_3S$) or Na-propionate was introduced. For inducing

intracellular alkalinization, 10 mM trimethylamine hydrochloride (TMA·HCl) replaced equimolar NaCl in the ACSF. A 3M KCl/3% agarose salt bridge reference electrode was used in experiments utilizing these three modified ACSFs. For bicarbonate- and CO_2-free condition, the ACSF was buffered only with HEPES and equilibrated with 100 % O_2 ("HEPES/O_2"): 20 mM $NaHCO_3$ was replaced with 20 mM HEPES (in addition to the original 3 mM), and glucose was increased to 20 mM to achieve a similar osmolarity to that of ACSF (~303 mosmol/L). The pH of "HEPES/O_2" was adjusted with NaOH at 34 °C to 7.32–7.34, which is the pH range of ACSF equilibrated with 5% CO_2/95% O_2, measured at 34 °C.

DCN cells in the slice were visualized by infrared differential interference contrast videomicroscopy on an Olympus BX51WI microscope with a 60X water-immersion objective (0.9 N.A., LUMPlanFL, Olympus, Japan). The ACSF or other saline solution was perfused at 2–3 ml/min through the recording chamber by a peristaltic pump (Minipulse 3, Gilson, Middleton, WI), and the temperature of the solution at the recording chamber was maintained at 34±0.5°C by an in-line heater (SH27B, Warner Instruments, Hamden, CT). Medium-sized cells in the molecular and fusiform cell layers of DCN were identified as CWCs if they showed complex spikes spontaneously or upon injection of depolarizing current. The data presented in this study were obtained with gramicidin perforated-patch recording (Rhee et al. 1994). The standard pipette solution for perforated patch recording contained of (in mM) 140 KCl, 10 NaCl and 10 HEPES (pH adjusted to 7.25 with KOH, 290 mOsm). Gramicidin was then added to this solution on the day of experiment at a final concentration of 40–100 μg/ml from a stock solution of 30–50 mg/ml DMSO. For simultaneous imaging, one or two acetoxymethyl (AM)

ester fluorescent dyes (see below) were added along with gramicidin. The maximum % of DMSO reached in the recording solution was 0.48 % when two AM dyes were included. The tip of the recording pipette was filled with the standard solution (without gramicidin or indicator dyes). The recording pipettes had a resistance of 3–6 MΩ when filled with the standard solution, and were prepared by pulling thick-walled filamented borosilicate glass capillaries (1B120F-4, World Precision Instruments, Sarasota, FL), and wrapped with Parafilm along one third the pipette's length from the tip to reduce capacitance. The detection of patch rupture was by a sudden offset in membrane potential. The liquid junction potential was not corrected, as discussed in a previous study (Kim and Trusselll, 2007).

Recordings were made with a BVC-700A (Dagan, Minneapolis MN) or MultiClamp 700B amplifier (Molecular Devices, Sunnyvale, CA) in conjunction with Digidata 1322A digitizer (Molecular Devices) and ClampEx software (pClamp 9.2, Molecular Devices). After the electrode had formed a seal (> 1GΩ) on the cell membrane in voltage-clamp (v-clamp), the progression of perforation (reduction in series resistance, R_s) was monitored in current-clamp (i-clamp) by periodic bridge balancing and by observing the growth in amplitudes of spontaneous fast spikes. The effect of glycine on spontaneous activity or on membrane potential (V_m) was examined and categorized from early on during perforation because it could be distinguished under a relatively high R_s. The glycine or GABA was pressure-ejected (Picospritzer II, General Valve, Fairfield, NJ) from a patch pipette pointed toward the cell body from 25–30 μm away. The duration and pressure of a puff were adjusted for each cell to elicit a 500-ms response: the ranges were 5–20 ms and 0.5–2 psi with 2 mM glycine, 100–300 ms and 2–

4 psi with 0.5 mM glycine or 0.5 mM GABA. Care was taken to minimize glycine/GABA applications, to avoid causing a significant change in intracellular [Cl^-] or [HCO_3^-] due to the flux through the glycine/GABA receptors. Glycine and GABA solutions were prepared in ACSF except during experiments involving HCO_3^-/CO_2 removal, for which glycine was dissolved in HEPES-buffered saline. Glycinergic/GABAergic postsynaptic potential (PSP) was evoked by 200-μsec 30–60 V pulses given through a glass stimulating electrode filled with ACSF. The recorded cell was kept in i-clamp mode except when the glycine reversal potential (E_{gly}) was measured. After the glycine response of spontaneous activity/V_m had been examined, the Na^+ channel blocker tetrodotoxin (TTX, 0.4 μM) and glutamate receptor blockers, DNQX (6,7-dinitroquinoxaline-2,3-dione, 10 μM) and APV (2-amino-5-phosphonovaleric acid, 100 μM) were added, and a bias current was given to keep the cell's V_m at –75 ~ –80 mV. I-clamp recording was sampled at 20 kHz and low-pass filtered at 10 kHz. The pipette capacitance was compensated in both i-clamp and v-clamp mode.

E_{gly} measurements

Voltage ramps (v-ramp) in v-clamp were used for measurement of E_{gly}, and were sampled at 40 kHz and low-pass filtered at 10 kHz. The v-ramp protocol consisted of 4 consecutive runs of a 1-sec-long unit stimulus that included a short –5 mV step followed by a 130-ms depolarizing ramp spanning 18–20 mV around the expected E_{gly} of the recorded cell (V_{HOLD} = –75 mV) (Fig. S1Bi). Glycine was puffed after the –5 mV step during the 1st and 3rd run. The average ramp voltage where the glycine responses and control responses crossed was taken as the raw E_{gly}. The R_s during an E_{gly}

measurement was estimated from dividing 5 mV by the average amplitude of the capacitative transient current (in nA) of the –5 mV step. The raw E_{gly} was corrected for the voltage error from the R_s with the following formula: E_{gly} = raw E_{gly} – ((average clamp current at raw E_{gly}) × R_s). The inclusion criteria for E_{gly} data was R_s < 60 MΩ. The R_s dropped to 20–40 MΩ within 40 minutes of forming a seal in most cells used in E_{gly} measurements.

The resting E_{gly} (measured >150 sec after any depolarization-induced spiking) was measured after an initial ~ 10 sec clamp to –75 mV. As shown in Fig. S1Di, a slow, negative drift in the resting E_{gly} was found in most cells. As the perforated-patch recording pipette contained 150 mM Cl^-, the negative drift was opposite to that expected if the pipette Cl^- leaked into the cell. The negative drift in E_{gly} was also recognized in i-clamp mode from the change in V_m response to glycine over time. The negative drift occurred both with the dye-free and dye-containing recording solution and was still observed when different pipette salts (145 K-gluconate, 4 NaCl, 4 NaOH, 10 HEPES, pH 7.25) were used. Occasionally, a positive drift in resting E_{gly} was seen under control conditions and was followed within a few minutes by the rupture of perforated patch; data from these recordings were not included.

We did not determine resting E_{gly} by plotting the amplitude of glycine-induced currents versus holding potential in v-clamp because the E_{gly} seemed to drift towards the holding potentials, particularly when the new potential was below –80 mV or above –60 mV suggestive of a passive Cl^- conductance. V-ramp protocol was adopted to minimize the drift of E_{gly} during measurements and to be able to follow the activity-induced change in E_{gly} (see Results).

Fluorescent imaging

Imaging experiments with the pH-sensitive dye SNARF-5F were mostly performed with a monochromator (Polychrome V)-based imaging system from Till Photonics (Munich, Germany) attached to the Olympus BX51WI microscope. Excitation wavelength was 547 nm, and emission was long-pass filtered above 600 nm (Chroma E590LPv2). Fluorescent images were acquired with IMAGO QE cooled CCD camera (Till Photonics) controlled by the TILLvisION 4.0 software. SNARF-5F was loaded into a cell by including the AM ester form (43 μM) in the recording pipette from which it diffused through the perforated patch and was de-esterified inside the cell (Filosa et al. 2002). The fluorescent intensity of the recorded cell increased with time as the dye accumulated (Fig. S2A). To minimize the phototoxicity and to keep the average raw intensity of cell body in different image series in a narrow range, the images were obtained (at 1 Hz) with 4x4 binning and the exposure time was adjusted as the baseline intensity increased (e.g. 150 ms for first imaging series collected ~30 min after the seal, gradually shortened to 50 ms over the next hour). For simultaneous pH-Ca or pH-Cl imaging, 2-photon scanning microscopy was utilized. Images of 256x256 pixels were acquired with a Prairie Technologies Ultima system using a Chameleon Ultra II Ti:sapphire pulsed laser (Coherent, Santa Clara, CA) (Roberts et al. 2008). For pH and Ca^{2+} imaging, the AM forms of SNARF-5F and either Fura-2 (100 μM) or Fluo-4 (76 μM) were included in the recording pipette for loading. Ca^{2+} dyes did not load as well as SNARF-5F through the patch membrane, but Fluo-4's loading could be improved by adding Pluronic F-127 (final concentration, 0.017%). The excitation wavelength was 800 nm for simultaneous pH-Ca imaging with Fluo-4, and 780 nm with Fura-2. For

concurrent pH and Cl^- imaging, Cl^--sensitive dye MQAE (N-(ethoxycarbonylmethyl)-6-methoxyquinolinium bromide) was loaded into the DCN slice by incubating the slice in 3 mM dye in ACSF for 8 min at 34 °C, and SNARF-5F was loaded from the recording pipette. MQAE and SNARF-5F were both excited by 750 nm laser light. For pH and Ca^{2+} imaging, fluorescent emission was split into two photomultiplier tubes using a dichroic mirror and band-pass filters for red (SNARF-5F) and green (Fluo-4 and Fura-2) light. For pH and Cl^- imaging, the green band pass filter was removed to collect all emission below 560 nm for the weak MQAE signal. As shown in an example of simultaneously recorded MQAE and SNARF-5F images in Fig. 6Bi, some of MQAE's fluorescence was caught in the red channel for SNARF-5F, but the impact of such on the SNARF signal was thought to be negligible considering the weak response of MQAE signal. The baseline MQAE fluorescence did not noticeably decrease, as expected from dye leakage or bleaching, either during a 150-sec run of experiment or over the ~1 hour of recording period. However, as experiments evoking a change in MQAE signal were repeated over time, the response magnitude became attenuated. With time, the typical inhomogeneous MQAE staining of the cell body (Marandi et al. 2002) also became more homogeneous. We suspect that the time-dependent loss of response is due to MQAE's conversion to a hydrolyzed (de-esterified) form having a reduced Cl^- sensitivity (Koncz and Daugirdas, 1994; Verkman, 1990). No glycine puff was given during 2-photon imaging experiments.

For both single-photon and 2-photon image series obtained, the "signal" was extracted from the average intensity (in arbitrary unit) of a region of interest (ROI) drawn along the periphery of the cell body (Fig. S2A). The average intensity of a background

region was subtracted from the SNARF signal but not from other dyes' signal because the signal to noise ratio was worsened by background subtraction. The time plot of fluorescence signal over a 150–200 sec period was corrected for the up-sloping baseline by fitting a straight line along the control period and subtracting the line from the signal. The initial intensity value before the line subtraction (F_0) was, then added back to all points and the plot of $(F–F_0)/F_0$ ("$\Delta F/F$") was produced. For the 800-sec image series involving weak acid or weak base challenge, the fitted straight line was not subtracted but used as F_0 in calculating $(F–F_0)/F_0$ to prevent the overestimation of ΔF in the later part of the 800-sec period. Although a linear increase in the baseline fluorescence was assumed for convenience, not infrequently the baseline-corrected SNARF-5F signals were found to deviate from 0 at the end of a 160-sec series when an intensity-attenuating response (acidification) was expected to have terminated. In such cases it was unclear whether it was a true signal or due to the failure of linear baseline correction. We mostly focused on the peak change in signal occurring within 30 sec from the control period, during which the linear extension of baseline is less likely to fail. Occasionally, a small abrupt increase in SNARF signal occurred not associated with a stimulus or a change in V_m (e.g. Figs. 5A black, 6A, 8Aii gray); whether this is an artifact or not is unknown. The peak signal in a time plot was selected by eye for single-photon SNARF-5F data, and by curve fitting or from the intersection of two fitted straight lines for the 2-photon MQAE or SNARF-5F data, respectively.

Drug application

All the pharmacological agents except glycine and GABA were applied by bath perfusion. DNQX (10 µM) and APV (100 µM) were co-applied for every occasion TTX was used. H_2DIDS (4,4'-diisothiocyano-1,2-diphenylethane-2,2'-disulphonic acid) was directly dissolved in ACSF each day of experiment, but other drugs were diluted from a stock solution in water (TTX, APV, glycine, GABA) or DMSO (all others). Drugs were obtained from Sigma-Aldrich (St Louis, MO) with the exception of TTX (Alomone labs, Jerusalem, Israel), APV, DNQX (Ascent scientific, Weston-Super-Mare, UK) and H_2DIDS (Invitrogen, Carlsbad, CA). Carboxyeosin diacetate used was from Sigma-Aldrich (n = 3) or Invitrogen (n = 2). All fluorescent dyes and Pluronic F-127 were from Invitrogen. When $CdCl_2$ or $CoCl_2$ was used, KH_2PO_4 in the bathing solution was replaced with KCl to prevent precipitation.

Data analysis

Data were analyzed with Clampfit (Molecular Devices), Microsoft Excel and KyPlot (KyensLab, Tokyo, Japan). Numerical values were given as mean ± S.D. where available. Two-tailed *t*-test (paired or unpaired) or Kolmogorov-Smirnov test was used to compare two groups of data, and one-way ANOVA and the multiple comparisons (Tukey-Kramer test) were used for three or more groups of data. Level of significance was at 0.05 for all statistical tests.

RESULTS

Glycine response of cartwheel cells

Depolarizing, excitatory glycine responses have been reported in CWCs using microelectrode or extracellular cell-attached recording (Golding and Oertel 1996; Tzounopoulos et al. 2004). We reevaluated the prevalence of depolarizing glycine responses using gramicidin perforated-patch recording, and found that cells varied in their response from depolarization to hyperpolarization, suggestive of variable glycine reversal potential (E_{gly}). For spontaneously spiking cells, the effect of glycine was categorized as excitatory, inhibitory or mixed. Excitation (Fig. 1A) was recognized as an increase in spike frequency with a clear depolarization. Mixed responses (Fig. 1B) consisted of a depolarized pause followed by a higher frequency firing at the decay of the response. Reducing the puff pressure or duration for this group did not reveal an increase but a decrease or no change in spiking at the onset of response. This is expected if E_{gly} is a few mV below spike threshold, such that shunting depolarization provided a platform for higher frequency spiking as the glycine receptors are closing (Gulledge and Stuart 2003). An inhibitory glycine response (Fig. 1C), a decrease or pause in spiking, was observed with the V_m driven to levels from just 5 mV below the fast spike threshold (~ –65 mV) to –84 mV. The glycine responses in CWCs that did not spike spontaneously (V_m –81.4 ± 2.8, n = 127) consisted of depolarizing or hyperpolarizing deflections of V_m; in some of these cases (11 of 127), spikes were evoked at the peak of a depolarizing response. The proportions of cells showing the three types of glycine response are shown in Table 1; for the standard pipette solution, the excitatory, mixed and inhibitory proportions were 31, 12, and 57 %, respectively (n=113).

Several potential factors, either biological or experimental, could influence the distribution of response polarity. For example, higher proportion of inhibitory responses was observed in cells recorded with a pipette solution containing an AM-ester dye (SNARF-5F or Fluo-4, see data below on imaging). Another potential factor that could impact the distribution is postnatal age, as intracellular [Cl^-] is higher during the first 1-2 weeks after birth, resulting in transient excitatory response to GABA or glycine (Ben-Ari et al. 2007). This concern was ruled out by comparing between the group of CWCs recorded with the dye containing solution and the group with no dye. No significant difference was found in the age distribution of all cells showing excitatory responses vs. inhibitory responses (Kolmogorov-Smirnov test, $p = 0.99$; 22.4 ± 2.4 days, $n = 57$, excitation vs. 22.4 ± 2.6 days, $n = 148$, inhibition). No difference was present in the ages of mice recorded with or without AM dyes (Kolmogorov-Smirnov test, $p = 0.65$; 22.3 ± 2.5 days, $n = 113$, no dye vs. 22.5 ± 2.5 days, $n = 129$, with dye). Thus, age is not a factor affecting glycine responses in our data set. More interestingly, we observed an association between the type of glycine response and whether the cell's spontaneous activity included complex spikes or was all simple spiking. In the current study, 19 % of spontaneously spiking cells (47 of 242) were complex-spiking, and among these the excitatory response was observed in only one, while the inhibitory response was seen in 85.1 % of them (Table 1). This suggests a possible relation between E_{gly} and complex spike activity, which is described below.

Activity-dependent shift in the glycine response

A series of experiments were designed to obtain qualitative description of the effects of spike activity on glycine responses and to suggest the cellular mechanisms that are tested in detail later in this study. Four cells showing depolarizing glycine responses, two simple-spiking cells and two silent cells, were induced to fire complex spikes for a long period by sustained depolarizing current injection (50–150 pA for 57–137 sec in different cells), and their glycine responses were monitored in 10–15 sec intervals. As shown in Fig. 2A, the glycine responses shifted negative, i.e., becoming less excitatory or more inhibitory as complex spiking continued, and when the spiking was terminated, a hyperpolarizing glycine response was observed, which shifted back to depolarizing over the next 100–200 sec. These results suggest a negative shift in E_{gly}.

To contrast the relative effects of simple and complex spikes, the type of spikes in the train were controlled by the magnitude of a given duration of the stimulus. To facilitate the comparison of glycine response amplitudes, cells were silenced to –80 mV, and 6 cell showing depolarizing glycine response at –80 mV were chosen. As shown in Fig. 2B (top), although a reversal to a hyperpolarizing glycine response did not occur, complex spiking resulted in a negative shift in the peaks of glycine responses (*, –1.7 ± 0.7 mV, n = 6) 20-30 sec after the stimulus ended. By contrast, after simple spiking (including cases where the single onset complex spike was present; Fig. 2B bottom) such a negative shift was barely noticeable (–0.1 ± 0.2 mV, n = 6). Interestingly, however, the peak of the first glycine response after simple spiking (o) was 0.1–3.3 mV more positive than that before the stimulus, despite riding on a prominent afterhyperpolarization (4 of 6 cells). A positive shift in E_{gly} is expected to develop during a long depolarization and to

decay on repolarization in the presence of a passive Cl^- conductance, as $[Cl^-]_i$ would change along with the V_m. A similar negative shift was seen in $GABA_A$ component of the responses to puffing 500 μM GABA after complex spiking (8–14 sec duration, n = 7 cells, not shown).

CWCs receive mixed glycinergic/GABAergic synapses from other CWCs (Roberts et al. 2008). We evoked glycinergic/GABAergic PSPs by stimulating in the deep layer of DCN in the presence of glutamate receptor blockers (100 μM APV, 10 μM DNQX) at 0.5–0.7 Hz. The reversal in the polarity of evoked PSPs from depolarizing to hyperpolarizing, indicating a negative shift in E_{gly}, again could be induced by complex spiking, in one cell at native V_m (zero bias current; Fig. 3A) and in 7 cell at hyperpolarized V_m (Fig. 3B cell 1 and 2). For 3 cells in which the evoked PSPs were hyperpolarizing even when V_m was brought near –80 mV, 10-sec of complex spiking made the PSPs more hyperpolarizing (Fig. 3B cell 3). The difference in the average amplitude of PSPs between the pre-activity period and the 15th–20th sec post-activity period was from –0.4 to –2.2 mV in 10 cells (average –1.3 mV, complex spiking induced for 10~16 sec by 100~250 pA).

The CWC's complex spike requires Ca^{2+} channels (Kim and Trussell 2007), and thus a complex spike results in a larger rise in intracellular Ca^{2+} than does a simple spike (Molitor and Manis 2003; Roberts et al. 2008). To investigate whether the Ca^{2+} influx is sufficient for the negative shift in glycine response to occur, high threshold Ca^{2+} spikes were evoked in the presence of Na^+ channel blocker TTX, 0.4 μM. Ca^{2+} spikes were evoked in seven cells that had a depolarizing glycine response at V_m = –80 mV, and glycine was puffed every 8 sec (Fig. 4A). In all 7 cells, the glycine response shifted

negative by the third puff during Ca^{2+} spiking. After Ca^{2+} spike trains, the V_m was depolarized compared to the pre-Ca^{2+} spiking level, lacking the afterhyperpolarization seen after complex spiking. This depolarization made the negative shift in E_{gly} obvious, as it facilitated conversion of the glycine response to a hyperpolarizing one: the peaks of hyperpolarizing glycine responses after Ca^{2+} spiking (at –78 to –93 mV in 5 cells) were more negative than the depolarizing peaks of glycine responses before Ca^{2+} spiking (at –79 to –74 mV).

Measurement of E_{gly}

We used a voltage-clamp protocol to measure E_{gly} and document the time course of its change after spike-train stimuli (Fig. S1Bi, see Methods). To avoid the slow negative drift in E_{gly} (see Methods, Fig. S1Di) representative resting E_{gly} was assessed as early as possible during patch perforation, as long as $R_s < 60$ MΩ (in TTX). With this criterion, the mean resting E_{gly} from 164 cells was –74.3 ± 5.8 mV. Table 2 lists E_{gly} values subgrouped with respect to spontaneous activity, response to glycine, and presence of AM dye in the recording pipette. The difference between spiking cells' E_{gly} and that of silent cells was insignificant (*t*-test, $p = 0.60$). E_{gly} was most negative in cells with inhibitory responses and most positive for those with excitatory responses. The difference among the three response groups was significant (one-way ANOVA, $p < 0.001$). While the E_{gly} difference between the excitatory group and mixed group was not significant in pairwise comparison (Tukey-Kramer test, $p = 0.56$), the differences in the other pairwise group comparisons were significant ($p < 0.001$). For comparison with CWCs, we examined glycine responses in fusiform cells which are the principal neuron of the DCN and postsynaptic to CWCs. All showed hyperpolarizing, inhibitory

responses to glycine (n = 28) and the E_{gly} measured in 4 cells was –83.9 ± 0.7 mV (in TTX). The fusiform cell showing more negative E_{gly} than the CWC and only inhibitory responses to glycine are in agreement with Golding and Oertel (1996)'s findings.

A protocol using mixed voltage and current clamp recording modes was set up to monitor the time course of E_{gly} shifts in relation to a period of activity. V_m and glycine responses were recorded in current clamp for 150–180 sec interrupted every 15 sec or less by the ramp protocol; an ~ 8 sec burst of complex or Ca^{2+} spiking was induced at t = 35 sec (Fig. S1A–C). Shown in Fig. 4B is the distribution of peak negative E_{gly} shifts (difference between the most negative E_{gly} after Ca^{2+} spiking and the mean of pre-Ca^{2+} spiking values) versus the number of Ca^{2+} spikes evoked during the 8-sec depolarization (n = 148 measurements; Pearson's r = –0.66, $p<0.001$). Initially, we evoked enough Ca^{2+} spiking in each cell to recognize a clear negative shift in glycine responses during current-clamp after the stimulus (e.g., Fig. S1A–C, 4D) and confirmed that the E_{gly} shifted negative. However, for cells with the largest shifts (> 5 mV), E_{gly} would often fail to recover fully within 120 sec after the Ca^{2+} spiking or would settle to a more negative level than the control level. Additionally in some cases Ca^{2+} spiking would continue beyond the 8-sec current injection. Therefore, we adjusted the current injection in each cell to prevent runaway spiking and to achieve ≤ 5 mV of negative E_{gly} shift. As shown in Fig. 4D, the most negative shift in E_{gly} occurred at one of the first three measurements after Ca^{2+} spiking (at 2, 8.5, or 19.5 sec, mean 9.3 ±.5.9 sec, n = 61 series with ≥ 1.5 mV peak negative shifts from 61 cells). Restoration of E_{gly} occurred over 100–130 sec, and single exponential fits for recovery gave a mean time constant of 35 ± 11 sec (n = 34 cells).

The 8s challenge protocol was also run in cells in the absence of TTX to examine the E_{gly} shift with complex or simple spiking. E_{gly} shifted negative by up to 4 mV after an 8-sec stimulus evoked with a maximum of 250 pA injection (Fig. 4Cii). In 32 E_{gly} series (from 32 cells, 29 with AM dye and 3 without dye) where > 1 mV peak negative shift occurred with complex spiking, the time of peak was most often (18 of 32) at the 19.5 sec point, and two had the peak at 34 sec. Thus, the average peak time (16.3 ± 7.8 sec, n = 32) was later than with Ca^{2+} spiking. The first data point (2 sec) after complex spiking was not as negatively shifted as that after Ca^{2+} spiking, showing a small positive shift in some cases. Fig. 4C shows the maximal negative shift in E_{gly} plotted against the shift at the 2-sec time point for individual experiments obtained with Ca^{2+} spiking (limited to 1–4 mV shifts for comparison with complex spiking-induced shifts), complex spiking and simple spiking. These data show that with only Ca^{2+} spiking, the magnitude of peak negative shifts was greater, and an initial positive shift was rarely observed. Such initial positive shifts were more common with complex spiking, and especially with simple spiking; as discussed below, these positive shifts appear to reflect passive elevation in intracellular Cl^- that are opposed by a Ca^{2+} dependent mechanism.

Ca^{2+}-dependent and passive E_{gly} shifts

To test whether Ca^{2+} influx triggers the negative shift of E_{gly}, Ca^{2+} in ACSF was removed ("zero-Ca^{2+}", $MgCl_2$ substitution of $CaCl_2$, in TTX, n = 8). Removal of Ca^{2+} depolarized V_m (restored to between –75 and –80 mV with bias current), and shifted resting E_{gly} between +2 to –4 mV in different cells. As illustrated in Fig. 4E, 8-sec current injection in TTX and zero-Ca^{2+} depolarized the cells strongly but without spiking

activity. Following the stimulus, there was no negative shift in E_{gly}, even with currents as large as 500 pA (n = 8 cells). Rather, the E_{gly} immediately shifted positive after the strongest depolarization, and this positive shift decayed within 60 sec (Fig. 4Eii). While the negative shift in E_{gly} when spikes were present peaked at 8.5 sec or 19.5 sec after stimulus in 6 of the 8 cells, the positive shift in zero-Ca^{2+} peaked at 2 sec (the first measured time point) in 7 of 8 cells. The simplest explanation for the transient positive shift in E_{gly} is a rise in intracellular Cl^- through a passive conductance during the depolarization. Such a Cl^- conductance is expected also to mediate the influx of Cl^- during the control condition with Ca^{2+} spiking. The fact that the E_{gly} was often more negative than the control level soon after (at 2 sec) Ca^{2+} spiking and that it could drop further during the next 10 or 20 sec indicates that Cl^- was actively removed or that a constitutive Cl^- accumulation was inhibited by a Ca^{2+}-triggered mechanism. Fig. 4F illustrates the contrasting direction of E_{gly} shifts induced by the same amount of current injection in control and zero-Ca^{2+}, as well as the tendency for both directions of shifts to increase with the amount of current injected in 6 cells. The average of the largest negative shift from each cell was –2.4 ± 2.2 mV and that for the positive shift was 2.2 ± 1.2 mV. Thus, the Ca^{2+}-dependent process opposed a passive process, shifting E_{gly} negative by nearly 5 mV in this protocol.

A hypothesis for the mechanism of Ca^{2+}-dependent negative E_{gly} shift

A negative shift in E_{gly} is expected to result from a reduction in intracellular Cl^- and/or HCO_3^-. HCO_3^- is less permeable than Cl^- through both the glycine and GABA receptor (Bormann et al. 1987), and at constant P_{CO2}, the intracellular concentration,

$[HCO_3^-]_i$, is expected to be set by the intracellular pH (pH_i) (Roos and Boron 1981). On the other hand, $[Cl^-]_i$ in neurons is possibly regulated by K^+-Cl^- cotransporters (KCC), Na^+-K^+-Cl^- cotransporters (NKCC) and the anion (Cl^--HCO_3^-) exchangers, Na^+-independent (AE) or Na^+-driven (NDCBE) (Farrant and Kaila 2007) (Fig. 8Di). To date, the specific expression of each transporter species in CWCs is not known, but we have assumed that all four kinds are functioning in setting up a hypothesis for the mechanism of Ca^{2+}-dependent negative E_{gly} shift in CWCs. For KCCs or NKCCs to cause a decrease in $[Cl^-]_i$ with Ca^{2+} spiking, their activity needs to be increased or decreased, respectively, with a rise in intracellular Ca^{2+}. However, given the depolarized V_m during Ca^{2+} spiking, extracellular K^+ should elevate, and the electrochemical driving force thus may not be in favor of KCC transporting Cl^- out of the cell. The possibility of the NKCC inactivation causing the drop in $[Cl^-]_i$ after Ca^{2+} spiking was thought to be low, considering that a clear (> 2 mV) negative E_{gly} shift with Ca^{2+} spiking could be seen in cells having resting E_{gly} below –80 mV as well as in those with their resting E_{gly} above –70 mV, the NKCC-mediated baseline influx of Cl^- being likely to be less in the former. Indeed, blockade of NKCC with bumetanide did not prevent the effect of Ca^{2+} spiking on E_{gly} (Supplemental Results). The Cl^--HCO_3^- exchangers, AE and NDCBE, have been studied mostly in the context of pH_i regulation: AE mediates influx of Cl^- while exporting HCO_3^- activated by intracellular alkalinization, and NDCBE, known as an acid extruder, moves Cl^- out in exchange for HCO_3^- driven by the Na^+ gradient (Chesler 2003; Romero et al. 2004). Intracellular acidification has been shown to occur with spiking activity or depolarization in various types of neurons often in a Ca^{2+}-dependent way, and the proposed mechanisms have been replacement of H^+ by Ca^{2+} in intracellular binding sites, mitochondrial Ca^{2+}

uptake leading to H^+ release and cytosolic Ca^{2+} removal by Ca^{2+}-H^+ ATPases of plasma membrane (PMCA) or endoplasmic reticulum (SERCA) (Ballanyi and Kaila 1998; Chesler 2003). Therefore, we propose that complex or Ca^{2+} spiking leads to a Ca^{2+}-dependent intracellular acidification, which brings NDCBE into extruding Cl^- and causing a negative shift in E_{gly} (Fig. 8Dii). Also contributing to the negative shift in E_{gly} is the lowering of $[HCO_3^-]_i$ during the intracellular acidification (Kaila et al. 1993), provided that P_{CO2} is constant and carbonic anhydrase is present promoting fast equilibration of the reaction, $CO_2 + H_2O \leftrightarrow H^+ + HCO_3^-$ (Roos and Boron 1981). We tested key elements of this hypothesis, examining whether i) the pH_i decreased with Ca^{2+}/complex spiking and the decrease was Ca^{2+}-dependent, ii) E_{gly} could shift negative with an intracellular acidification not associated with electrical activity, and iii) blocking NDCBE could eliminate the negative E_{gly} shift.

Activity-dependent and Ca^{2+}-dependent intracellular acidification

Changes in pH_i were monitored with the fluorescent indicator SNARF-5F ("SNARF"). To maintain the perforated patch condition, the dye was introduced into the cell by including the AM ester form in the recording pipette, which we found would diffuse through the perforated patch and get de-esterified. This loading method led to a steady increase in the baseline intracellular fluorescence over the course of the recording due to accumulation of the de-esterified indicator (Fig. S2A). A change in pH_i was detected by measuring SNARF's emission at wavelengths > 600 nm, where the fluorescence intensity decreased with a decrease in pH. SNARF images were taken at 1 Hz during a run of the 8s challenge protocol to measure simultaneously the change in pH_i

and E_{gly} after complex/Ca^{2+} spiking. Shown in Fig. 5A are the concurrent changes in SNARF signal and E_{gly} induced by simple (red) and complex (black) spiking in one cell. Similar profiles were observed in 9 other cells. In all cells, the pH_i fell during both complex and simple spiking, and the recovery to near control level occurred within the next 120 sec beginning immediately after the spikes terminated. The degree of acidification, however, was greater with complex spiking than with simple spiking in each cell, the peak SNARF signal 119–240 % (mean 171 %) larger with complex spiking ($p < 0.001$, paired *t*-test, n = 10). Complex spiking was evoked with 150–250 pA in different cells, and the resulting acidification and peak negative E_{gly} shift were –95 ± 16 in 1000ΔF/F (n = 10) and –1.9 ± 0.2 mV (n = 6). The corresponding values for simple spiking, evoked with 70–200 pA in the same group of cells, were –57 ± 11 in 1000ΔF/F (n = 10) and –0.8 ± 0.2 mV (n = 6). The fact that complex spiking led to a larger pH_i decrease than simple spiking suggests that the intracellular acidification may be proportional to the increase in $[Ca^{2+}]_i$. However, that an obvious negative E_{gly} shift was only observed with complex spiking suggests that the intracellular acidification may need to be larger than a threshold level to be associated with a negative E_{gly} shift.

Ca^{2+} spiking was found to cause the same pattern of pH_i change, a fall during the activity and the recovery beginning with termination of the activity, as complex spiking and simple spiking did (Fig. 5Bi-ii, controls). As illustrated in Fig. 5Bi-ii, the acidification elicited by Ca^{2+} spiking under control conditions became unnoticeable (Fig. 5Bi, n = 5 cells) or largely reduced (Fig. 5Bii, n = 3 cells) when the same amount of current injection was given in zero-Ca^{2+} (replaced with Co^{2+} or Mg^{2+}) or in 300 μM Cd^{2+}. Switching perfusion to those containing 2.4 mM Co^{2+} (zero-Ca^{2+}) or 300 μM Cd^{2+} caused

the resting E_{gly} to shift positive by 4–7 mV with an apparent shrinkage of the cell body. Nevertheless, there was an additional positive shift in E_{gly} immediately after depolarization (n=8 cells), just as in the previous experiments without SNARF. The 1000ΔF/F values at the end of the 8-sec current injection are plotted against the peak negative E_{gly} shift (in control condition) and the peak positive E_{gly} shift (in Ca^{2+} block) for the 8 cells in Fig. 5Biii. The average reduction in acidification by Ca^{2+} block was 66 ± 9 in 1000ΔF/F for the 8 data series in the plot. In Ca^{2+} block conditions, another current injection 100–250 pA larger than that used for evoking Ca^{2+} spikes was given in 7 of the 8 cells. While a larger current injection, i.e. larger depolarization, caused the positive E_{gly} shift to increase in all cells, the pH_i response to a larger current injection appeared the same in 5 of the 7 cells (Fig. 5Bi-ii), but in 2 other cells, one in zero-Ca^{2+} (Co^{2+}) and the other in 300 μM Cd^{2+}, the larger current injection revealed or enhanced a small acidification during the current injection.

Change in $[Ca^{2+}]_i$ and pH_i were monitored simultaneously with respect to an 8-sec complex spiking taking advantage of the overlapping 2-photon excitation spectra of the fluorescent indicators. The Ca^{2+} indicator Fluo-4 (n = 3) or Fura-2 (n = 5) was loaded into the cell along with SNARF by including their AM forms in the recording pipette. As shown in Fig. 5C, the rise and fall in $[Ca^{2+}]_i$ was rapid, and thus restricted to the period of spiking, in sharp contrast to the prolonged decrease in pH_i. The $[Ca^{2+}]_i$ peaked at the end of the depolarization and then within 5 sec fell to about 10–15 % (3 cells with Fluo-4) or 20–25 % (5 cells with Fura-2) of the peak. The relatively fast clearance of the Ca^{2+} rise compared to that of H^+ (pH_i recovery) after complex spiking suggests that the slow

recovery of pH_i is not secondary to a gradual recovery of Ca^{2+} but rather reflects slow H^+ removal.

Activity-independent changes in pH_i and E_{gly}

The shared Ca^{2+}-dependence and the coincidence of intracellular acidification and the negative E_{gly} shift after complex/Ca^{2+} spiking having been confirmed, the next step in testing our hypothesis was to show that the pH_i decrease is a necessary intermediate in the process of Ca^{2+}-induced negative E_{gly} shift. For this, preventing or reducing the pH_i decrease during Ca^{2+} spiking by blocking the PMCA and SERCA was attempted using carboxyeosin, an inhibitor of Ca^{2+}-H^+ ATPases (Gatto et al. 1995). This compound (diacetate form, 40 or 80 μM) was not useful both to its intrinsic fluorescence, which precluded monitoring of pH_i with SNARF and to its suppression of Ca^{2+} spikes, with only 1–3 spikes evoked at the onset of an 8-sec depolarization (see Choi and Eisner 1999).

We next examined whether E_{gly} shifts negative with an activity-independent intracellular acidification induced by a weak acid (Roos and Boron 1981; Kaila et al. 1993). Sodium propionate, 20 mM, was perfused for 100–120 sec while cells were held at –75 mV in voltage clamp (in TTX), with periodic E_{gly} measurements. In order to maintain the same $[Cl^-]_o$ throughout the period of E_{gly} measurements, cells were bathed in a solution containing 20 mM Na-methanesulfonate instead of Na-propionate before and after the propionate challenge (Kaila et al. 1993). Simultaneous records of pH_i change and E_{gly} during propionate wash-in and wash-out were obtained from 5 cells as shown in Fig. 6Ai. In all cases, the E_{gly} shifted negative (peak shift of –4.9 ± 1.6 mV compared to

the mean E_{gly} during 100 sec before propionate) as pH_i dropped during propionate perfusion (peak acidification of –84 ± 31 in 1000ΔF/F). Upon propionate wash-out, a small overshoot in pH above baseline level was observed (37 ± 26 in 1000ΔF/F), accompanied in 4 of 5 cases by a concurrent overshoot in E_{gly}, 1.6 ± 0.6 mV.

In the part of our hypothesis relating the pH_i decrease to the negative E_{gly} shift via action of NDCBE and a decrease in $[HCO_3^-]_i$, equally possible is a pH_i increase causing a positive E_{gly} shift via AE and an increase in $[HCO_3^-]_i$. To determine if an alkalinization would shift E_{gly} positive, the weak base trimethylamine ("TMA", 10 mM) was applied (Kaila et al. 1993). A parallel positive shift in E_{gly} was observed along with the TMA-induced intracellular alkalinization in all 4 cells examined (Fig 6Aii; peak shifts were 1.9 ± 0.3 mV in E_{gly} and 40 ± 9 in 1000ΔF/F). Moreover, an undershoot occurred upon TMA washout in pH_i and E_{gly}, of –51 ± 9 in 1000ΔF/F and –2.6 ± 0.9 mV, respectively. The overshoot and undershoot in pH_i during wash-out of weak acid and weak base are believed to be the consequence of activation of pH_i regulation mechanisms during intracellular acidification and alkalinization, respectively (Roos and Boron 1981). With both weak acid and weak base challenges, the E_{gly} was found to shift negative with a pH_i decrease and to shift positive with a pH_i increase. The Spearman's correlation coefficient (ρ) between E_{gly} and decimated SNARF signal (in 1000ΔF/F) was calculated for each run of propionate or TMA challenge. With propionate, the average correlation coefficient for the whole duration (800 sec) of run was 0.61 ± 0.09 ($p < 0.05$ for all 5 cases) and that for the 135-sec period of wash-in to wash-out was 0.88 ± 0.10 ($p < 0.05$ for all 5 cases). For TMA runs, the coefficient for whole duration was 0.73 ± 0.11 ($p < 0.05$ for all 4 cases) and that for the 160-sec period of wash-in and out was 0.78 ± 0.23 (p

< 0.05 in 3 cases, p > 0.05 in one). Thus far, the activity-independent pH_i decrease or increase causing negative or positive shift in E_{gly} have been confirmed.

Simultaneous monitoring of Cl^-_i and pH_i

A pH_i change may affect E_{gly} through the NDCBE/AE-mediated change in $[Cl^-]_i$, and/or through the passive change in $[HCO_3^-]_i$ along with pH_i. To examine whether $[Cl^-]_i$ actually changes during the activity-dependent negative E_{gly} shift, we used MQAE, a fluorescent dye quenched by Cl^- and relatively insensitive to pH changes(Marandi et al. 2002; Verkman 1990). MQAE loading of CWCs was done by incubating slices in the indicator. MQAE (3 mM) was loaded for 8 min at 34 °C; longer incubations or higher concentrations led to excessive depolarization and inability to maintain firing. With SNARF loaded from the recording pipette, simultaneous monitoring of pH_i and Cl^-_i by 2-photon imaging (Fig 6Bi) was done in CWCs held silent in current clamp. The MQAE fluorescence was found to increase (a decrease in Cl^-_i) after sufficient complex spiking in each cell examined, and the return to baseline took place over similar time scale as that of pH_i (Fig. 6Bii). Eight sec of depolarization-induced simple spiking examined in 4 cells did not induce a change in MQAE fluorescence while complex spiking did so in the same cells (not shown). The peak increase in MQAE signal was 33–73 in 1000ΔF/F (average 47, n = 15) after an 8-sec complex spiking evoked by 100–250 pA in different cells, and the corresponding peak decrease in SNARF signal ranged –64 to –135 in 1000ΔF/F (average –88). Interestingly, the peak in MQAE fluorescence occurred at 15.4 ± 5.4 sec from the end of complex spiking while the peak acidification was at 1.9 ± 1.5 sec (average difference, 13.5 ± 5.3 sec, paired *t*-test, p < 0.001, n = 15). The large difference

in time course for MQAE and SNARF signals argues against the possibility that MQAE fluorescence might have originated from a decrease in non-Cl^- quencher anion, such as HPO_4^{2-} and HCO_3^-, whose concentration is dependent on pH_i (Koncz and Daugirdas 1994). The time to peak of MQAE fluorescence (15 sec) was similar to that of the E_{gly} shift (16.3 sec), indicating that the E_{gly} change reflects a change in $[Cl^-]_i$.

Block of the negative E_{gly} shift by H_2DIDS

Anion exchangers, NDCBE and AE, are known to be sensitive to block by disulfonic stilbene derivatives such as DIDS and SITS (Romero et al. 2004). Using H_2DIDS, an analog of DIDS, to block NDCBE, we asked whether the change in E_{gly} can be blocked despite activity-dependent intracellular acidification. H_2DIDS (100 μM) attenuated the glycine responses but did not prohibit determination of E_{gly}. Several effects of H_2DIDS were observed prior to testing its effects on the activity-dependent shift. In H_2DIDS, the *resting* E_{gly} (in TTX) changed by –3.6 ± 2.0 mV (from control resting E_{gly} of –72 ~ –85 mV, p = 0.007, paired *t*-test, n = 6) and V_m hyperpolarized (not measured but evident from the positive shift in holding current at –75 mV). H_2DIDS increased the Ca^{2+} spikes number in response to current injection, and often the spiking did not cease immediately after termination of the stimulus. Therefore, cells were kept in voltage clamp at –75 mV throughout a run of simultaneous pH_i and E_{gly} monitoring except for 10 sec when a glycine puff and an 8-sec depolarization were given in current clamp. The greater number of Ca^{2+} spikes evoked in H_2DIDS led to a larger pH_i decrease than under control condition in each cell examined (219 ± 58 % increase in number of spikes evoked with the same current (70–300 pA in different cells) and 168 ± 34 % larger

acidification peak in SNARF signal, n = 6) (Fig. 7A, B). Importantly, however, the negative E_{gly} shift was eliminated by H_2DIDS after the excessive Ca^{2+} spiking in H_2DIDS (+0.4 ~ +1.5 mV (mean +0.9) shift compared to –1.4 ~ –4.1 mV (mean –2.6) in control conditions, n = 5; Fig. 7C). The small positive E_{gly} shift peaked at 2-sec point after Ca^{2+} spiking in H_2DIDS and is probably due to accumulation of Cl^- through a passive H_2DIDS-insensitive mechanism. The elimination of negative E_{gly} shift in H_2DIDS excludes the possibility that the negative E_{gly} shift in control conditions was primarily caused by the reduction in $[HCO_3^-]_i$ during the pH_i decrease rather than by the reduction in $[Cl^-]_i$, supporting our conclusions with MQAE.

The recovery time course of pH_i appeared slower in H_2DIDS in all cases examined, and this was evident in the cell of Fig. 7A, in which an acidification of similar magnitude to that in control experiment was obtained with a smaller current injection in H_2DIDS. In addition, the peak acidification in H_2DIDS did not occur at or immediately after the end of 8-sec depolarization (at 1.3 ± 0.6 sec in controls, n = 6) but was delayed to a later time than in control conditions (difference in time to peak 15.2 ± 8.2 sec, n = 6) (Fig. 7A, B). This suggests that the production of acid continues beyond the duration of depolarizing current injection, and the mechanism inhibited by H_2DIDS normally works to remove the acid fast enough for the pH_i to begin rising immediately after the depolarization. Though the H_2DIDS-sensitive acid removal mechanism may be the Na^+-HCO_3^- cotransporter (Chen et al. 2008b; Romero et al. 2004) as well as the NDCBE, that the slowed pH_i recovery occurred together with the block of negative E_{gly} shift in H_2DIDS supports the involvement of NDCBE.

Block of the negative E_{gly} shift by HCO_3^-/CO_2 removal

Although we interpreted the effects of H_2DIDS in terms of the block of NDCBE, the drug may also have inhibited KCC. For example, H_2DIDS and DIDS block KCC in red blood cells (Culliford et al. 2003; Delpire and Lauf 1992). To confirm that the Cl^--HCO_3^- exchangers, rather than the KCC, is involved in the negative E_{gly} shift after Ca^{2+} spiking, we investigated whether removal of HCO_3^- and CO_2 could block the negative E_{gly} shift. In addition to disabling NDCBE, HCO_3^- removal is expected to eliminate the contribution of lowered $[HCO_3^-]_i$ to the negative E_{gly} shift during a pH_i decrease. For HCO_3^-/CO_2-free condition, $NaHCO_3$ in ACSF was replaced with equimolar HEPES, and the solution was gassed with 100 % O_2 ("HEPES/O_2"). After >10 min of perfusion with HEPES/O_2, the resting E_{gly} of CWCs shifted by +0.4 ± 1.8 mV (range –3.4 ~ +2.7 mV, n = 12, p = 0.50 with paired *t*-test), and the excitability slightly increased in 9 of 12 cells. Substantial loss of HCO_3^- current through the glycine receptor in HEPES/O_2 was inferred from the observation that the biphasic, the later phase depolarizing, glycine response that was inducible by prolonging the glycine puff in CWCs was lost in HEPES/O_2 (not shown; Backus et al. 1998; Cordero-Erausquin et al. 2005; Staley et al. 1995).

Although reduced, the negative E_{gly} shift with 8-sec Ca^{2+} spiking persisted in HEPES/O_2 in all cells examined (Fig 8Ai), contrary to our expectation. However, the degree of negative E_{gly} shift on an intracellular acidification appeared lessened in HEPES/O_2 compared with that in the control, HCO_3^-/CO_2-buffered, condition. This was supported by the following findings: 1) in 5 cases (from 5 cells) of control-HEPES/O_2 pair of E_{gly}/pH_i series with 8-sec depolarization in which the number of evoked Ca^{2+} spikes was similar (0 to 4 more Ca^{2+} spikes in HEPES/O_2), the peak acidification was

larger (by 165 ± 22 % in SNARF ΔF/F) in HEPES/O_2 than in control condition (p = 0.002, paired *t*-test) while the magnitude of negative E_{gly} shift was 0.1 ± 0.9 mV less in HEPES/O_2 (p = 0.79, paired *t*-test)(Fig. 8Ai). 2) in 8 cases (from 8 cells) of control-HEPES/O_2 pair in which the negative E_{gly} shift was similar in magnitude (0 to 0.4 mV larger in HEPES/O_2), the peak acidification was larger (by 176 ± 22 %) again in HEPES/O_2 than in controls (p < 0.001, paired *t*-test) with 5.8 ± 6.2 more Ca^{2+} spikes evoked in HEPES/O_2 (p = 0.034, paired *t*-test). Also noted was that the time of peak negative E_{gly} shift became delayed to the next measurement point (10 to 15 sec later) in 6 of 12 cells subjected to HEPES/O_2, including 3 cells in which the peak time in control condition was at the first point (2 sec) after spiking (e.g. Fig 8Ai).

Despite perfusion of a nominally HCO_3^-/CO_2-free solution, CO_2 may still be produced by oxidative metabolism in cells (Voipio and Ballanyi 1997). Hydration of CO_2 could then generate sufficient HCO_3^- in the slice to drive NDCBE. Therefore, we minimized endogenous HCO_3^- production by blocking carbonic anhydrase which catalyzes the hydration of CO_2. Acetazolamide ("AZA"), a membrane-permeable inhibitor of carbonic anhydrase, added in HEPES/O_2 at 50 μM caused the resting E_{gly} of CWCs to shift negative by 4.6 ± 2.6 mV (from –64 ~ –81 mV, n = 10, p < 0.001, paired *t*-test). The excitability increased in AZA/HEPES/O_2 to the degree cells would not stop Ca^{2+} spiking after an 8-sec depolarization, so E_{gly}/pH_i series were obtained in voltage clamp as described above for H_2DIDS experiments. In AZA/HEPES/O_2, the negative E_{gly} shift was absent after an 8-sec Ca^{2+} spiking in all 10 cells examined (Fig. 8Aii). Instead, E_{gly} was positively shifted, which peaked at 8–55 sec after spiking, rather than immediately (~2 sec) (9 of 10 cells; Fig. 8Aii, B). The maximal positive E_{gly} shift over

several runs of E_{gly}/pH_i series with different current injections in single cells ranged 1.6–3.1 mV (average 2.3 mV, after 22–96 Ca^{2+} spikes evoked by 27–190 pA in different cells, n = 10).

AZA/HEPES/O_2 also had effects indicative of reduced control of pH_i. During experiments with AZA/HEPES/O_2, attempts were made to evoke similar numbers of Ca^{2+} spikes in AZA to that before AZA addition by reducing the amount of injected current during E_{gly}/pH_i series. Fig. 8C shows the peak acidification (i) and half-time of pH_i recovery (ii) plotted against the peak negative and positive E_{gly} shift for HEPES/O_2 and AZA/HEPES/O_2, respectively, for 6 cells in which the numbers of evoked Ca^{2+} spikes were similar between the two conditions (≤3 spike difference). The difference between the HEPES/O_2 and AZA/HEPES/O_2 conditions in peak acidification was not significant ($p = 0.24$, paired *t*-test), but the half-recovery time was longer by 166 ± 21 % in AZA ($p < 0.001$, paired *t*-test) as well as the time of peak acidification (delayed by 3.2 ± 1.7 sec in AZA, $p = 0.006$, paired *t*-test). Thus, like H_2DIDS in HCO_3^-/CO_2-buffered conditions, the addition of AZA in HEPES/O_2 slowed the pH_i recovery. We also tested AZA in HCO_3^-/CO_2-buffered condition. Resting E_{gly} again shifted negative by 1.8 ± 1.0 mV in AZA ($p = 0.002$, paired *t*-test, n = 8), and the excitability increased. After Ca^{2+} spiking under AZA, the E_{gly} shifted negative, and the recovery from acidification began without delay in all cells examined. Comparing control-AZA pairs of E_{gly}/pH_i series with similar number of evoked Ca^{2+} spikes (1 to 7 more spikes in AZA, n = 5 cells), however, the negative E_{gly} shift was smaller by 1.2 ± 0.5 mV in AZA ($p = 0.005$, paired *t*-test) while the peak acidification was 139 ± 20 % larger in AZA ($p = 0.002$, paired *t*-test). This effect, reduced coupling between pH_i decrease and E_{gly} shift, was similar to that observed

in HEPES/O_2. Taken together, these results suggest that the mechanism responsible for the negative E_{gly} shift is H_2DIDS-sensitive and HCO_3^--dependent, but may be able to function at low bicarbonate level (see Discussion).

DISCUSSION

We have identified a novel postsynaptic mechanism for short-term (10's of seconds) enhancement of the effectiveness of inhibition following a period of excitation. A shift in $E_{GABA/IPSP}$ that is dependent on postsynaptic activity have been reported in hippocampal neurons (Fiumelli et al. 2005) and subthalamic neurons (Wang et al. 2006). While the $E_{GABA/IPSP}$ shift in both of these regions is Ca^{2+}-dependent, it differs from the situation in CWC in several major respects. These reported shifts were long-lasting (> 30 min) and often of opposite direction to that seen in CWC. The E_{GABA} shift in hippocampal cells were depolarizing and were induced with 5 min of 10 Hz or 2.5 min of 20 Hz singly-evoked spikes. In subthalamic neurons, negative or positive shift in E_{IPSP} appeared after evoking rebound bursts at 0.1 Hz for 100 sec depending on the intra-burst frequency of the rebound burst. Unlike the positive E_{gly} shift in CWCs, the positive shift in this study was eliminated by application of Ca^{2+} channel blockers. The proposed mechanism for the E_{GABA} shift in hippocampal neurons was Ca^{2+}-mediated down regulation of KCC2. It may be that the mechanism we have identified is of general significance but precedes the longer lasting Cl^- shifts described above. Given its dependence on dynamic control of intracellular Cl^- and pH, the drop in E_{gly} we describe may have been missed in studies that do not employ perforated patch recording.

E_{gly} and its relation to changes in intracellular Cl^-

Glycine responses in different CWCs ranged from depolarizing excitation to hyperpolarizing inhibition, reflecting the range of resting E_{gly} (–58 to –87 mV). The relation between these values for E_{gly} and $[Cl^-]_i$ can be understood using the Goldman-Hodgkin-Katz (GHK) voltage equation, $E_{gly} = (RT/F) \ln((([Cl^-]_i + r\,[HCO_3^-]_i)/([Cl^-]_o + r\,[HCO_3^-]_o))$. This is illustrated in Fig. S3A-B for a range of $[HCO_3^-]_i$, 6–18 mM (corresponding to pH_i 6.78–7.25), with the ratio (*r*) of HCO_3^- permeability (P_{HCO3}) to that of Cl^- (P_{Cl}) of 0.2 (A) or 0.1 (B) (P_{HCO3}/P_{Cl} for glycine receptors has been measured to be 0.11 (Bormann et al. 1987) or 0.4 (Fatima-Shad and Barry 1993). The pH_i indicated for each curve of different $[HCO_3^-]_i$ in Fig. S3 is derived from $[HCO_3^-]_i/[HCO_3^-]_o = 10^{(pHi-pHo)}$ at fixed pH_o = 7.30 and $[HCO_3^-]_o$ = 20 mM, based on the assumption that the partial pressure, solubility, and the dissociation constant of CO_2 is equal intra- and extracellularly (Roos and Boron 1981). As apparent in Fig. S3A from the increasing vertical separation between curves toward the lower left corner, the influence of $[HCO_3^-]_i$ on E_{gly} increases toward smaller $[Cl^-]_i$ (Kaila and Voipio 1990b). For example, over an arbitrary resting pH_i of 6.95 – 7.15, the possible E_{gly} at $[Cl^-]_i$ of 4 mM is –84.4 ~ –80.2 mV (Δ 4.2 mV) and that at $[Cl^-]_i$ of 12 mM –61.5 ~ –59.6 mV (Δ 1.9 mV). Using the same range of resting pH_i and the two extreme values of the measured resting E_{gly}, –58 and –87 mV, the range of resting $[Cl^-]_i$ among CWCs is found to be 2–14 mM (This value could be higher due to drift in E_{gly}; See Supplemental Discussion). E_{gly} shifted negative after an 8-sec period of complex or Ca^{2+} spiking, whereas it shifted positive immediately and transiently after 8-sec of all-simple spiking or after spike-free depolarizations. The pH_i was found to drop during spike activity, particularly during

Ca^{2+}-dependent spikes. By considering the complex relation between pH, E_{gly}, and $[Cl^-]_i$, it is clear that an activity-dependent drop in E_{gly} could be associated with relative small decreases, or even increases, in $[Cl^-]_i$ depending on the change in pH (See Supplemental Discussion and Fig. S3D). This is expected given the HCO_3^- permeability of the glycine receptor.

Mechanism of the time-dependent E_{gly} shifts after spiking terminates

We hypothesized that complex/Ca^{2+} spiking caused a Ca^{2+}-dependent intracellular acidification, and that the E_{gly} shifted negative as a result of lowered $[HCO_3^-]_i$ and NDCBE-mediated Cl^- extrusion in response to the acidification. The intracellular acidification was found to occur with all types of evoked spiking (simple, complex, and Ca^{2+} spikes; see discussion below on acidification). Regarding the mechanism of Cl^- extrusion, our evidence supports a role of NDCBE in the negative E_{gly} shift: a decrease in $[Cl^-]_i$ could be seen with complex spiking, and a H_2DIDS-sensitive HCO_3^--dependent mechanism was responsible for the negative E_{gly} shift after complex/Ca^{2+} spiking. The contribution of lowered $[HCO_3^-]_i$ during acidification to the activity-dependent negative E_{gly} shift does not appear as important as the NDCBE-mediated decrease in $[Cl^-]_i$, based on the following: 1) when the Cl^--HCO_3^- exchangers were blocked under H_2DIDS, E_{gly} did not shift negative in the face of a greater fall in pH_i, 2) in nominally HCO_3^-/CO_2-free Ringer (HEPES/O_2), where the impact of change in $[HCO_3^-]_i$ on E_{gly} is expected to be greatly reduced even if a few millimolar level of intra- and extracellular HCO_3^- is considered (Fig. S3C), the E_{gly} could shift negative in comparable range of magnitude to that in control condition. It appears that the Na^+-driven Cl^--HCO_3^- exchange could run at

a reduced rate with a few millimolar extracellular HCO_3^- in HEPES/O_2, such that the E_{gly} shifted negative by the fall in $[Cl^-]_i$, consistent with the reported K_m or K_i for $[HCO_3^-]_o$ of Na^+-driven or Na^+-independent Cl^--HCO_3^- exchange of 1 to 10 mM (Boron et al. 1981; Boron and Russell 1983; Cassel et al. 1988; Olsnes et al. 1986; Vaughan-Jones 1986).

The peak negative shift in E_{gly} was observed often 9–20 sec after an 8-sec complex/Ca^{2+} spiking whereas the intracellular acidification peaked within 2 sec from termination of spiking. To explain this delay, we first consider the change in $[HCO_3^-]_i$ and components of Cl^- flux during and after evoked spiking. The labels in parenthesis below refer to those in Fig. S3D. $[HCO_3^-]_i$ is expected to decrease during spike activity (*b*-*c*), reach minimum at termination of activity (*c*) and then recover (*c*-*e*) with all types of evoked spiking, mirroring the change in the pH_i; this assumes that pH_o and CO_2 tension are constant and that the intra- and extracellular carbonic anhydrase activity is sufficient to keep the reaction $CO_2 + H_2O \leftrightarrow H^+ + HCO_3^-$ at equilibrium during the time scale of activity-dependent intracellular acidification and recovery. Passive Cl^- conductance is expected to mediate a large influx during the depolarization associated with evoked spiking (*b*-*c*). At other periods (*a*-*b*, *c*-*e*) the flux can be either inward or outward depending on the difference between the E_{Cl} and V_m, and may thus not exert as big an influence as during the depolarization. The activity of NDCBE may be negligible at the resting pH_i but increase with intracellular acidification (Boyarsky et al. 1988; Cassel et al. 1988; Roos and Boron 1981). The Cl^- efflux mediated by NDCBE would thus increase during the activity-induced pH_i decrease (*b*-*c*) and then decrease as the pH_i recovers. If indeed there is significant Cl^- influx provided by AE at rest, it would decrease during activity (*b*-*c*) and then recover afterwards, as the activity of AE is known

to diminish with intracellular acidification (Boyarsky et al. 1988; Leem et al. 1999; Olsnes et al. 1986). Regarding KCC and NKCC, the activity of NKCC2, KCC2 and KCC3 may be inhibited at acidic pH_i (Bergeron et al. 2003; see also Russell 2000), suggesting that Cl^- flux through these may be reduced during the time around the peak decrease in pH_i.

What mechanisms might underlie the time-dependent E_{gly} change after evoked spiking? These will reflect a complex, and dynamic interplay between different processes. During the period of evoked spiking (period *b*-*c* in Fig. S3D), the major pathways for Cl^- flux are the influx through passive conductance and NDCBE-mediated efflux dependent on the pH_i decrease. If the intracellular acidification during spiking becomes large enough, the NDCBE-mediated Cl^- efflux would be able to bring $[Cl^-]_i$ below the baseline level, and as a result the immediate E_{gly} (Fig. S3D, 'Q') after spiking would be negative to the baseline. Otherwise, $[Cl^-]_i$ would rise during spiking, and remain higher than the baseline immediately after spiking stops; at this time, depending on magnitude of decrease in $[HCO_3^-]_i$, the E_{gly} could be positive to (Q′) or slightly negative to (Q) the baseline level, the former corresponding to the case with simple spiking. During the early period after spiking (*c*-*d*), there is no longer a large influx of Cl^- through the passive conductance, but NKCC- and AE-mediated Cl^- influxes are likely to oppose the Cl^- efflux by NDCBE. The pH_i during this period begins gradually recovering, the NDCBE-mediated Cl^- efflux, plus any other efflux, is likely to outweigh the net influx provided by NKCC and AE. Consequently, $[Cl^-]_i$ would fall until the balance between the net Cl^- efflux and the net influx is reversed as the pH_i further recovers: thus, the E_{gly} shifts negative during early after spiking (Q→R), and its most

negative traversal is delayed to the peak pH_i decrease. Less commonly, the negative peak in E_{gly} was observed immediately after complex spiking or Ca^{2+} spiking in some cells. This may be explained by either that the net Cl^- efflux did not dominate over the net influx during the early period after spiking (*c*-*d*) due to the low activity of NDCBE or that the decrease in $[HCO_3^-]_i$, which peaks at termination of spiking, exerted more influence on E_{gly} than the change in $[Cl^-]_i$. The evidence for the latter may be found in the observation that the time of peak negative E_{gly} shift became delayed to the next measurement point in 6 of 12 cells subjected to HEPES/O_2, including 3 cells in which the negative peak in E_{gly} was immediately after spiking in control condition (e.g. Fig 8Ai).

Activity-induced intracellular acidification

The decrease in intracellular pH occurring with V_m depolarization or action potential firing has been recognized in various neurons starting from studies in invertebrates (e.g. Ahmed and Connor 1980; Thomas and Meech 1982), and the acidification's dependence on Ca^{2+} influx was demonstrated in a number of these studies (reviewed in Ballanyi and Kaila 1998; Chesler 2003). The pH_i decrease during evoked spiking in CWCs required Ca^{2+} entry, as depolarizations given in zero Ca^{2+} or after Ca^{2+} channel blockade induced little or no acidification. We did not investigate the mechanism of Ca^{2+}-dependent pH_i decrease in CWCs, but it could occur via multiple pathways: displacement of H^+ by Ca^{2+} in intracellular binding sites, mitochondrial Ca^{2+}/H^+ exchange, PMCA or SERCA-mediated Ca^{2+}extrusion, and stimulation of metabolic acid production (Ballanyi and Kaila, 1998; Chesler, 2003). The present study has a significance in that the spiking-induced pH_i decrease was demonstrated with the

gramicidin perforated-patch recording in mammalian neurons, while many previous studies utilized whole-cell recording (Meyer et al. 2000; Ritucci et al. 2005; Trapp et al. 1996a; Trapp et al. 1996b; Willoughby and Schwiening 2002). We found that the complex spiking-induced acidification was smaller and decayed faster in cells recorded whole-cell than in those recorded in perforated-patch condition (Fig. S2B). Willoughby and Schwiening (2002) have shown in whole-cell recorded cerebellar Purkinje cells that acidic pH_i transients induced by depolarization or spiking were greater in dendrites than in soma. Given the large dendritic Ca^{2+} signals characteristic of CWCs (Roberts et al. 2008), complex/Ca^{2+} spiking could induce a larger negative E_{gly} shift in dendrites than that we recorded at the soma.

We recorded several non-CWCs including fusiform cells in DCN with pH imaging and found that the activity-dependent pH_i decrease did not occur as readily as in CWCs, requiring high frequency spiking (~100 Hz) evoked with a large current injection (300–500 pA) to produce a degree of acidification comparable to that seen with ~50 Hz simple spiking in CWCs (not shown). It may be that CWCs have increased tendency to acidify compared to other cells, thus are better suited to the negative shift in E_{gly}, and it could arise from any of the following: less H^+ buffering, less efficient acid removal, larger Ca^{2+} influx and less Ca^{2+} buffering.

It is worth noting that a rise in neuronal $[Cl^-]_i$ has been reported in some circumstances of V_m depolarization and intracellular acidification, such as anoxia, ischemia (oxygen-glucose deprivation), glutamate agonist or high K^+ solution application (Inglefield and Schwartz-Bloom 1998; Jiang et al. 1992; Pond et al. 2006; Slemmer et al. 2004; Van Damme et al. 2003). Among these, ischemia is a complex situations in which

a rise in $[Na^+]_i$, $[Ca^{2+}]_i$, and decrease in pH_i and pH_o all occur together, with the lactic acid production regarded as the main cause of acidification (Lipton 1999). The mechanism of increase in $[Cl^-]_i$ proposed or implicated in above studies was the influx of Cl^- through channels under the depolarized V_m. It might be that the severe V_m depolarization which may not subside fast after removal of these stimuli (ischemia, glutamate perfusion, etc.) would prevent possible NDCBE-mediated Cl^- efflux to drive $[Cl^-]_i$ below the baseline.

Functional relevance of shifts in E_{gly}

The glycine effect on spontaneous activity was variable in different CWCs. The resting E_{gly} appears to be an important determinant in this, as there was a significant difference in its level between the excitatory response group of CWCs and the inhibitory group. The broad range of CWCs' resting E_{gly} with the upper end reaching above the average fast spike threshold (–60 mV; Kim and Trussell, 2007) is thought to have resulted in the spectrum of responses comprising obvious excitation and hyperpolarizing inhibition. Furthermore, in individual CWCs the glycine effect could become more inhibitory or switch from excitation to inhibition with prolonged complex spiking, and this also occurred through a negative shift in E_{gly}. On the other hand, the E_{gly} was found to be shifted positive just after a period simple spiking or some cases of complex spiking, which suggests that the positive shift existed during spiking. However, because the V_m is also depolarized during spiking (or during increased rate of spiking), the positive shift in E_{gly} is not thought to promote the glycine effect toward the excitation. Rather, the positive E_{gly} shift, which originates from the passive Cl^- conductance, may serve to

reduce the increase in inhibitory glycine effect (E_{gly}–V_m) that occurs immediately with a V_m depolarization. Golding and Oertel (1996) proposed that the weakly excitatory glycinergic and GABAergic input in CWCs at rest could become inhibitory when the cell fires at a higher rate (i.e. V_m depolarization) not discriminating whether the activity involves complex spikes and apparently assuming the $E_{gly/GABA}$ remains the same. A similar view to Golding and Oertel (1996) on the sign of the GABAergic input in cerebellar molecular layer interneurons, which also could to be both excitatory and inhibitory, has been presented by Chavas and Marty (2003). It should be noted that the activity-dependent E_{gly} shifts we observed were associated with a rather long duration of spiking and that if the activity change were of short duration or of small change in frequency, the passive and pH-dependent components might be equal, and thus serve to stabilize E_{gly}.

It is unclear why there is a difference in the observation of inhibitory glycine response in CWCs at rest between the study of Golding and Oertel (1996) and of us using similar mouse slice preparation, no hyperpolarizing PSP being seen at the resting V_m in the former study. However, the prevalence of hyperpolarizing PSPs at resting V_m of CWCs in Manis et al. (1994) or the increased CWC spiking found after strychnine or bicuculline *in vivo* in Davis and Young (2000) may have something to do with the dataset consisting of spontaneous complex spiking cells: the CWCs in the former study were all-complex spiking except three which fired both simple and complex spikes, and the latter *in vivo* study selected complex-spiking units to record. We found that few spontaneously complex spiking cells showed excitatory responses with many of these cells showing inhibitory responses to glycine. It could be that the more negative resting E_{gly} in these

cells is associated with a lower resting pH_i or dominance in activity of KCC over NKCC. In the former case, whether the low rate of spontaneous complex spikes causes the standing intracellular acid load is curious.

The prolonged high frequency complex spiking used in the present study to induce a noticeable negative E_{gly} shift may only rarely occur in physiological settings. However when such activity happens, the increase in glycinergic/GABAergic inhibition through the negative E_{gly} shift is expected to reduce the frequency of complex spikes or terminate the complex spiking in a CWC. For cells postsynaptic to a CWC, the DCN principal cells or other CWCs, this mechanism would limit the frequency of the large burst-form PSPs originating from presynaptic complex spikes (Roberts et al. 2008; Tzounopoulos et al. 2004), and thus limit the maximal glycinergic inhibition or excitation coming from a CWC. In the perspective of inhibitory interneuron network, the variation in CWCs' resting E_{gly} enabling both excitatory and inhibitory connections seems to stabilize the inhibition the network provides to the principal neurons, compared to having only one kind of connection, as has been suggested for cerebellar interneurons (Chavas and Marty 2003). It would be of interest to examine other neuronal cell types with $E_{gly/GABA}$ range spread over excitatory level for the presence of the activity-dependent and intracellular acidification-dependent shift in $E_{gly/GABA}$.

SUPPLEMENTAL RESULTS

Effect of bumetanide.

We have tried blocking NKCC with bumetanide (50 μM) to rule out the possibility that inactivation of NKCC during Ca^{2+} spiking contributes to the negative E_{gly}

shift after Ca^{2+} spiking (n = 5). The resting E_{gly} (in TTX, without dye) shifted by –3.4 ± 1.7 mV (p = 0.012, paired *t*-test) during the initial 15 min of bumetanide superfusion, and then remained relatively stable (ΔE 0–0.6 mV) over the next 15 min. The largest shift (–6.1 mV) in resting E_{gly} was observed from a cell with a control resting E_{gly} of –69.8 mV, the most positive among the 5 cells, and the smallest shift (–1.1 mV) was from a cell with the most negative control E_{gly} (–76.7 mV). The correlation coefficient (*r*) between the control resting E_{gly} and the magnitude of negative shift in resting E_{gly} in bumetanide was –0.88 (n = 5, p = 0.049). Among the four cells in which resting E_{gly} were measured > 10 min after bumetanide wash-out, only the cell that had the largest negative shift in the drug showed a partial recovery (by 2.2 mV) in E_{gly}, and in others the E_{gly} shifted further negative by 0.5 to 1.3 mV. The Ca^{2+} spiking-induced negative E_{gly} shift persisted in bumetanide with similar magnitude to control condition in all 5 cells. In 2 of 5 cells, the half-time of recovery from the negative E_{gly} shift appeared delayed by about 5 sec in bumetanide compared to under control conditions, but in other cells the time course was almost identical.

$[Ca^{2+}]_i$ change associated with weak acid/base application.

Changes in $[Ca^{2+}]_i$ during intracellular acidification or alkalinization induced with weak acid or base have been reported in various cell types, but the direction of change was rather inconsistent across different studies. For example, increase in $[Ca^{2+}]_i$ was shown during both the intracellular alkalinization and acidification induced by NH_4Cl or other weak base and weak acid by Batlle et al. (1993), Martinez-Zaguilan et al. (1996), OuYang et al. (1994) and Wu et al. (1999), but a decrease in $[Ca^{2+}]_i$ during

NH_4Cl-induced intracellular alkalinization has also been demonstrated by Iino et al. (1994) and Kaila and Voipio (1990). Whether in CWCs, the propionate-induced acidification and the TMA-induced alkalinization were associated with a rise and fall in $[Ca^{2+}]_i$, respectively, may also be questioned. If this is true, then both the weak acid-mediated and the complex spiking-mediated negative shift in E_{gly} may be regarded as a consequence of Ca^{2+}'s modulation of Cl^- transporters. We did not monitor $[Ca^{2+}]_i$ during the propionate or TMA challenge but have done simultaneous Fura-2 and SNARF imaging with NH_4Cl on 5 CWCs held at –75 mV in v-clamp (in TTX). Five mM NH_4Cl for CWCs caused a barely noticeable alkalinization at wash-in, which was soon followed by an acidification during the presence of NH_4Cl (2 min). The peak intracellular acidification occurred within 1 min of NH_4Cl wash out (–153.6 ± 28 in 1000ΔF/F, n = 5). In none of the 5 CWCs, was there a noticeable change in Fura-2 signal ($Ca^{2+}{}_i$) during wash-in and out of NH_4Cl, while an 8-sec complex spiking or Ca^{2+} spiking produced a clear signal (–276 ± 46 in 1000ΔF/F) in the same cells. Therefore, considering that the NH_4Cl-induced intracellular acidification is larger than that by propionate (–84 ± 31 in 1000ΔF/F), it seemed unlikely that $[Ca^{2+}]_i$ rose significantly during the propionate-induced acidification in CWCs.

SUPPLEMENTAL DISCUSSION

Potential causes of slow negative drift in E_{gly}

The actual range of $[Cl^-]_i$ in CWCs may lie in higher values than that estimated with the GHK equation because there was the tendency for the resting E_{gly} to drift negative with time, and the reported resting E_{gly} values are those obtained some time after the drift had been noticed. The reason for the slow negative drift over time in resting E_{gly}

is not clear. It is possible that, during the gramicidin perforated-patch recording, activation of KCCs and/or inactivation of NKCC (lowering $[Cl^-]_i$) occurred or an intracellular acidification (lowering $[HCO_3^-]_i$) developed. Slow intracellular acidification may occur unrelated to the perforated-patch recording due to possible build-up of metabolically generated acids in slice (cf. Trapp et al. 1996a); however, this is unlikely in our case given that the negative drift in E_{gly} is generally faster during the early period of recording. The more negative resting E_{gly} in AM dye-loaded cells may be associated with lower resting pH_i levels due to increased intracellular acid generation from the de-esterification reaction, the byproducts of which are acetic acid and formaldehyde (which can be converted to formic acid). However, the acid build-up from AM ester hydrolysis is not expected to be too large because acetic acid and formaldehyde can diffuse out of the cell, and acetate may also be eliminated from the cell along with a H^+ by monocarboxylate transporters (Pierre and Pellerin 2005).

E_{gly} shifts viewed with the Goldman-Hodgkin-Katz equation

A typical change in E_{gly} and pH_i associated with complex/Ca^{2+} spiking and simple spiking is drawn in Fig. S3D with labeled time periods and E_{gly} points. The change in $[Cl^-]_i$ involved in the activity-dependent shifts in E_{gly} was estimated by identifying points along the curves of E_{gly} vs. $[Cl^-]_i$ at different pH_i levels assuming constant CO_2 tension and pH_o (GHK equation with $P_{HCO3}/P_{Cl} = 0.2$; Fig. S3A). The finding from such examination is described below with labels in parenthesis referring to Fig. S3D. 1) The decrease in $[Cl^-]_i$ that can occur with a negative shift in E_{gly} associated with a pH_i decrease (P→Q or P→R) is less than, i.e. limited by, what would occur

without a pH_i change. This leads to prediction of less than 1.6 mM and 0.7 mM decrease in $[Cl^-]_i$ for a 3 mV negative shift accompanied with a pH_i decrease from E_{gly} –60 mV and –80 mV, respectively. The $[Cl^-]_i$ decreases less the larger the intracellular acidification for a given magnitude of negative E_{gly} shift. 2) For a negative E_{gly} shift associated with a pH_i decrease (P→Q) and for a positive E_{gly} shift occurring with a pH_i increase (R→S), it is possible for the $[Cl^-]_i$ to change in the opposite direction to that of pH_i if the pH_i change is large enough. For example, if pH_i = 7.15 ($[HCO_3^-]_i$ = 14 mM) and E_{gly} = –72 mV ($[Cl^-]_i$ = 6.5 mM) in baseline condition and the E_{gly} shifts by –1 mV (i.e. P→Q), then $[Cl^-]_i$ must *rise* if the pH_i falls more than 0.06 unit ($\Delta[HCO_3^-]_i$ = –1.7 mM). If the E_{gly} shifts by –3 mV (to –75 mV), the $[Cl^-]_i$ rises for acidification > 0.20 pH unit ($\Delta[HCO_3^-]_i$ = –5.0 mM). 3) However if the E_{gly} goes negative with a pH_i rise (Q→R) or shifts positive with a pH_i drop (P′→Q′), the $[Cl^-]_i$ is bound to fall (Q→R) or rise (P′→Q′), and the change in $[Cl^-]_i$ is greater than that without a pH_i change. For example, if the E_{gly} and pH_i at baseline is –72 mV and 7.15, respectively, and each shifts by +1 mV and –0.04 after simple spiking (P′→Q′), the increase in $[Cl^-]_i$ is 0.56 mM, which is 0.2 mM larger than what is expected without a pH_i change.

The predictions of the effect of pH_i decrease (i.e. lowered $[HCO_3^-]_i$) on the E_{gly} shifts were based on a P_{HCO3}/P_{Cl} of 0.2 for the glycine receptor. The influence of $[HCO_3^-]_i$ on the magnitude of E_{gly} shifts becomes less if the P_{HCO3}/P_{Cl} is smaller (Fig. S3B) or if the concentration of intracellular and extracellular HCO_3^- is low at the same P_{HCO3}/P_{Cl} (Fig. S3C). It should be added that the P_{CO2} and pH_o may not be constant during the spiking activity associated with E_{gly} shifts (Chesler 2003; Voipio and Kaila 1993), which

would compromise our estimations of $[Cl^-]_i$ change based on constant values of P_{CO2}, pH_o, and $[HCO_3^-]_o$.

We do not know the absolute values of resting pH_i or the magnitude of pH_i decrease induced by complex /Ca^{2+} spiking in CWCs. However, 20 mM propionate caused a similar range of peak changes in SNARF signal (–5 ~ –12 % ΔF/F) to that observed with complex/Ca^{2+} spiking in CWCs; moreover, intracellular acidifications of 0.04–0.15 pH unit were observed with 20 mM propionate in other cell types in HCO_3^--buffered condition (Jacobs et al. 2008; Saarikoski et al. 1997; Xiong et al. 2000). Thus, assuming CWCs buffer pH at a level similar to that of other cells, the peak decrease in pH_i with complex/Ca^{2+} spiking may have been less than 0.2 pH units in HCO_3^--buffered condition. Therefore, at least for cases where the peak negative E_{gly} shifts of > 3 mV occurred after some recovery from peak acidification (e.g. Fig 5Bi control, 280 pA trace), the $[Cl^-]_i$ must have fallen below baseline level, probably by 1~2 mM. Given that the predicted decrease in $[Cl^-]_i$ was generally less than 2 mM with up to 4 mV negative shift in E_{gly}, it is understandable that the increase in MQAE fluorescence (reflecting a decrease in $[Cl^-]_i$) was weak and became noticeable after rather excessive induction of complex spiking in each cell tested (Fig 6Bii); a ~1 mM change in $[Cl^-]_i$ seems unlikely to yield a detectable change in MQAE signal based on the intracellular calibration curve of Marandi et al. (2000).

Factors contributing to resting E_{gly} in CWCs

Given the discussion above, it is clear that in individual cells, the levels of $[Cl^-]_i$ and $[HCO_3^-]_i$ together determine the E_{gly}. The mechanism determining the resting E_{gly} in

CWCs was not the focus of the present study, but some hints were gathered from the change in resting E_{gly} observed with certain experimental conditions. NKCC1 is likely to provide a steady inward transport of Cl^- in CWCs as bumetanide shifted the resting E_{gly} negative. In some cells, the H_2DIDS or AZA/HEPES/O_2-induced negative shift in resting E_{gly} involved conversion to a hyperpolarizing glycine response (e.g. Fig 7A). This suggests that the resting Cl^- extrusion mechanism partially survived in H_2DIDS, and thus is most likely due to KCC. AE-mediate Cl^- influx may contribute to steady-state $[Cl^-]_i$, given that H_2DIDS or AZA (in HCO_3^-/CO_2-buffered or HCO_3^-/CO_2-free Ringer) shifted resting E_{gly} negative. However, this result could have arisen from block of constitutively active Na^+-HCO_3^- co-transport. The net transport direction of the electroneutral Cl^--HCO_3^- exchange by AE is determined by the transmembrane concentration gradient of Cl^- and HCO_3^- (equilibrium when $[Cl^-]_i/[Cl^-]_o = [HCO_3^-]_i/[HCO_3^-]_o$), and thus it can be made to work in the reverse mode (Cl^- efflux and HCO_3^- influx) if bath Cl^- is lowered or the intracellular pH_i is decreased enough (Vaughan-Jones 1986). In our experimental setting of $[Cl^-]_o$ = 136.8 mM, $[HCO_3^-]_o$ = 20 mM and pH_o = 7.30, the reversal pH_i for AE's transport direction seems to be very low (e.g. 6.24 if $[Cl^-]_i$ = 12 mM, 5.94 if $[Cl^-]_i$ = 6 mM), thus AE is expected to transport Cl^- inward under most conditions. However, while AE's participation in maintenance of high $[Cl^-]_i$ has been suggested in some smooth muscle cells (reviewed in Chipperfield and Harper 2000) and in cardiac Purkinje fibers (Vaughan-Jones 1986), whether AE can provide significant Cl^- influx at the resting pH_i (6.90–7.30) in neurons is not yet known. The Cl^--HCO_3^- exchange activity in several non-neuronal cell types as well as in AE2- or AE3-transfected cell lines has been shown to be rather low at baseline pH_i increasing steeply at alkaline pH_i (> ~ 7.2) (Boyarsky et

al. 1988; Jiang et al. 1994; Lee et al. 1991; Leem et al. 1999; Olsnes et al. 1986). Considering that the Cl^- influx by AE is accompanied by gain of acid equivalents, mechanisms removing acid, such as Na^+-H^+ exchangers (NHEs) or Na^+-HCO_3^- co-transporters (NBCs), may need to work in concert with AE for it to contribute to intracellular Cl^- level without disturbing the resting pH_i (Vaughan-Jones 1986).

Table 1. Numbers and proportions of glycine response types in spontaneously spiking CWCs

	n	[%]	exc.	(%)	mix.	(%)	inh.	(%)
no dye	113		35	(31.0)	14	(12.4)	64	(56.6)
complex-spiking	30	[26.5]	1	(3.3)	3	(10.0)	26	(86.7)
simple-spiking	83	[73.5]	34	(41.0)	11	(13.3)	38	(45.8)
AM dye	129		22	(17.1)	23	(17.8)	84	(65.1)
complex-spiking	17	[13.2]	0	(0)	3	(17.6)	14	(82.4)
simple-spiking	112	[86.8]	22	(19.6)	20	(17.9)	70	(62.5)
total	242		57	(22.3)	37	(15.3)	148	(61.2)
complex-spiking	47	[19.4]	1	(2.1)	6	(12.8)	40	(85.1)
simple-spiking	195	[80.6]	56	(28.7)	31	(15.9)	108	(55.4)

% values in [] are the proportion of complex-spiking or simple-spiking cells.

Table 2. Resting E_{gly} of cartwheel cells

		n	E_{gly} (mV)	SD	range
Total		164	–74.3	5.8	−87.4, −58.0
spiking		101	–74.0	5.9	−87.0, −58.0
	exc	24	–68.5	4.6	−75.9, −58.0
	mix	16	–69.9	3.0	−77.1, −65.5
	inh	61	–77.3	4.5	−87.0, −68.3
silent (V_m –81.4 ± 2.8 mV)		63	–74.5	5.8	−87.4, −60.8
no dye		92	–73.1	5.3	−85.0, −58.0
SNARF–AM		72	–75.6	6.3	−87.4, −63.2

See Supplemental Discussion for the possible cause of more negative E_{gly} in AM-dye loaded cells.

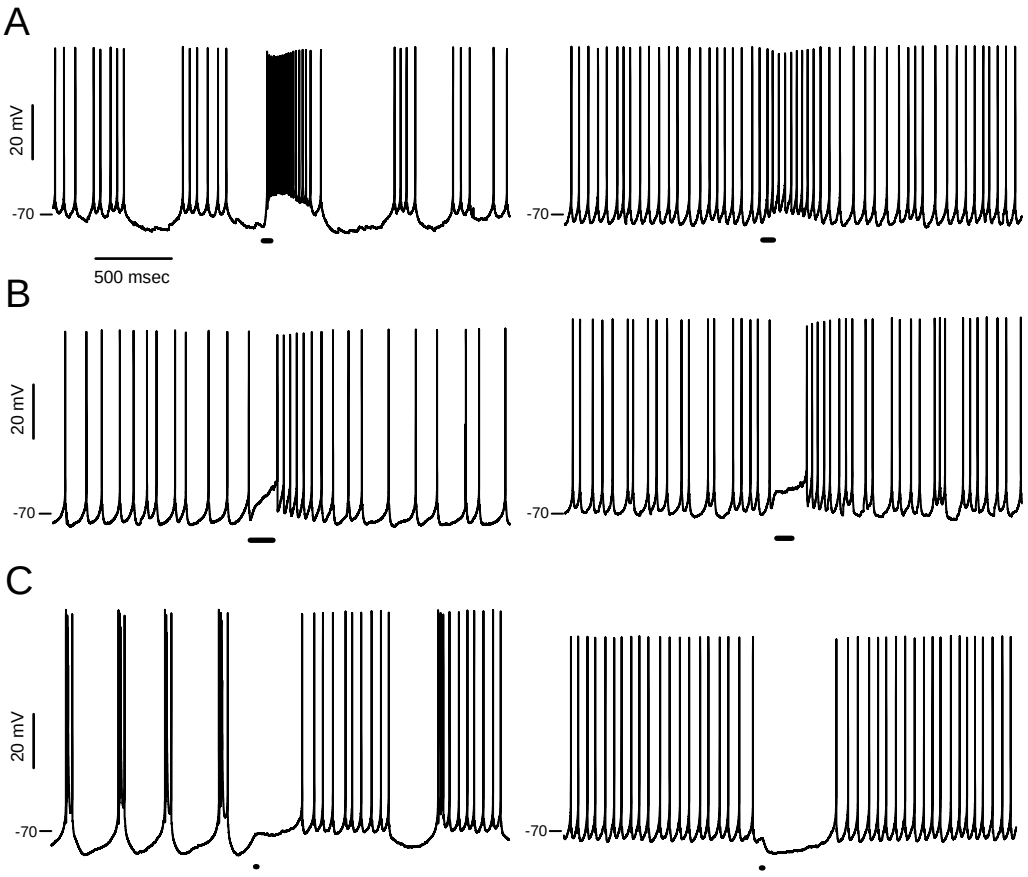

Figure 1. Three types of glycine response in spontaneously spiking CWCs Examples of excitory, A, mixed, B, and inhibitory, C, responses to a glycine puff during spontaneous activity. The duration of the glycine puff is indicated with a bar, and the glycine concentration was 0.5, 0.5, 0.5, 0.5, 2, 2 mM for the six cells in left-to-right, top-to-bottom order.

Figure 2. Activity-dependent shifts in the glycine response.

(A) An example of the negative glycine response shift occurring with prolonged complex spiking. An all-simple-spiking cell with excitatory glycine response was injected 100 pA at t = 0, with which the complex spikes began appearing at t = 27 s. The weakly inhibitory effect of glycine at t = 23 s became more inhibitory (t = 105 s) as complex spiking continued. After termination of depolarization, the glycine responses were hyperpolarizing until the 4th response (t = 182), and the recovery to the excitatory response took ~100 seconds (t = 242 s). Arrowheads indicate time of a 500 μM glycine puff, and the red line is drawn at –70 mV for reference.

(B) Comparison of the change in glycine responses following simple spiking and complex spiking. An all-simple-spiking cell with inhibitory glycine (2 mM) response was silenced with –110 pA bias current and induced to fire late complex spikes (top) or trains of simple spikes (bttom), with an 8-sec step of 250 pA and 170 pA, respectively. Insets show the expansion of a 0.8-sec segment at 7 sec into depolarization. The red line is aligned to the peaks of glycine responses before the evoked activity.

The negative shift in glycine response is noticeable (∗) after complex spiking, while an immediate positive shift is obvious (o) after simple spiking. The vertical line in the middle of bottom trace is a complex spike evoked on top of a postsynaptic potential.

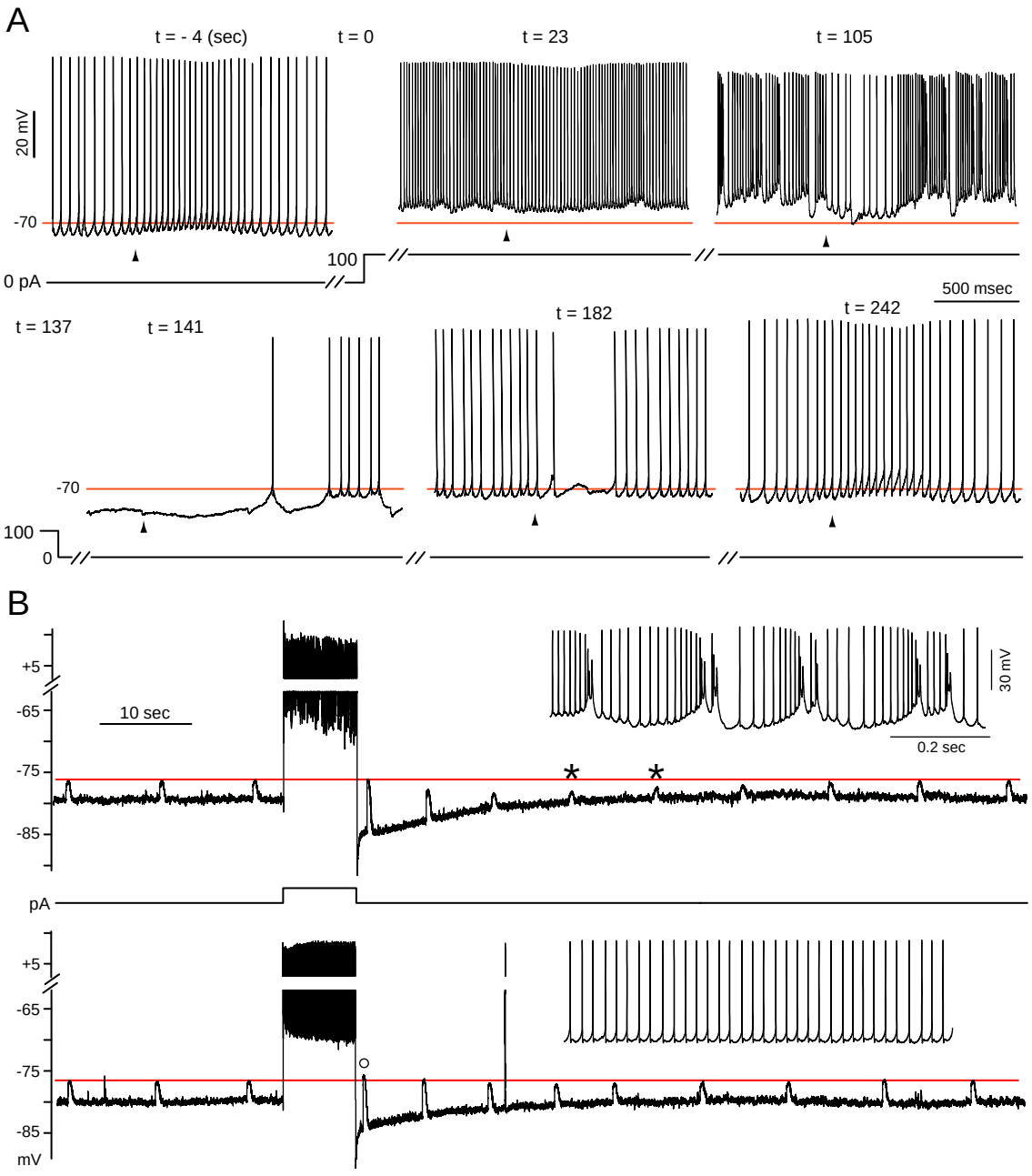
A
t = - 4 (sec)
t = 0
t = 23
t = 105
20 mV
-70
0 pA
100
500 msec
t = 137
t = 141
t = 182
t = 242
-70
100
0
B
+5
-65
-75
-85
10 sec
30 mV
0.2 sec
pA
+5
-65
-75
-85
mV

Figure 2

Figure 3. More evidence of negative shift in $E_{gly.}$

(A) Glycinergic/GABAergic PSPs were evoked at 0.5 Hz in a cell spontaneously spiking in bursts of simple spikes in the presence of 100 μM APV and 10 μM DNQX. The downward deflections of the stimulus artifacts are clipped. Four segments from a 150-sec-long V_m recording are shown in sequence. Complex spiking was induced after 20 sec of control period by 75 pA injection (depol) for 30 sec, and the inset above shows the expansion of a 0.8-sec segment at 25 sec into depolarization. Shown at bottom are overlays of 5–6 evoked PSPs chosen from the period indicate above. The PSPs were depolarizing at V_m –77 mV during the pre-depolarization period. Just after the depolarization and complex spiking, PSPs were hyperpolarizing even at –81 mV but became depolarizing at –77 mV again over the next 100 sec.

(B) More examples of evoked glycinergic/GABAergic PSPs shifting negatively after complex spiking. The bias current during pre-depolarization period for cell 1, 2 and 3 was –45, –60 and 0 pA, respectively, and the current was adjusted post-depolarization to hold the V_m close to the pre-depolarization level.

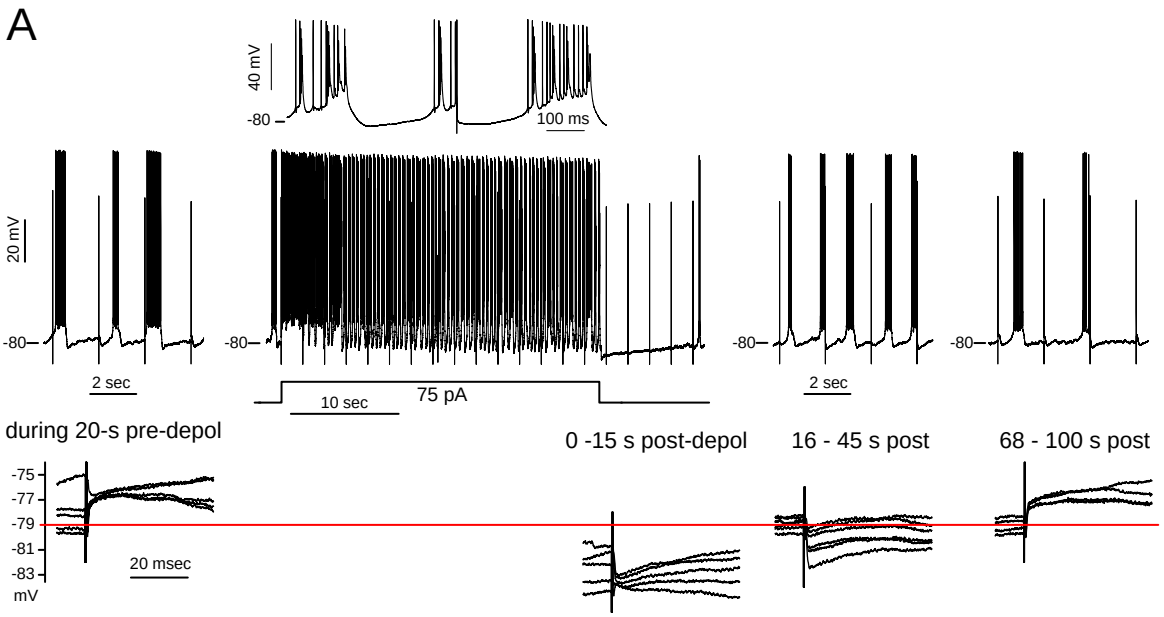

B

	20-s pre-depol	depol & complex spikes induced with	15-35 s post-depol	85-115 s post-depol
cell 1	-77 -79 -81 mV, 20 msec	100 pA, 10-sec	-77 -79 -81	-77 -79 -81
cell 2	-73 -75 -77	200 pA, 16-sec	-73 -75 -77	-73 -75 -77
cell 3	-78 -80 -82	200 pA, 10-sec	-78 -80 -82	-78 -80 -82

Figure 3

Figure 4. Ca^{2+}-dependent and -independent E_{gly} shifts.

All data in the figure except (Cii-iii) were obtained in TTX and glycine (2 mM) responses are marked with arrowheads.

(A) An example of glycine responses shifting negative during long Ca^{2+} spiking. Ca^{2+} spikes were evoked for 42 sec by +70 pA from –30 pA bias. A negative shift and recovery in E_{gly} was evident as the polarity of glycine responses changed from depolarization to hyperpolarization after Ca^{2+} spiking and back to depolarization. The hyperpolarization to –80 mV at 2 sec into depolarization was an afterhyperpolarization of the first Ca^{2+} spike, and the fluctuation of V_m during 10 sec after Ca^{2+} spiking is thought to be a manifestation of the intrinsic bistability of CWCs.

(B) Plot of the peak negative shift in E_{gly} versus the number of high-threshold Ca^{2+} spikes evoked during an 8-sec challenge protocol. Dots represent 148 E_{gly} series from 83 CWCs. 104 series are from 55 cells recorded with AM dye solution and 44 series from 28 cells without dye.

(C) The shifts in E_{gly} at 2 sec after an 8-sec Ca^{2+} spiking (i), complex spiking (ii), or simple spiking (iii) are plotted against the peak negative shift of the E_{gly} series. Dots in each plot represent single E_{gly} series from different cells and the numbers are 44, 29, and 8 for (i), (ii), and (iii), respectively.

(D-E) Data from one cell comparing glycine responses and E_{gly} measurements in control condition (B) with those in zero-Ca (C). Time 0 is the moment the 8-sec depolarizing current injection terminated. (Di) After 56 high-threshold Ca^{2+} spikes induced with a 220 pA injection, the glycine response shifted negative. (Dii) The E_{gly} series measured along with the V_m recording in (Di) is shown (●) with two other series obtained with different

amount of current injections. The negative E_{gly} shifts peaked at 8.5 sec. The holding current at the –75 mV holding potential (I_H) of the v-ramp protocol is plotted below for reference. (Ei,ii) The V_m and E_{gly} series in zero-Ca (replaced with Mg^{2+}) are displayed in the same way as in (D). After a depolarization in zero-Ca, no negative shift but a positive shift in E_{gly} occurred. Bias current was –40 pA in (Di) and –55 pA in (Ei).

(F) Bar graphs showing the peak change in E_{gly} after an 8-sec current injection (amount in pA indicated above each bar) in control condition and in zero-Ca, from 6 cells. Number of Ca^{2+} spikes evoked is shown in parenthesis under each bar belonging to control conditions.

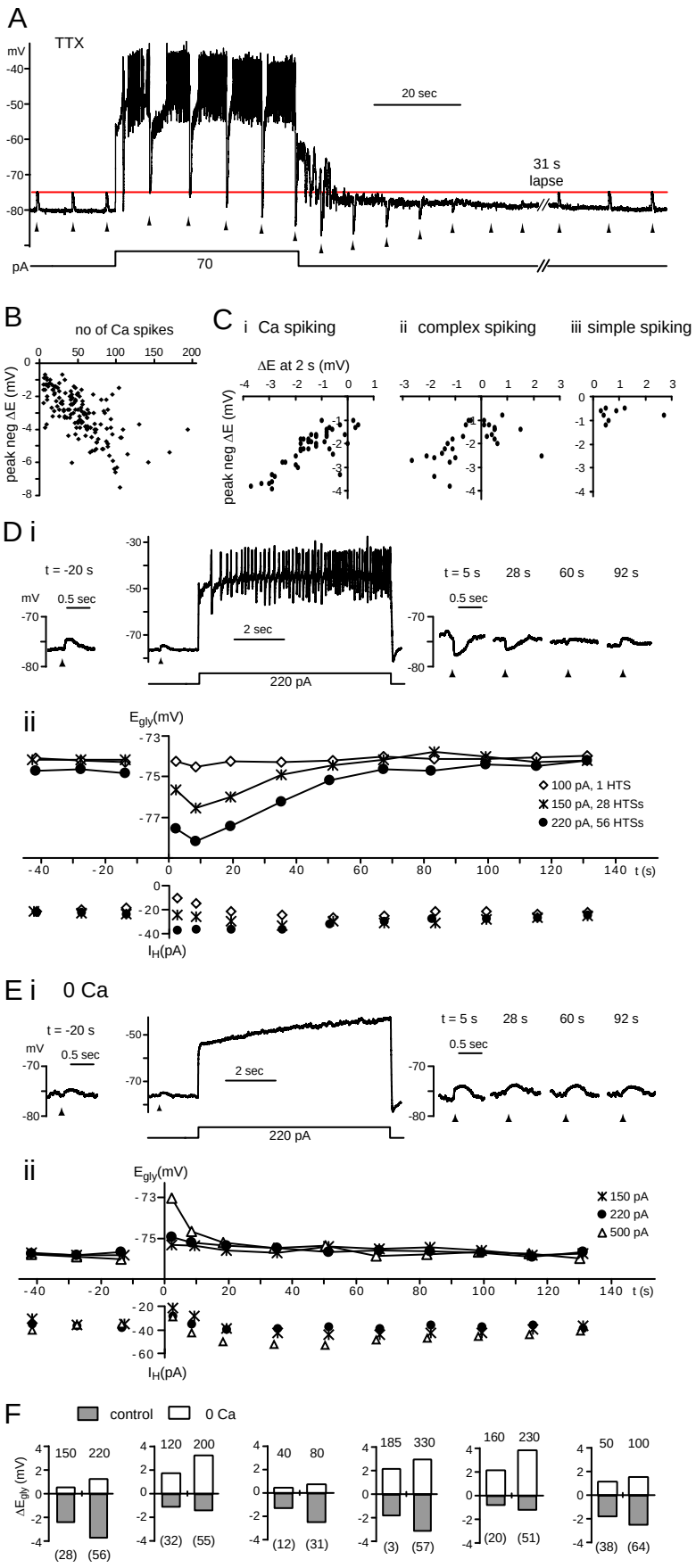
A
TTX
mV
-40
-50
-60
-70
-80
20 sec
31 s
lapse
pA
70
B
no of Ca spikes
0
50
100
150
200
peak neg ΔE (mV)
C
i Ca spiking
ii complex spiking
iii simple spiking
ΔE at 2 s (mV)
peak neg ΔE (mV)
D i
t = -20 s
mV
0.5 sec
2 sec
220 pA
t = 5 s
28 s
60 s
92 s
ii
E_{gly}(mV)
100 pA, 1 HTS
150 pA, 28 HTSs
220 pA, 56 HTSs
t (s)
I_H(pA)
E i
0 Ca
ii
150 pA
220 pA
500 pA
F
control
0 Ca
ΔE_{gly} (mV)
150
220
120
200
40
80
185
330
160
230
50
100
(28)
(56)
(32)
(55)
(12)
(31)
(3)
(57)
(20)
(51)
(38)
(64)

Figure 4

Figure 5. Ca^{2+}-dependent intracellular acidification.

(A) Simultaneous monitoring of pH_i and E_{gly} with respect to an 8-sec simple spiking (red) and complex spiking (black) in one cell. Arrowheads indicate glycine (2 mM) responses. The pH-sensitive dye SNARF-5F's signal is the average fluorescence intensity of a region of interest drawn inside cell body. An intracellular acidification, manifest as a decrease in SNARF's signal, was found to occur both during simple spiking and complex spiking. Black bar above SNARF traces indicate the duration of 8-sec depolarizing current injection evoking simple spiking or complex spiking.

(B) The intracellular acidification was also seen with Ca^{2+} spiking (in TTX) and inhibited by zero-Ca (replaced with Co^{2+} or Mg^{2+}) or 300 μM Cd^{2+}. (Bi-ii) Simultaneously obtained SNARF signal and E_{gly} from two cells. The 8-sec depolarizing current injections evoking Ca^{2+} spikes or just depolarization in Ca^{2+} block are marked with thick bars above SNARF traces. The amount of injected current is shown beside each symbol along with the number of evoked Ca^{2+} spikes in parenthesis. An example of apparent complete block (Bi) and incomplete block (Bii) of the depolarization-induced acidification by zero-Ca is shown. (Biii) Plot relating the change in SNARF signal to the peak negative E_{gly} shift in control condition and the peak positive E_{gly} shift in Ca^{2+} block condition for 8 cells.

(C) The change in pH_i and $[Ca^{2+}]_i$ induced by 8-sec complex spiking were simultaneously detected by 2-photon imaging of SNARF-5F and Fluo-4 or Fura-2. Two examples from different cells are shown. The duration of 8-sec depolarizing current injection evoking complex spikes is indicated by the shaded rectangle. The excitation wavelengths were 800 nm (Ci) and 780 nm (Cii).

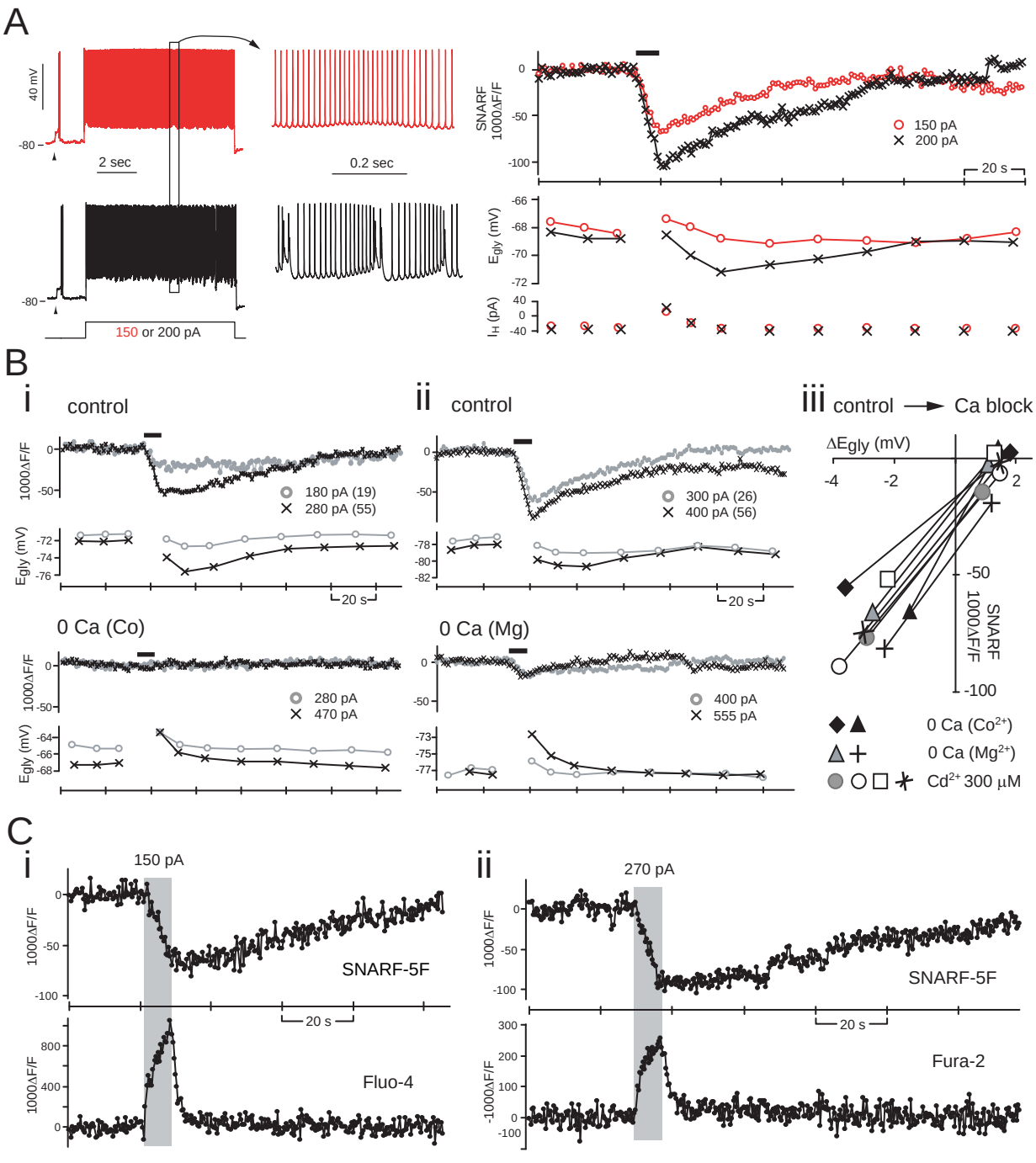
A
40 mV
-80
2 sec
0.2 sec
150 or 200 pA
SNARF
1000ΔF/F
150 pA
200 pA
20 s
Egly (mV)
IH (pA)
B
i control
ii control
iii control → Ca block
180 pA (19)
280 pA (55)
300 pA (26)
400 pA (56)
0 Ca (Co)
0 Ca (Mg)
280 pA
470 pA
400 pA
555 pA
ΔEgly (mV)
0 Ca (Co2+)
0 Ca (Mg2+)
Cd2+ 300 μM
C
i
150 pA
SNARF-5F
Fluo-4
ii
270 pA
Fura-2

Figure 5

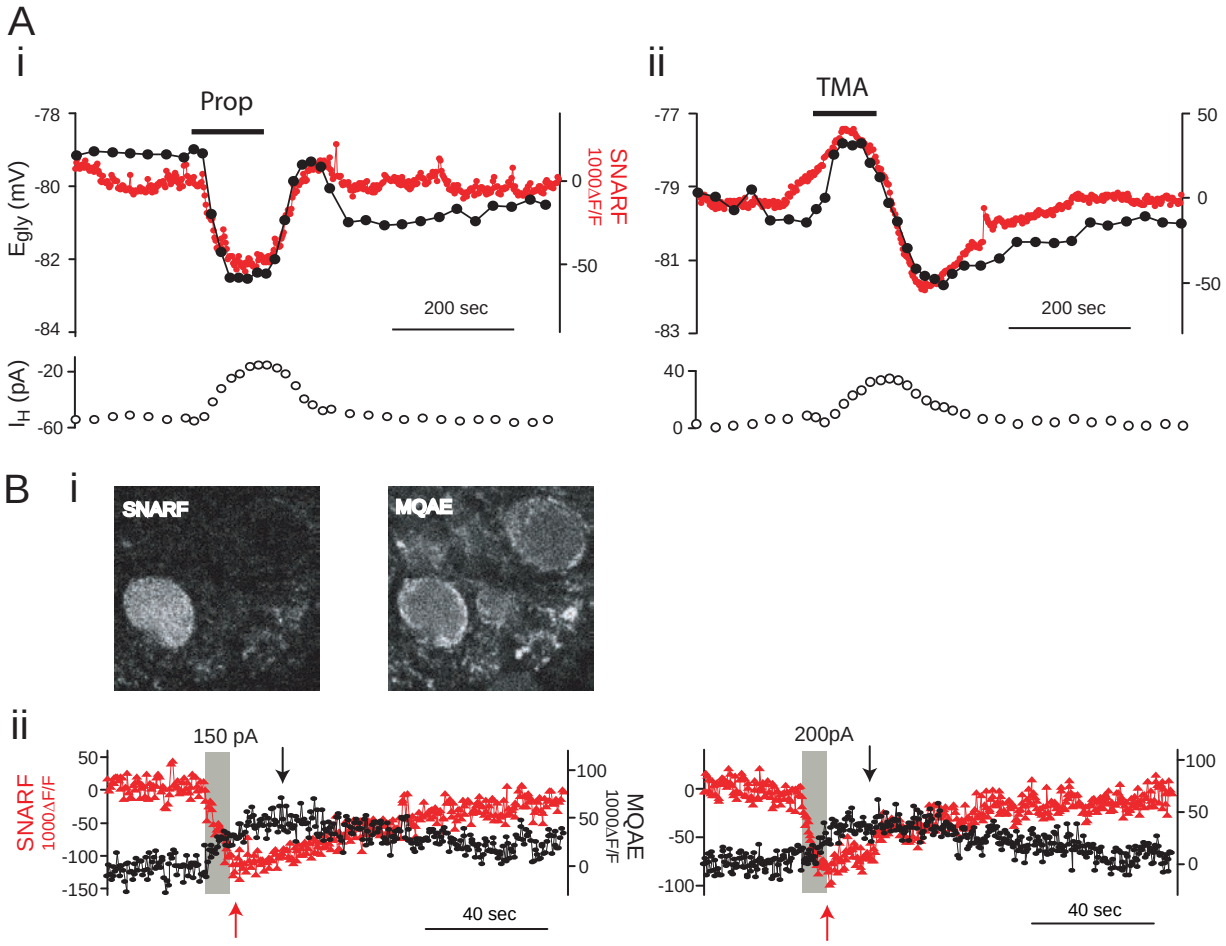

Figure 6. Activity-independent pHi and E_{gly} change and simultaneous Cl and pH imaging (A) Examples showing the concurrent changes in E_{gly} (left ordinate) and pH_i (right ordinate) induced during and after 20 mM sodium propionate (i) and 10 mM TMA (ii) perfusion for inducing intracellular acidification and alkalinization, respectively. SNARF images were obtained at 0.5 Hz while cells were held at -75 mV in v-clamp in TTX.
(B) Simultaneous 2-photon imaging of intracellular pH and Cl^- with SNARF and MQAE. Excitation wavelength at 750 nm. (Bi) Two images of one area taken at the same time through the red emission channel (SNARF) and green channel (MQAE). MQAE was bulk-loaded into DCN slice, and SNARF was loaded from the recording pipet on the left of the cell in lower left. Inhomogeneous staining with MQAE is typical. (Bii) Simultaneous records of pH_i (SNARF) and Cl^-_i (MQAE) obtained from two different cells. An 8-sec complex spiking was evoked during the period of gray rectangle with the indicated amount of current. The peak of each signal is indicated with an arrow.

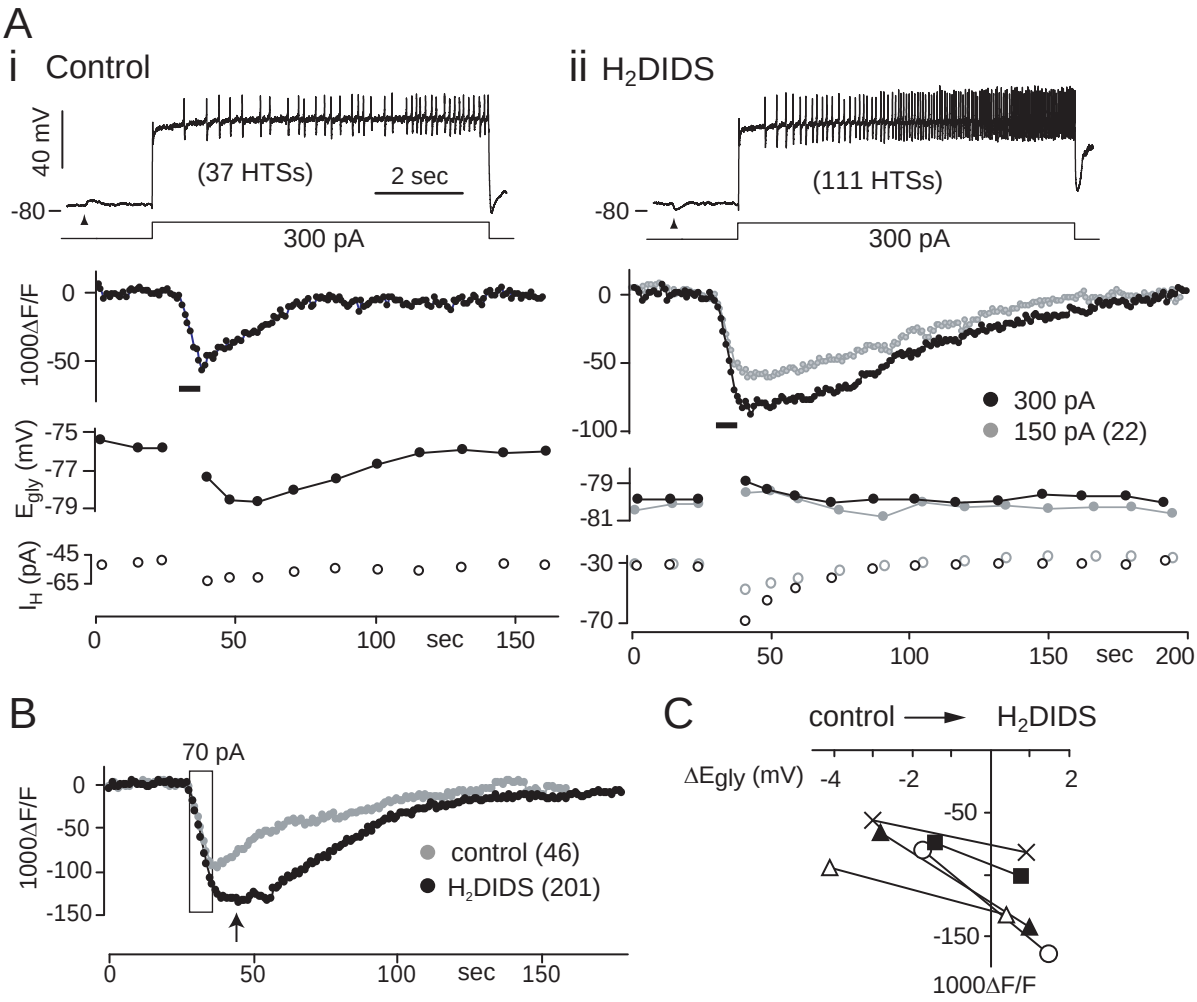

Figure 7. Block of the negative E_{gly} shift by H_2DIDS

(A) Simultaneously obtained SNARF signal and E_{gly} from one cell are shown for control condition (i) and in100 µM H_2DIDS (ii) along with the V_m trace of Ca^{2+} spiking. Thick bars indicate periods of 8-sec Ca^{2+} spiking. Arrowheads indicate time of 2 mM glycine puff. Number of evoked Ca^{2+} spikes is shown in parenthesis. The bias currents during 8-sec current injection were -80 pA and -55 pA for (i) and (ii), respectively.

(B) Another example showing the difference in magnitude and time course of pH_i change between the control condition and in H_2DIDS. The period of 8-sec Ca^{2+} spiking evoked with 70 pA is bound by a rectangle. Numbers of evoked Ca^{2+} spikes are shown in parenthesis. Arrow indicates the time of peak acidification in H_2DIDS.

(C) Plot of peak acidification (in SNARF's ΔF/F) against the peak negative E_{gly} shift in control condition and the peak positive E_{gly} shift in H_2DIDS. 5 cases (pairs) from different cells are shown. The same depolarizing current injection was used for control and H_2DIDS conditions in each of the 5 cases, but the amount ranged from 70 to 300 pA in different cases. The average of peak negative Egly shifts in controls is -2.6 ± 1.1 mV and that of peak positive shifts in H_2DIDS is 0.9 ± 0.4 mV for the 5 cases in the plot.

Figure 8. Block of the negative E_{gly} shift by HCO_3^-/CO_2 removal.

(A) The effect on E_{gly} and pH_i of removing HCO_3^-/CO_2 from perfusion (HEPES/O_2) (i), and then adding acetazolamide (AZA, 50 μM) (ii) in one cell. Superimposed control-treatment pairs of E_{gly}/pH_i series were chosen on the basis of similar number of evoked Ca^{2+} spikes during the 8-sec depolarization. The periods of 8-sec Ca^{2+} spiking are marked with thick bars. (Ai) The injected current and number of evoked Ca^{2+} spikes were 180 pA/16 and 120 pA/18 Ca^{2+} spikes for the control and HEPES/O_2, respectively. (Aii) The injected current and number of evoked Ca^{2+} spikes were 130 pA/30, 110 pA/31, and 110 pA/15 Ca^{2+} spikes for HEPES/O_2, after AZA addition (+AZA), and 17 min after removing AZA (–AZA), respectively. The effects of AZA were fully reversible if it had been applied for less than about 15 min.

(B) Another example showing the slowed pH_i recovery and positive E_{gly} shift after addition of AZA in HEPES/O_2 after Ca^{2+} spiking. Time of peak acidification in AZA is indicated with an arrow and the period of Ca^{2+} spiking is shaded. The injected current and number of evoked Ca^{2+} spikes were 170 pA/23 and 160 pA/22 Ca^{2+} spikes for the HEPES/O_2 and +AZA, respectively.

(C) Plot of peak acidification (i) and half-recovery time (ii) against the peak negative E_{gly} shift and the peak positive E_{gly} shift for HEPES/O_2 and +AZA for 6 cases (from different cells) in which the number of evoked Ca^{2+} spikes were similar between the two conditions. The number of evoked Ca^{2+} spikes in +AZA condition ranged 20–47 in the 6 cases. The difference in peak acidification was not significant, but the half-recovery time was significantly lengthened in AZA added to HEPES/O_2.

(D) Chloride transporters potentially affecting neuronal $[Cl^-]_i$ (i), and the proposed mechanism of activity-dependent negative shift in E_{gly} in CWCs (ii). KCC, the K^+-Cl^- cotransporters. NKCC, the Na^+-K^+-Cl^- cotransporters. AE, the Na^+-independent anion (Cl^--HCO_3^-) exchanger. NDCBE, the Na^+-driven Cl^--HCO_3^- exchanger, also known as NDAE.

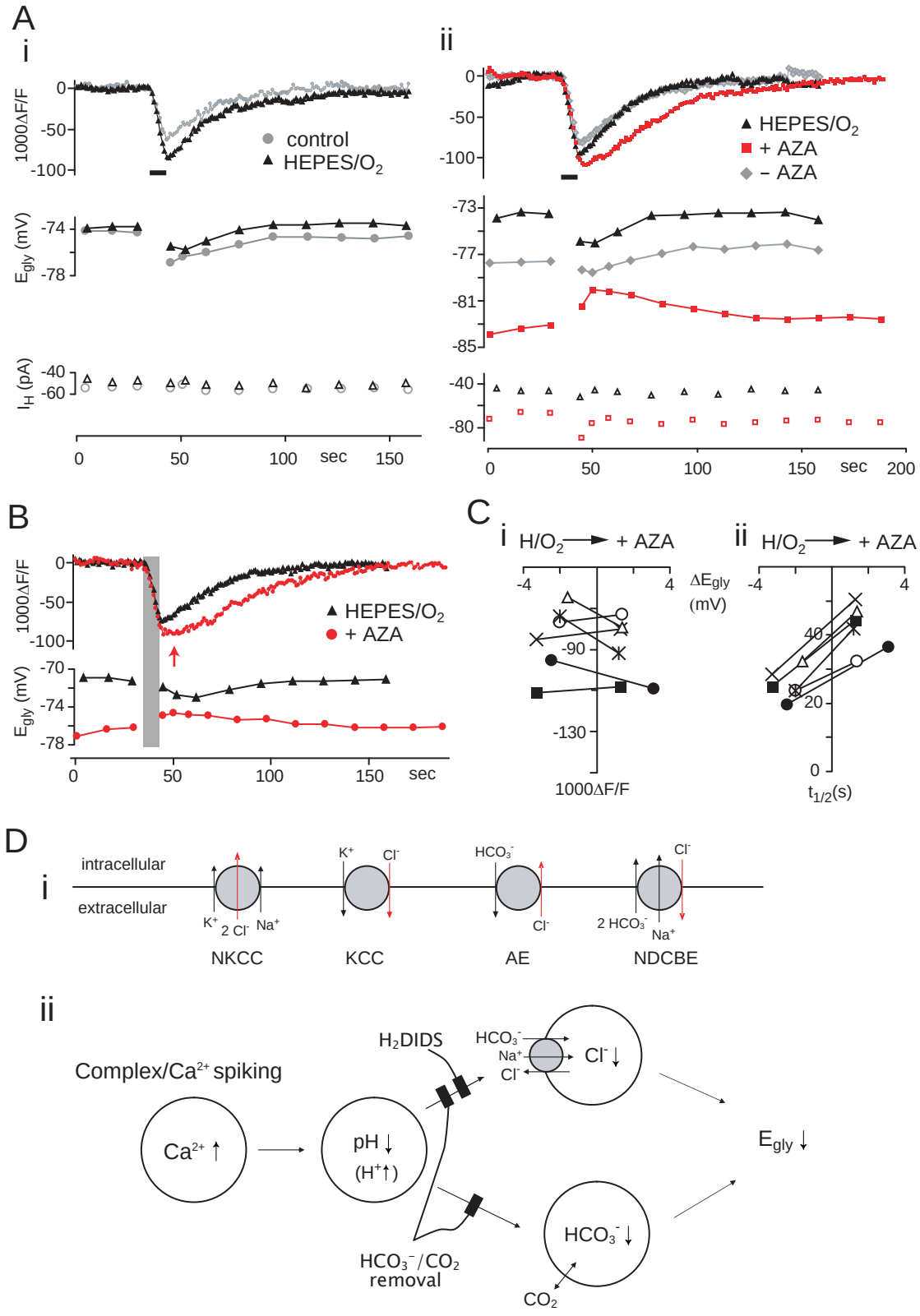
A
i
ii
1000ΔF/F
control
HEPES/O2
+ AZA
– AZA
Egly (mV)
IH (pA)
sec
B
C
i
ii
H/O2
+ AZA
ΔEgly (mV)
1000ΔF/F
t1/2(s)
D
i
intracellular
extracellular
NKCC
KCC
AE
NDCBE
ii
Complex/Ca2+ spiking
H2DIDS
pH ↓
(H+↑)
Egly ↓
HCO3−/CO2 removal
CO2

Figure 8

Figure S1. Measurement of E_{gly} with a voltage ramp protocol.

(A-C) An example showing how a series of E_{gly} measurements was made to generate the time plot of E_{gly} with respect to Ca^{2+} spiking in one cell. (A) The recording began at t = 0 (sec) in i-clamp with a bias current for setting the V_m close to –75 mV. In this cell, the V_m was hold below –75 mV with –30 pA bias to reduce the post-Ca^{2+} spiking depolarization. At t = 5 and every 15 sec (except just after Ca^{2+} spiking) the recording mode was switched to v-clamp for 4 sec to measure E_{gly} with the voltage ramp protocol (B). Ca^{2+} spiking was induced for 8 sec at t = 35 in i-clamp. The fragmented V_m traces with time designation are the response to 2 mM glycine puffed for 8 ms at the arrowhead. (Bi left) The unit voltage ramp command protocol was run 4 times consecutively to obtain 2 glycine responses (1st and 3rd run) and 2 control responses. (Bi right) Ramp responses obtained 5 sec before Ca^{2+} spiking, 8 sec after Ca^{2+} spiking, and at the end of the series. A trace without glycine (gray) and one with glycine (red) are superimposed. The uncorrected E_{gly} was taken from the voltage on the ramp where the two responses crossed. (Bii) I-V plot of glycine currents at different times with respect to Ca^{2+} spiking was generated by subtracting the control ramp response from that with glycine in each set of ramp responses. (C) Time plot of R_s-corrected E_{gly}. Gray rectangle shows the period of Ca^{2+} spiking. The recording was obtained in TTX 0.4 μM, APV 100 μM, and DNQX 10 μM.

(D) Slow negative drift in the resting E_{gly} in CWCs. E_{gly} was measured in TTX, DNQX and APV with the voltage ramp protocol. (Di) Each series of symbols represents measurements from one cell, and 24 cells are shown. Symbols are connected with a dotted line if one or more Ca^{2+}spike experiment as in (A-C) was run in between. The

first point in each series is the first E_{gly} with $R_s < 60$ MΩ. The last point in a series is the last measurement either before recording termination or before a drug was added. (Dii) Plot of difference in the resting E_{gly} between the last measurement and the first measurement versus the time elapsed between the two measurements. Dots represent single CWCs, and are from 94 cells including the cells shown in (Di).

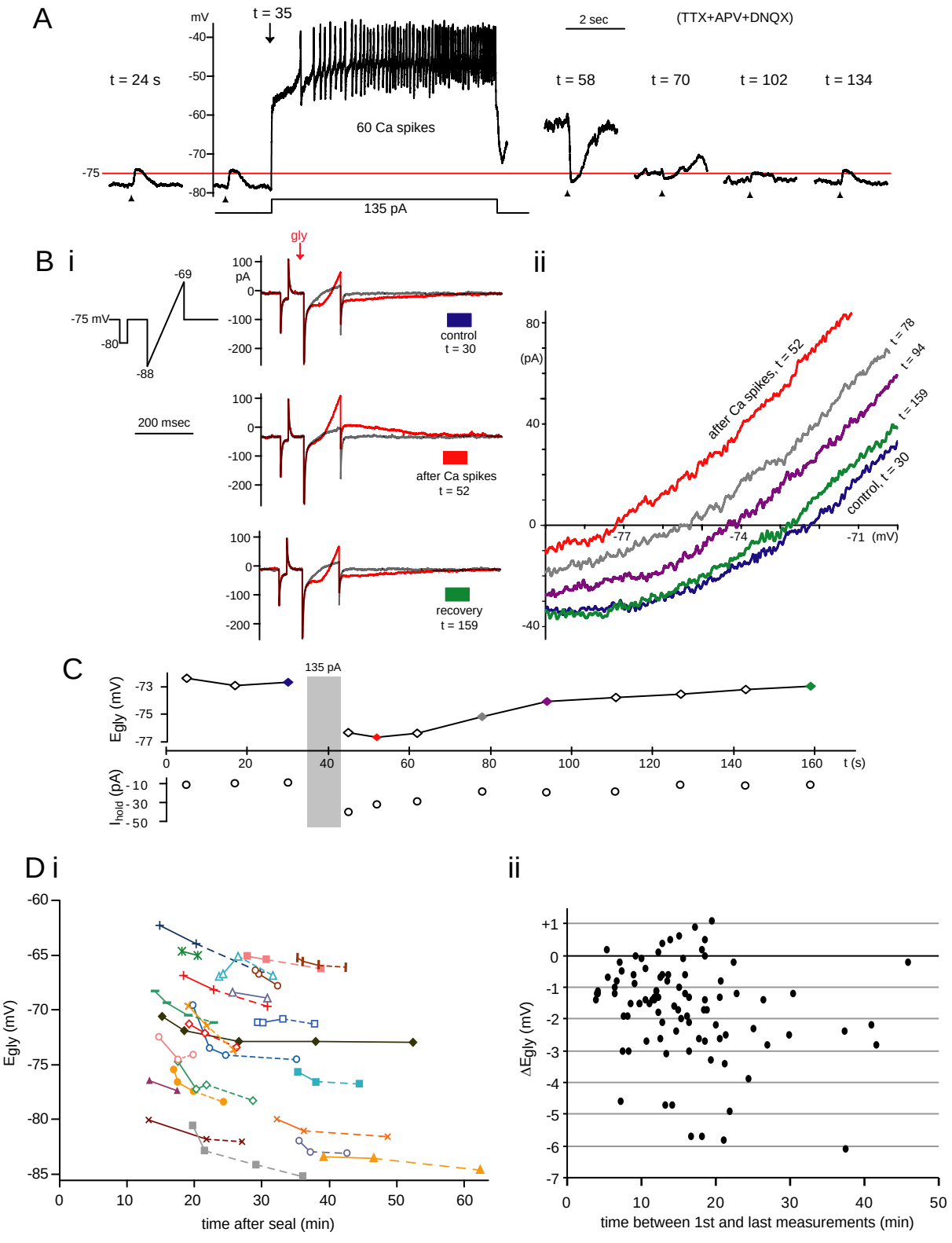
A
mV
t = 35
2 sec
(TTX+APV+DNQX)
t = 24 s
t = 58
t = 70
t = 102
t = 134
60 Ca spikes
135 pA
B i
gly
-69
-75 mV
-80
-88
200 msec
control
t = 30
after Ca spikes
t = 52
recovery
t = 159
ii
after Ca spikes, t = 52
t = 78
t = 94
t = 159
control, t = 30
(pA)
(mV)
C
135 pA
Egly (mV)
t (s)
Ihold (pA)
D i
Egly (mV)
time after seal (min)
ii
ΔEgly (mV)
time between 1st and last measurements (min)

Figure S1

Figure S2. Activity-induced intracellular acidifications detected with fluorescent imaging. (A) The SNARF fluorescence images and intensity signals at acquisition. Excitation at 547 nm, emission filtered at > 600 nm. A CWC was loaded with SNARF-5F by diffusion of the AM form of dye from the recording pipette. In each image shown in the top row, the ROIs are placed inside the cell body, over the recording pipette on the right of cell body, and in the background. The fluorescence in the recording pipette is from the intracellular compartment invaginated into the pipette tip. (Ai, bottom) The average fluorescent intensity of the 3 ROIs (top) as appeared in the image acquisition software during a 8s challenge protocol. A 150 pA current injection evoked complex spikes during the period indicated with thick bar. (Aii bottom) An example showing the detection of patch rupture from an abrupt fall in the fluorescence of the ROI drawn over the recording pipette.

(B) pH imaging performed with a different dye, pHrodo (A gift from Daniel Beecham, Molecular Probes/Invitrogen) This rhodamine-based dye (excited at 555 nm, emission filtered at > 600 nm) increases fluorescence as pH decreases. In both (Bi) and (Bii) the image and the bottom pH trace are from one cell, and the top trace is from a different cell. (Bi) pHrodo loaded into a CWC through perforated patch with 50 μM of AM ester form in a recording solution composed of (in mM) 147 K-gluconate, 4 NaCl, 4 NaOH, 10 HEPES. The nearby area was stained by the dye leaking from the recording pipette when the cell was patched. The acidification on complex spiking induced with an 8-sec current injection occurred in the same pattern as that seen with SNARF. (Bii) pH imaging in whole-cell configuration was done using the free acid form of pHrodo (100 μM) in a K-gluconate-based recording solution containing 9 mM HEPES and nucleotides (pH 7.30).

8-sec current injections evoking complex spikes induced an acidification, but unlike with perforated patch recording, the acidification decayed faster and was followed by apparent rebound alkalinization and acidification.

(C) An example showing the correlation in pH_i and E_{gly} change in a situation where additional spontaneous Ca^{2+} spiking (c) occurred after the 8-sec current injection (a). V_m traces at bottom correspond to the shaded period indicated with the same letter in the simultaneously obtained pH and E_{gly} plot above. The arrowhead indicates the time of a 2 mM glycine puff. In TTX, APV and DNQX with –10 pA bias current.

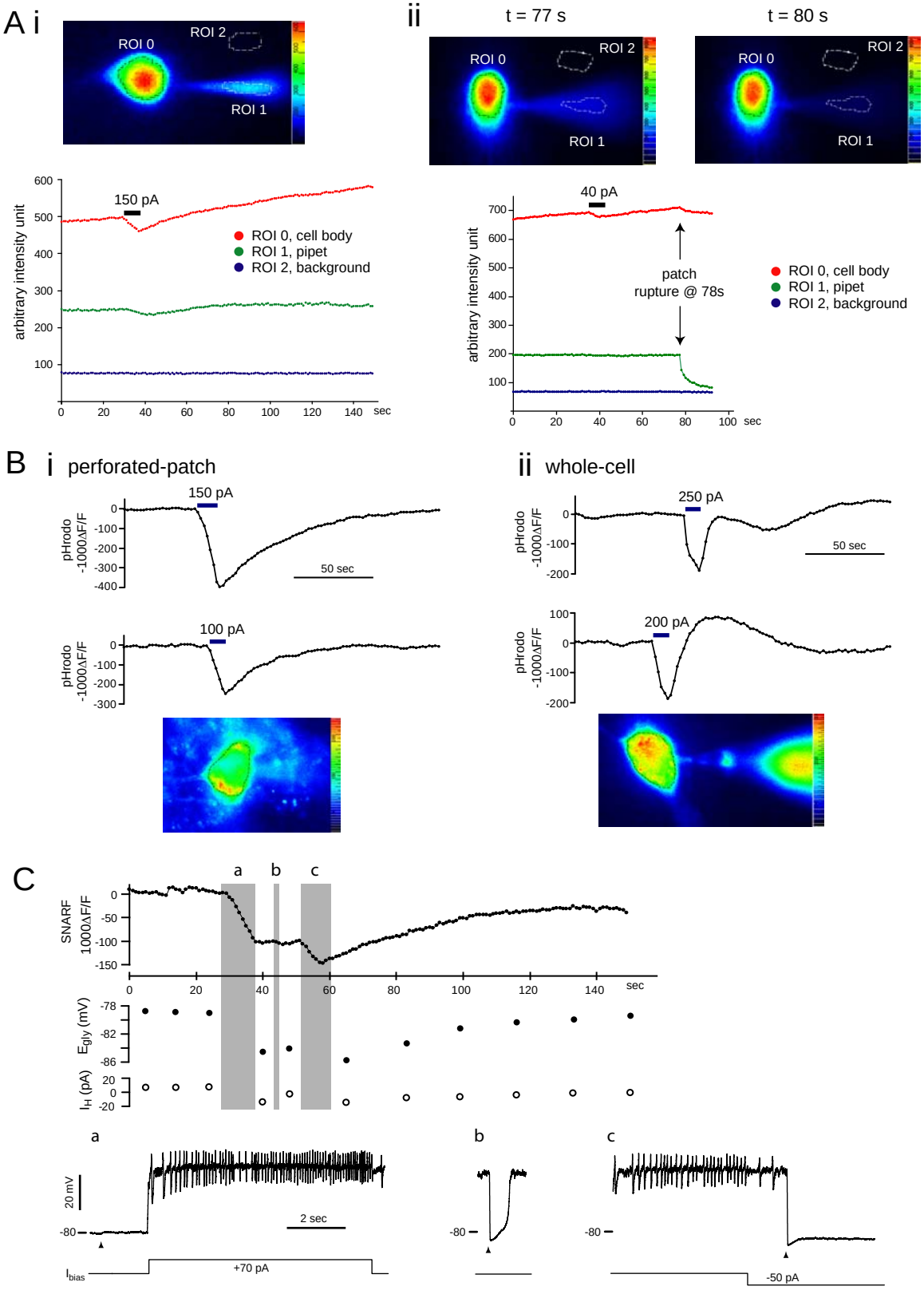
A i
ROI 0
ROI 2
ROI 1
ii
t = 77 s
t = 80 s
150 pA
arbitrary intensity unit
ROI 0, cell body
ROI 1, pipet
ROI 2, background
sec
40 pA
patch
rupture @ 78s
B i perforated-patch
ii whole-cell
pHrodo
-1000ΔF/F
50 sec
100 pA
250 pA
200 pA
C
a
b
c
SNARF
1000ΔF/F
E_{gly} (mV)
I_H (pA)
20 mV
2 sec
+70 pA
-50 pA
I_{bias}

Figure S2

Figure S3. Plots of E_{gly} vs. $[Cl^-]_i$ according to the Goldman-Hodgkin-Katz equation. (A-B) Each curve represents the relation between $[Cl^-]_i$ and E_{gly} according to the Goldman-Hodgkin-Katz voltage equation with the P_{HCO3}/P_{Cl} at 0.2 (A) or 0.1 (B) for the glycine receptor at a given $[HCO_3^-]_i$ ranging 6–18 mM. The pH_i indicated is derived from $[HCO_3^-]_i/[HCO_3^-]_o = 10^{(pHi-pHo)}$ at fixed pH_o = 7.30 and $[HCO_3^-]_o$ = 20 mM, based on the assumption that the partial pressure, solubility, and the dissociation constant of CO_2 is equal intra- and extracellularly. The plot of E_{Cl} is also drawn according to the Nernst equation. The temperature used in equations is 34 °C.

(C) The curves were generated as in (A) but with 3 mM $[HCO_3^-]_o$ in equilibrium with 7.2 mmHg CO_2 at pH_o 7.2, a potential condition of slices in nominally HCO_3^-/CO_2-free Ringer. The value of P_{CO2} was derive from the assumed 1% endogenous CO_2 taken from Lamsa and Kaila (1997), and the pH_o was set lower than that of the HCO_3^-/CO_2-free Ringer, 7.30, as it has been known to occur (e.g. Voipio and Ballanyi, 1997; Chesler and Rice, 1991).

(D) Schematic of typical time-dependent change in average V_m, E_{gly}, pH_i associated with an 8-sec complex/Ca^{2+} spiking (Di) and simple spiking (Dii).

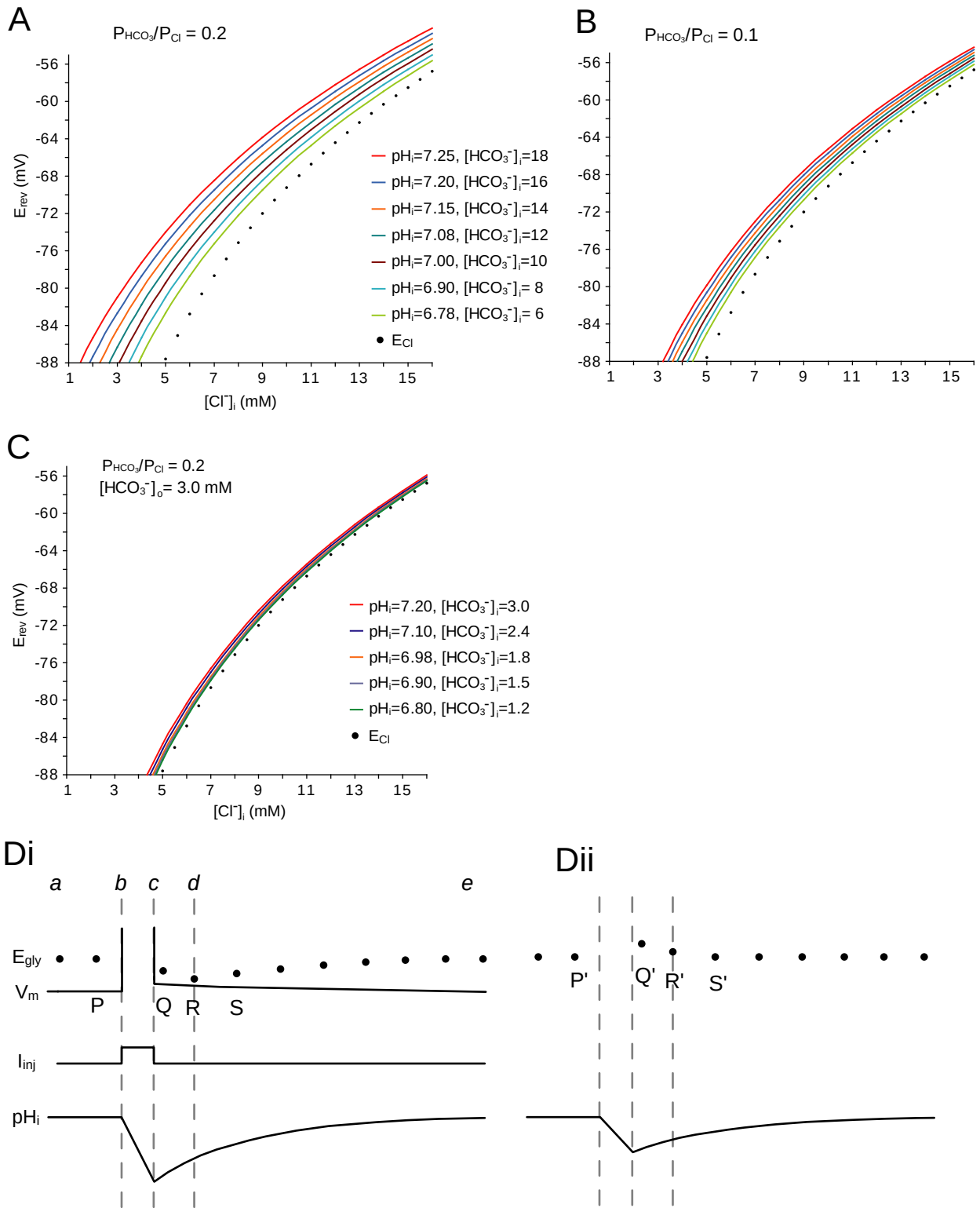
A
P_{HCO_3}/P_{Cl} = 0.2
E_{rev} (mV)
$[Cl^-]_i$ (mM)
pH_i=7.25, $[HCO_3^-]_i$=18
pH_i=7.20, $[HCO_3^-]_i$=16
pH_i=7.15, $[HCO_3^-]_i$=14
pH_i=7.08, $[HCO_3^-]_i$=12
pH_i=7.00, $[HCO_3^-]_i$=10
pH_i=6.90, $[HCO_3^-]_i$= 8
pH_i=6.78, $[HCO_3^-]_i$= 6
E_{Cl}
B
P_{HCO_3}/P_{Cl} = 0.1
C
P_{HCO_3}/P_{Cl} = 0.2
$[HCO_3^-]_o$= 3.0 mM
pH_i=7.20, $[HCO_3^-]_i$=3.0
pH_i=7.10, $[HCO_3^-]_i$=2.4
pH_i=6.98, $[HCO_3^-]_i$=1.8
pH_i=6.90, $[HCO_3^-]_i$=1.5
pH_i=6.80, $[HCO_3^-]_i$=1.2
Di
Dii
a
b
c
d
e
E_{gly}
V_m
I_{inj}
pH_i
P
Q
R
S
P'
Q'
R'
S'

Figure S3

SUMMARY and CONCLUSIONS

Factors contributing to complex spike generation in cartwheel cells

The single fast action potential of cartwheel cells characteristically possesses an afterdepolarization (ADP) following the fast afterhyperpolarization (fAHP), and these two were found important in controlling the complex spiking tendency. More fAHP suppressed complex spike generation: spontaneously all-simple-spiking cells showed deeper fAHP than the complex-spiking cells, and treatments reducing fAHP, BK channel block and BAPTA, increased complex spikes. On the other hand, more ADP enhanced complex spiking as supported by the opposite effect of SK channel block and T-type Ca^{2+} channel block, with the former increasing both the ADP and the complex spike frequency. The slow underlying depolarization of complex spikes has been believed to be Ca^{2+}-dependent. The current work revealed that it is shaped by different subtypes of Ca^{2+} channels depending on the level of V_m from which the spike arises: the high-threshold type Ca^{2+} channels, L and P/Q, contribute to complex spikes appearing at depolarized V_m and the low-threshold type, T and/or R, to spikes arising from hyperpolarized V_m. Balancing the depolarizing influence of various Ca^{2+} channels, Ca^{2+}-activated K^+ channels limit complex spiking in cartwheel cells, coupled with probably P/Q-, T- and R-type Ca^{2+} channels. SK channels control the duration of slow depolarization of complex spikes as well as ADP of single spikes, and BK channels enhance repolarization of single spike.

Future directions

For studying the spike characteristics of cartwheels cells, whole-cell recording

should be avoided because it alters the action potential waveforms and the pattern of spiking, spontaneous or evoked. Considering the gradual loss of fAHP and increase in complex spiking tendency seen during the course of whole-cell recording, it is suspected that BK channel activity was weakened due to lowered intracellular Ca^{2+} (higher Ca^{2+}-buffering than normal) or wash-out of a regulatory factor. In the current study, a gradient in the degree of complex spiking was found among spontaneously spiking cells. The majority fired only simple spikes, and those showing complex spikes ranged in the frequency between one complex spike in tens of second and ~6 spikes per second. Whether the complex spiking behavior can be regulated is of interest. Neuromodulators may do so by inducing a change in intracellular Ca^{2+} level or affecting Ca^{2+} or Ca^{2+}-activated K^+ channel properties. One candidate mechanism is the activation the metabotrophic glutamate receptor, mGluR1, which is known to be expressed in cartwheel cells (Wright et al., 1996; Petralia et al., 1996). Preliminary application of (1S,3R)-ACPD, an agonist for group I&II mGluRs, induced increased complex spiking in several cartwheel cells. This effect needs to be examined in detail using specific agonists and antagonists of mGluR1.

The mechanism of activity-dependent change in E_{gly} in cartwheel cells

Glycine effect in different cartwheel cell varied from depolarizing excitation to hyperpolarizing inhibition. The resting E_{gly} of cartwheel cells distributed over a 30 mV range with the mean of cells showing excitatory responses to glycine significantly less negative than that of cells showing inhibitory responses. Interestingly, the E_{gly} was found to shift negative transiently when complex spiking was induced with long depolarizing

current injection but shift positive when simple spiking was induced with a weaker depolarization. The transient negative shift in E_{gly} was Ca^{2+}-dependent; it could occur with Ca^{2+} spikes, and removal of bath Ca^{2+} eliminated the negative shift leaving a positive shift, which suggests the presence of a passive Cl^- conductance. The known phenomenon of Ca^{2+}-dependent intracellular acidification was hypothesized as the underlying mechanism of Ca^{2+}-dependent negative E_{gly} shift, i.e., lowering of $[Cl^-]_i$ or $[HCO_3^-]_i$. Intracellular acidification indeed was detected with complex spiking activity but also to a lesser extent with simple spiking. That Ca^{2+} removal blocked both the acidification and the negative E_{gly} shift and that the weak acid-induced, activity-independent acidification was effective in shifting E_{gly} negative also supported the hypothesis. Subsequently, the decrease in $[Cl^-]_i$ observed with complex spiking-induced intracellular acidification and the block of the negative E_{gly} shift by H_2DIDS indicated that the Na^+-driven Cl^--HCO_3^- exchanger (NDCBE)-mediated recovery from acidification caused E_{gly} to shift negative. The reversible activity-dependent shifts in E_{gly} would serve to suppress excessive complex spiking and promote moderate rate of activity.

Future directions

It is of interest to investigate further what contributes to the variation in the resting E_{gly} among cartwheel cells. Immunohistochemical examination on the expression of Cl^- transporters, KCC2, NKCC1, NDCBE and AE3, as well as Na^+-HCO_3^- cotransporters in cartwheel cells can be conducted to answer questions such as whether those transporters mentioned in the current study are really expressed and whether there is a variation in the level of expression for Cl^- accumulating and Cl^- extruding proteins

among different cartwheel cells. If AE is detected in cartwheel cells, the possibility of AE contributing to the maintenance of Cl^- influx, as the negative shift in resting E_{gly} on H_2DIDS application implicates, can be tested by ruling out whether the resting pH_i declines in H_2DIDS; monitoring the resting pH_i during perfusion of H_2DIDS with ratiometric pH imaging using BCECF or SNARF would be the way. Also, whether the higher proportion of inhibitory glycine responses in spontaneously complex spiking cells, i.e., more negative E_{gly} in these cells, is due to prevailing expression of Cl^- extruders or more acidic resting pH_i is in question. Comparison of the resting pH among multiple cells using ratiometric pH imaging of a pH dye loaded into the whole slice accompanied with extracellular recording could help testing the possibility of lower resting pH_i in complex spiking cells.

REFERENCES

Ahmed Z and Connor JA. Intracellular pH changes induced by calcium influx during electrical activity in molluscan neurons. *J Gen Physiol* 75: 403-426, 1980.

Akemann W and Knopfel T. Interaction of Kv3 potassium channels and resurgent sodium current influences the rate of spontaneous firing of Purkinje neurons. *J Neurosci* 26: 4602-4612, 2006.

Athanassiadis T, Westberg KG, Olsson KA, and Kolta A. Physiological characterization, localization and synaptic inputs of bursting and nonbursting neurons in the trigeminal principal sensory nucleus of the rat. *Eur J Neurosci* 22: 3099-3110, 2005.

Atherton JF and Bevan MD. Ionic mechanisms underlying autonomous action potential generation in the somata and dendrites of GABAergic substantia nigra pars reticulata neurons in vitro. *J Neurosci* 25: 8272-8281, 2005.

Backus KH, Deitmer JW, and Friauf E. Glycine-activated currents are changed by coincident membrane depolarization in developing rat auditory brainstem neurones. *J Physiol* 507: 783-794, 1998.

Ballanyi K and Kaila K. Activity-evoked changes in intracellular pH. In: *pH and Brain Function*, edited by Kaila K and Ransom BR. New York: Wiley-Liss, 1998, p. 291-308.

Barry PH. JPCalc, a software package for calculating liquid junction potential corrections in patch-clamp, intracellular, epithelial and bilayer measurements and for correcting junction potential measurements. *J Neurosci Methods* 51: 107-116, 1994.

Batlle DC, Peces R, LaPointe MS, Ye M, and Daugirdas JT. Cytosolic free calcium regulation in response to acute changes in intracellular pH in vascular smooth muscle. *Am J Physiol Cell Physiol* 264: C932-943, 1993.

Ben-Ari Y, Gaiarsa JL, Tyzio R, and Khazipov R. GABA: a pioneer transmitter that excites immature neurons and generates primitive oscillations. *Physiol Rev* 87: 1215-1284, 2007.

Bergeron MJ, Gagnon E, Wallendorff B, Lapointe J-Y, and Isenring P. Ammonium transport and pH regulation by K+-Cl- cotransporters. *Am J Physiol Renal Physiol* 285: F68-78, 2003.

Berglund K, Schleich W, Krieger P, Loo LS, Wang D, Cant NB, Feng G, Augustine GJ, and Kuner T. Imaging synaptic inhibition in transgenic mice expressing the chloride indicator, Clomeleon. *Brain Cell Biol* 35: 207-228, 2006.

Berrebi AS, Morgan JI, and Mugnaini E. The Purkinje cell class may extend beyond the cerebellum. *J Neurocytol* 19: 643-654, 1990.

Berrebi AS and Mugnaini E. Distribution and targets of the cartwheel cell axon in the dorsal cochlear nucleus of the guinea pig. *Anat Embryol (Berl)* 183: 427-454, 1991.

Bezprozvanny I and Tsien RW. Voltage-dependent blockade of diverse types of voltage-gated Ca2+ channels expressed in Xenopus oocytes by the Ca2+ channel antagonist mibefradil (Ro 40-5967). *Mol Pharmacol* 48: 540-549, 1995.

Billups D and Attwell D. Control of intracellular chloride concentration and GABA response polarity in rat retinal ON bipolar cells. *J Physiol* 545: 183-198, 2002.

Bormann J, Hamill OP, and Sakmann B. Mechanism of anion permeation through channels gated by glycine and gamma-aminobutyric acid in mouse cultured spinal neurones. *J Physiol* 385: 243-286, 1987.

Boron WF, McCormick WC, and Roos A. pH regulation in barnacle muscle fibers: dependence on extracellular sodium and bicarbonate. *Am J Physiol* 240: C80-89, 1981.

Boron WF and Russell JM. Stoichiometry and ion dependencies of the intracellular-pH-regulating mechanism in squid giant axons. *J Gen Physiol* 81: 373-399, 1983.

Boyarsky G, Ganz MB, Sterzel RB, and Boron WF. pH regulation in single glomerular mesangial cells. II. Na+-dependent and -independent Cl(-)-HCO3- exchangers. *Am J Physiol* 255: C857-869, 1988.

Brett CL, Kelly T, Sheldon C, and Church J. Regulation of Cl--HCO3- exchangers by cAMP-dependent protein kinase in adult rat hippocampal CA1 neurons. *J Physiol* 545: 837-853, 2002.

Brockhaus J and Ballanyi K. Synaptic inhibition in the isolated respiratory network of neonatal rats. *Eur J Neurosci* 10: 3823-3839, 1998.

Brown MC and Ledwith JV, 3rd. Projections of thin (type-II) and thick (type-I) auditory-nerve fibers into the cochlear nucleus of the mouse. *Hear Res* 49: 105-118, 1990.

Brumback AC and Staley KJ. Thermodynamic regulation of NKCC1-mediated Cl-cotransport underlies plasticity of GABA(A) signaling in neonatal neurons. *J Neurosci* 28: 1301-1312, 2008.

Brumberg JC, Nowak LG, and McCormick DA. Ionic mechanisms underlying repetitive high-frequency burst firing in supragranular cortical neurons. *J Neurosci* 20: 4829-4843, 2000.

Cant NB. The Cochlear Nucleus: Neuronal Types and Their Organization. In: *The Mammalian Auditory Pathway: Neuroanatomy*, edited by Webster DB, Popper AN and Fay RR. New York: Springer-Verlag, 1992.

Cassel D, Scharf O, Rotman M, Cragoe EJ, Jr., and Katz M. Characterization of Na+-linked and Na+-independent Cl-/HCO3- exchange systems in Chinese hamster lung fibroblasts. *J Biol Chem* 263: 6122-6127, 1988.

Cavelier P and Bossu JL. Dendritic low-threshold Ca2+ channels in rat cerebellar Purkinje cells: possible physiological implications. *Cerebellum* 2: 196-205, 2003.

Chagnac-Amitai Y, Luhmann HJ, and Prince DA. Burst generating and regular spiking layer 5 pyramidal neurons of rat neocortex have different morphological features. *J Comp Neurol* 296: 598-613, 1990.

Chavas J and Marty A. Coexistence of excitatory and inhibitory GABA synapses in the cerebellar interneuron network. *J Neurosci* 23: 2019-2031, 2003.

Chen LM, Kelly ML, Parker MD, Bouyer P, Gill HS, Felie JM, Davis BA, and Boron WF. Expression and localization of Na-driven Cl-HCO(3)(-) exchanger (SLC4A8) in rodent CNS. *Neuroscience* 153: 162-174, 2008.

Chen LM, Kelly ML, Rojas JD, Parker MD, Gill HS, Davis BA, and Boron WF. Use of a new polyclonal antibody to study the distribution and glycosylation of the sodium-coupled bicarbonate transporter NCBE in rodent brain. *Neuroscience* 151: 374-385, 2008.

Chesler M. Regulation and Modulation of pH in the Brain. *Physiol Rev* 83: 1183-1221, 2003.

Chesler M and Rice ME. Extracellular alkaline-acid pH shifts evoked by iontophoresis of glutamate and aspartate in turtle cerebellum. *Neuroscience* 41: 257-267, 1991.

Chipperfield AR and Harper AA. Chloride in smooth muscle. *Prog Biophys Mol Biol* 74: 175-221, 2000.

Choi HS and Eisner DA. The effects of inhibition of the sarcolemmal Ca-ATPase on systolic calcium fluxes and intracellular calcium concentration in rat ventricular myocytes. *Pflugers Archiv European Journal of Physiology* 437: 966-971, 1999.

Cordero-Erausquin M, Coull JA, Boudreau D, Rolland M, and De Koninck Y. Differential maturation of GABA action and anion reversal potential in spinal lamina I neurons: impact of chloride extrusion capacity. *J Neurosci* 25: 9613-9623, 2005.

Crunelli V, Toth TI, Cope DW, Blethyn K, and Hughes SW. The 'window' T-type calcium current in brain dynamics of different behavioural states. *J Physiol (Lond)* 562: 121-129, 2005.

Culliford SJ, Ellory JC, Lang H-J, Englert H, Staines HM, and Wilkins RJ. Specificity of Classical and Putative Cl - Transport Inhibitors on Membrane Transport Pathways in Human Erythrocytes. *Cell Physiol Biochem* 13: 181-188, 2003.

Damkier HH, Nielsen S, and Praetorius J. Molecular expression of SLC4-derived Na+-dependent anion transporters in selected human tissues. *Am J Physiol Regul Integr Comp Physiol* 293: R2136-2146, 2007.

Davis KA and Young ED. Granule cell activation of complex-spiking neurons in dorsal cochlear nucleus. *J Neurosci* 17: 6798-6806, 1997.

Davis KA and Young ED. Pharmacological evidence of inhibitory and disinhibitory neuronal circuits in dorsal cochlear nucleus. *J Neurophysiol* 83: 926-940, 2000.

Davson H and Segal MB. *Physiology of the CSF and Blood-Brain Barriers*. Boca Raton: CRC Press, 1996.

DeFazio RA, Heger S, Ojeda SR, and Moenter SM. Activation of A-type gamma-aminobutyric acid receptors excites gonadotropin-releasing hormone neurons. *Mol Endocrinol* 16: 2872-2891, 2002.

Del Negro CA, Koshiya N, Butera RJ, Jr., and Smith JC. Persistent sodium current, membrane properties and bursting behavior of pre-botzinger complex inspiratory neurons in vitro. *J Neurophysiol* 88: 2242-2250, 2002.

Delpire E and Lauf PK. Kinetics of DIDS inhibition of swelling-activated K-Cl cotransport in low K sheep erythrocytes. *J Membr Biol* 126: 89-96, 1992.

Deschenes M, Roy JP, and Steriade M. Thalamic bursting mechanism: an inward slow current revealed by membrane hyperpolarization. *Brain Res* 239: 289-293, 1982.

Do MT and Bean BP. Subthreshold sodium currents and pacemaking of subthalamic neurons: modulation by slow inactivation. *Neuron* 39: 109-120, 2003.

Duebel J, Haverkamp S, Schleich W, Feng G, Augustine GJ, Kuner T, and Euler T. Two-photon imaging reveals somatodendritic chloride gradient in retinal ON-type bipolar cells expressing the biosensor Clomeleon. *Neuron* 49: 81-94, 2006.

Ehrlich I, Lohrke S, and Friauf E. Shift from depolarizing to hyperpolarizing glycine action in rat auditory neurones is due to age-dependent Cl- regulation. *J Physiol* 520 Pt 1: 121-137, 1999.

Eller P, Berjukov S, Wanner S, Huber I, Hering S, Knaus HG, Toth G, Kimball SD, and Striessnig J. High affinity interaction of mibefradil with voltage-gated calcium and sodium channels. *Br J Pharmacol* 130: 669-677, 2000.

Ertel EA. Pharmacology of Cav3(T-tpye) Channels. In: *Calcium Channel Pharmacology*, edited by McDonough SI. New York: Kluwer Academic/Plenum Publishers, 2004, p. 183-236.

Fagni L, Bossu JL, and Bockaert J. Inhibitory effects of dihydropyridines on macroscopic K+ currents and on the large-conductance Ca2+-activated K+ channel in cultured cerebellar granule cells. *Pflugers Arch* 429: 176-182, 1994.

Farrant M and Kaila K. The cellular, molecular and ionic basis of GABA(A) receptor signalling. *Prog Brain Res* 160: 59-87, 2007.

Fatima-Shad K and Barry PH. Anion permeation in GABA- and glycine-gated channels of mammalian cultured hippocampal neurons. *Proc Biol Sci* 253: 69-75, 1993.

Fenwick EM, Marty A, and Neher E. A patch-clamp study of bovine chromaffin cells and of their sensitivity to acetylcholine. *J Physiol* 331: 577-597, 1982.

Filosa JA, Dean JB, and Putnam RW. Role of intracellular and extracellular pH in the chemosensitive response of rat locus coeruleus neurones. *J Physiol* 541: 493-509, 2002.

Fiumelli H, Cancedda L, and Poo MM. Modulation of GABAergic transmission by activity via postsynaptic Ca2+-dependent regulation of KCC2 function. *Neuron* 48: 773-786, 2005.

Franceschetti S, Guatteo E, Panzica F, Sancini G, Wanke E, and Avanzini G. Ionic mechanisms underlying burst firing in pyramidal neurons: intracellular study in rat sensorimotor cortex. *Brain Res* 696: 127-139, 1995.

Gatto C, Hale CC, Xu W, and Milanick MA. Eosin, a potent inhibitor of the plasma membrane Ca pump, does not inhibit the cardiac Na-Ca exchanger. *Biochemistry* 34: 965-972, 1995.

Golding NL, Jung H-y, Mickus T, and Spruston N. Dendritic calcium spike initiation and repolarization are controlled by distinct potassium channel subtypes in CA1 pyramidal neurons. *J Neurosci* 19: 8789-8798, 1999.

Golding NL and Oertel D. Context-dependent synaptic action of glycinergic and GABAergic inputs in the dorsal cochlear nucleus. *J Neurosci* 16: 2208-2219, 1996.

Golding NL and Oertel D. Physiological identification of the targets of cartwheel cells in the dorsal cochlear nucleus. *J Neurophysiol* 78: 248-260, 1997.

Grichtchenko II, Choi I, Zhong X, Bray-Ward P, Russell JM, and Boron WF. Cloning, Characterization, and Chromosomal Mapping of a Human Electroneutral Na+-driven Cl-HCO3 Exchanger. *J Biol Chem* 276: 8358-8363, 2001.

Grissmer S, Nguyen AN, Aiyar J, Hanson DC, Mather RJ, Gutman GA, Karmilowicz MJ, Auperin DD, and Chandy KG. Pharmacological characterization of 5 cloned voltage-gated K+ channels, types Kv1.1, Kv1.2, Kv1.3, Kv1.5, and Kv3.1, stably expressed in mammalian-cell lines. *Mol Pharmacol* 45: 1227-1234, 1994.

Gulacsi A, Lee CR, Sik A, Viitanen T, Kaila K, Tepper JM, and Freund TF. Cell type-specific differences in chloride-regulatory mechanisms and GABA(A) receptor-mediated inhibition in rat substantia nigra. *J Neurosci* 23: 8237-8246, 2003.

Gulledge AT and Stuart GJ. Excitatory actions of GABA in the cortex. *Neuron* 37: 299-309, 2003.

Hallworth NE, Wilson CJ, and Bevan MD. Apamin-sensitive small conductance calcium-activated potassium channels, through their selective coupling to voltage-gated calcium channels, are critical determinants of the precision, pace, and pattern of action

potential generation in rat subthalamic nucleus neurons in vitro. *J Neurosci* 23: 7525-7542, 2003.

Hentschke M, Wiemann M, Hentschke S, Kurth I, Hermans-Borgmeyer I, Seidenbecher T, Jentsch TJ, Gal A, and Hubner CA. Mice with a targeted disruption of the Cl-/HCO3- exchanger AE3 display a reduced seizure threshold. *Mol Cell Biol* 26: 182-191, 2006.

Hirsch JA and Oertel D. Intrinsic properties of neurones in the dorsal cochlear nucleus of mice, in vitro. *J Physiol* 396: 535-548, 1988.

Horn R and Marty A. Muscarinic activation of ionic currents measured by a new whole-cell recording method. *J Gen Physiol* 92: 145-159, 1988.

Iino S, Hayashi H, Saito H, Tokuno H, and Tomita T. Effects of intracellular pH on calcium currents and intracellular calcium ions in the smooth muscle of rabbit portal vein. *Exp Physiol* 79: 669-680, 1994.

Inglefield JR and Schwartz-Bloom RD. Optical imaging of hippocampal neurons with a chloride-sensitive dye: early effects of in vitro ischemia. *J Neurochem* 70: 2500-2509, 1998.

Isope P and Murphy TH. Low threshold calcium currents in rat cerebellar Purkinje cell dendritic spines are mediated by T-type calcium channels. *J Physiol* 562: 257-269, 2005.

Ito M. Cerebellar long-term depression: characterization, signal transduction, and functional roles. *Physiol Rev* 81: 1143-1195, 2001.

Jacobs S, Ruusuvuori E, Sipila ST, Haapanen A, Damkier HH, Kurth I, Hentschke M, Schweizer M, Rudhard Y, Laatikainen LM, Tyynela J, Praetorius J, Voipio J,

and Hubner CA. Mice with targeted Slc4a10 gene disruption have small brain ventricles and show reduced neuronal excitability. *Proc Natl Acad Sci U S A* 105: 311-316, 2008.

Jiang C, Agulian S, and Haddad GG. Cl- and Na+ homeostasis during anoxia in rat hypoglossal neurons: intracellular and extracellular in vitro studies. *J Physiol* 448: 697-708, 1992.

Jiang L, Stuart-Tilley A, Parkash J, and Alper SL. pHi and serum regulate AE2-mediated Cl-/HCO3- exchange in CHOP cells of defined transient transfection status. *Am J Physiol* 267: C845-856, 1994.

Jimenez C, Bourinet E, Leuranguer V, Richard S, Snutch TP, and Nargeot J. Determinants of voltage-dependent inactivation affect Mibefradil block of calcium channels. *Neuropharmacology* 39: 1-10, 2000.

Jung H-y, Staff NP, and Spruston N. Action potential bursting in subicular pyramidal neurons Is driven by a calcium tail current. *J Neurosci* 21: 3312-3321, 2001.

Kaila K and Voipio J. Dependence of intracellular free calcium and tension on membrane potential and intracellular pH in single crayfish muscle fibres. *Pflugers Archiv European Journal of Physiology* 416: 501-511, 1990.

Kaila K and Voipio J. GABA-Activated Bicarbonate Conductance: influence on E_{GABA} and on postsynaptic pH regulation. In: *Chloride Channels and Carriers in Nerve, Muscle, and Glial Cells*, edited by Alvarez-Leefmans FJ and Russell JM. New York: Plenum, 1990, p. 331-353.

Kaila K and Voipio J. Postsynaptic fall in intracellular pH induced by GABA-activated bicarbonate conductance. *Nature* 330: 163-165, 1987.

Kaila K, Voipio J, Paalasmaa P, Pasternack M, and Deisz RA. The role of bicarbonate in GABAA receptor-mediated IPSPs of rat neocortical neurones. *J Physiol* 464: 273-289, 1993.

Kanaka C, Ohno K, Okabe A, Kuriyama K, Itoh T, Fukuda A, and Sato K. The differential expression patterns of messenger RNAs encoding K-Cl cotransporters (KCC1,2) and Na-K-2Cl cotransporter (NKCC1) in the rat nervous system. *Neuroscience* 104: 933-946, 2001.

Kandel ER and Spencer WA. Electrophysiology of hippocampal neurons. II. After-potentials and repetitive firing. *J Neurophysiol* 24: 243-259, 1961.

Kanold PO and Young ED. Proprioceptive information from the pinna provides somatosensory input to cat dorsal cochlear nucleus. *J Neurosci* 21: 7848-7858, 2001.

Khaliq ZM and Raman IM. Axonal propagation of simple and complex spikes in cerebellar Purkinje neurons. *J Neurosci* 25: 454-463, 2005.

Kim U and Chung LY. Dual GABAergic synaptic response of fast excitation and slow inhibition in the medial habenula of rat epithalamus. *J Neurophysiol* 98: 1323-1332, 2007.

Kim Y and Trussell LO. Ion channels generating complex spikes in cartwheel cells of the dorsal cochlear nucleus. *J Neurophysiol* 97: 1705-1725, 2007.

Koncz C and Daugirdas JT. Use of MQAE for measurement of intracellular [Cl-] in cultured aortic smooth muscle cells. *Am J Physiol* 267: H2114-2123, 1994.

Konnerth A, Dreessen J, and Augustine GJ. Brief dendritic calcium signals initiate long-lasting synaptic depression in cerebellar Purkinje cells. *Proc Natl Acad Sci U S A* 89: 7051-7055, 1992.

Kopito RR, Lee BS, Simmons DM, Lindsey AE, Morgans CW, and Schneider K. Regulation of intracellular pH by a neuronal homolog of the erythrocyte anion exchanger. *Cell* 59: 927-937, 1989.

Kuner T and Augustine GJ. A genetically encoded ratiometric indicator for chloride: capturing chloride transients in cultured hippocampal neurons. *Neuron* 27: 447-459, 2000.

Kyrozis A and Reichling DB. Perforated-patch recording with gramicidin avoids artifactual changes in intracellular chloride concentration. *J Neurosci Methods* 57: 27-35, 1995.

Lamsa K and Kaila K. Ionic Mechanisms of Spontaneous GABAergic Events in Rat Hippocampal Slices Exposed to 4-Aminopyridine. *J Neurophysiol* 78: 2582-2591, 1997.

Larkum ME, Zhu JJ, and Sakmann B. A new cellular mechanism for coupling inputs arriving at different cortical layers. *Nature* 398: 338-341, 1999.

Lee BS, Gunn RB, and Kopito RR. Functional differences among nonerythroid anion exchangers expressed in a transfected human cell line. *J Biol Chem* 266: 11448-11454, 1991.

Leem CH, Lagadic-Gossmann D, and Vaughan-Jones RD. Characterization of intracellular pH regulation in the guinea-pig ventricular myocyte. *J Physiol* 517 (Pt 1): 159-180, 1999.

Leniger T, Thone J, Bonnet U, Hufnagel A, Bingmann D, and Wiemann M. Levetiracetam inhibits Na+-dependent Cl-/HCO3- exchange of adult hippocampal CA3 neurons from guinea-pigs. *Br J Pharmacol* 142: 1073-1080, 2004.

Lipton P. Ischemic Cell Death in Brain Neurons. *Physiol Rev* 79: 1431-1568, 1999.

Lisman JE. Bursts as a unit of neural information: making unreliable synapses reliable. *Trends Neurosci* 20: 38-43, 1997.

Llinas R and Sugimori M. Electrophysiological properties of in vitro Purkinje cell somata in mammalian cerebellar slices. *J Physiol* 305: 171-195, 1980.

Llinas R, Sugimori M, Lin JW, and Cherksey B. Blocking and isolation of a calcium channel from neurons in mammals and cephalopods utilizing a toxin fraction (FTX) from funnel-web spider poison. *Proc Natl Acad Sci U S A* 86: 1689-1693, 1989.

Mainen ZF and Sejnowski TJ. Influence of dendritic structure on firing pattern in model neocortical neurons. *Nature* 382: 363-366, 1996.

Manis PB, Spirou GA, Wright DD, Paydar S, and Ryugo DK. Physiology and morphology of complex spiking neurons in the guinea pig dorsal cochlear nucleus. *J Comp Neurol* 348: 261-276, 1994.

Marandi N, Konnerth A, and Garaschuk O. Two-photon chloride imaging in neurons of brain slices. *Pflugers Arch* 445: 357-365, 2002.

Martin RL, Lee JH, Cribbs LL, Perez-Reyes E, and Hanck DA. Mibefradil block of cloned T-type calcium channels. *J Pharmacol Exp Ther* 295: 302-308, 2000.

Martina M, Yao GL, and Bean BP. Properties and functional role of voltage-dependent potassium channels in dendrites of rat cerebellar Purkinje neurons. *J Neurosci* 23: 5698-5707, 2003.

Martinez-Zaguilan R, Gurule MW, and Lynch RM. Simultaneous measurement of intracellular pH and Ca2+ in insulin-secreting cells by spectral imaging microscopy. *Am J Physiol* 270: C1438-1446, 1996.

Marty A and Llano I. Excitatory effects of GABA in established brain networks. *Trends Neurosci* 28: 284-289, 2005.

Mason A and Larkman A. Correlations between morphology and electrophysiology of pyramidal neurons in slices of rat visual cortex. II. Electrophysiology. *J Neurosci* 10: 1415-1428, 1990.

May BJ. Role of the dorsal cochlear nucleus in the sound localization behavior of cats. *Hear Res* 148: 74-87, 2000.

McCormick DA and Bal T. Sleep and arousal: thalamocortical mechanisms. *Annu Rev Neurosci* 20: 185-215, 1997.

McDonough SI and Bean BP. Mibefradil inhibition of T-type calcium channels in cerebellar purkinje neurons. *Mol Pharmacol* 54: 1080-1087, 1998.

McKay BE and Turner RW. Kv3 K+ channels enable burst output in rat cerebellar Purkinje cells. *Eur J Neurosci* 20: 729-739, 2004.

McKay BE and Turner RW. Physiological and morphological development of the rat cerebellar Purkinje cell. *J Physiol* 567: 829-850, 2005.

Meech RW and Thomas RC. Voltage-dependent intracellular pH in Helix aspersa neurones. *J Physiol* 390: 433-452, 1987.

Meera P, Wallner M, and Toro L. A neuronal beta subunit (KCNMB4) makes the large conductance, voltage- and Ca2+-activated K+ channel resistant to charybdotoxin and iberiotoxin. *Proc Natl Acad Sci U S A* 97: 5562-5567, 2000.

Metz AE, Jarsky T, Martina M, and Spruston N. R-type calcium channels contribute to afterdepolarization and bursting in hippocampal CA1 pyramidal neurons. *J Neurosci* 25: 5763-5773, 2005.

Meyer TM, Munsch T, and Pape HC. Activity-related changes in intracellular pH in rat thalamic relay neurons. *Neuroreport* 11: 33-37, 2000.

Miyakawa H, Lev-Ram V, Lasser-Ross N, and Ross WN. Calcium transients evoked by climbing fiber and parallel fiber synaptic inputs in guinea pig cerebellar Purkinje neurons. *J Neurophysiol* 68: 1178-1189, 1992.

Molitor SC and Manis PB. Dendritic Ca2+ transients evoked by action potentials in rat dorsal cochlear nucleus pyramidal and cartwheel neurons. *J Neurophysiol* 89: 2225-2237, 2003.

Monsivais P, Clark BA, Roth A, and Hausser M. Determinants of action potential propagation in cerebellar Purkinje cell axons. *J Neurosci* 25: 464-472, 2005.

Mugnaini E, Berrebi AS, Dahl AL, and Morgan JI. The polypeptide PEP-19 is a marker for Purkinje neurons in cerebellar cortex and cartwheel neurons in the dorsal cochlear nucleus. *Arch Ital Biol* 126: 41-67, 1987.

Mugnaini E and Morgan JI. The neuropeptide cerebellin is a marker for two similar neuronal circuits in rat brain. *Proc Natl Acad Sci U S A* 84: 8692-8696, 1987.

Neher E. Correction for liquid junction potentials in patch clamp experiments. *Methods Enzymol* 207: 123-131, 1992.

Nelken I and Young ED. Two separate inhibitory mechanisms shape the responses of dorsal cochlear nucleus type IV units to narrowband and wideband stimuli. *J Neurophysiol* 71: 2446-2462, 1994.

Niespodziany I and Poulain P. Electrophysiology of the neurons in the area of the enkephalinergic magnocellular dorsal nucleus of the guinea-pig hypothalamus, studied by intracellular and whole-cell recordings. *Eur J Neurosci* 7: 1134-1145, 1995.

Nishimura Y, Asahi M, Saitoh K, Kitagawa H, Kumazawa Y, Itoh K, Lin M, Akamine T, Shibuya H, Asahara T, and Yamamoto T. Ionic Mechanisms Underlying Burst Firing of Layer III Sensorimotor Cortical Neurons of the Cat: An In Vitro Slice Study. *J Neurophysiol* 86: 771-781, 2001.

Oertel D and Young ED. What's a cerebellar circuit doing in the auditory system? *Trends Neurosci* 27: 104-110, 2004.

Olsnes S, Tonnessen TI, and Sandvig K. pH-regulated anion antiport in nucleated mammalian cells. *J Cell Biol* 102: 967-971, 1986.

Osen KK, Ottersen OP, and Storm-Mathisen J. Colocalization o f glycine-like and GABA-like immunoreactivities: a semiquantitative study of individual neurons in the dorsal cochlear nucleus of cat. In: *glycine neurotransmission*, edited by Ottersen OP and Storm-Mathisen J. New York: Wiley, 1990, p. 417-451.

Ou-yang Y, Mellergard P, and Siesjo BK. Regulation of intracellular pH in single rat cortical neurons in vitro: a microspectrofluorometric study. *J Cereb Blood Flow Metab* 13: 827-840, 1993.

OuYang YB, Mellergard P, Kristian T, Kristianova V, and Siesjo BK. Influence of acid-base changes on the intracellular calcium concentration of neurons in primary culture. *Exp Brain Res* 101: 265-271, 1994.

Parham K and Kim DO. Spontaneous and sound-evoked discharge characteristics of complex-spiking neurons in the dorsal cochlear nucleus of the unanesthetized decerebrate cat. *J Neurophysiol* 73: 550-561, 1995.

Paulsen O and Sejnowski TJ. Natural patterns of activity and long-term synaptic plasticity. *Curr Opin Neurobiol* 10: 172-179, 2000.

Payne JA, Stevenson TJ, and Donaldson LF. Molecular characterization of a putative K-Cl cotransporter in rat brain. A neuronal-specific isoform. *J Biol Chem* 271: 16245-16252, 1996.

Pearson MM, Lu J, Mount DB, and Delpire E. Localization of the K+-Cl- cotransporter, KCC3, in the central and peripheral nervous systems: expression in the choroid plexus, large neurons and white matter tracts. *Neuroscience* 103: 481-491, 2001.

Petralia RS, Wang YX, Zhao HM, and Wenthold RJ. Ionotropic and metabotropic glutamate receptors show unique postsynaptic, presynaptic, and glial localizations in the dorsal cochlear nucleus. *J Comp Neurol* 372: 356-383, 1996.

Pierre K and Pellerin L. Monocarboxylate transporters in the central nervous system: distribution, regulation and function. *J Neurochem* 94: 1-14, 2005.

Plotkin MD, Kaplan MR, Peterson LN, Gullans SR, Hebert SC, and Delpire E. Expression of the Na(+)-K(+)-2Cl- cotransporter BSC2 in the nervous system. *Am J Physiol* 272: C173-183, 1997.

Pocock G and Richards CD. Hydrogen Ion Regulation in Rat Cerebellar Granule Cells Studied by Single-Cell Fluorescence Microscopy. *Eur J Neurosci* 4: 136-143, 1992.

Pond BB, Berglund K, Kuner T, Feng G, Augustine GJ, and Schwartz-Bloom RD. The chloride transporter Na(+)-K(+)-Cl- cotransporter isoform-1 contributes to intracellular chloride increases after in vitro ischemia. *J Neurosci* 26: 1396-1406, 2006.

Portfors CV and Roberts PD. Temporal and frequency characteristics of cartwheel cells in the dorsal cochlear nucleus of the awake mouse. *J Neurophysiol* 98: 744-756, 2007.

Raman IM and Bean BP. Ionic currents underlying spontaneous action potentials in isolated cerebellar purkinje neurons. *J Neurosci* 19: 1663-1674, 1999.

Randall AD and Tsien RW. Contrasting biophysical and pharmacological properties of T-type and R-type calcium channels. *Neuropharmacology* 36: 879-893, 1997.

Rhee JS, Ebihara S, and Akaike N. Gramicidin perforated patch-clamp technique reveals glycine-gated outward chloride current in dissociated nucleus solitarii neurons of the rat. *J Neurophysiol* 72: 1103-1108, 1994.

Rickmann M, Orlowski B, Heupel K, and Roussa E. Distinct expression and subcellular localization patterns of Na+/HCO3- cotransporter (SLC 4A4) variants NBCe1-A and NBCe1-B in mouse brain. *Neuroscience* 146: 1220-1231, 2007.

Ritucci NA, Dean JB, and Putnam RW. Somatic vs. dendritic responses to hypercapnia in chemosensitive locus coeruleus neurons from neonatal rats. *Am J Physiol Cell Physiol* 289: C1094-1104, 2005.

Rivera C, Voipio J, Payne JA, Ruusuvuori E, Lahtinen H, Lamsa K, Pirvola U, Saarma M, and Kaila K. The K+/Cl- co-transporter KCC2 renders GABA hyperpolarizing during neuronal maturation. *Nature* 397: 251-255, 1999.

Roberts MT, Bender KJ, and Trussell LO. Fidelity of Complex Spike-Mediated Synaptic Transmission between Inhibitory Interneurons. *J Neurosci* 28: 9440-9450, 2008.

Rocha-Gonzalez HI, Mao S, and Alvarez-Leefmans FJ. Na+,K+,2Cl- cotransport and intracellular chloride regulation in rat primary sensory neurons: thermodynamic and kinetic aspects. *J Neurophysiol* 100: 169-184, 2008.

Romero MF, Fulton CM, and Boron WF. The SLC4 family of HCO 3 - transporters. *Pflugers Arch* 447: 495-509, 2004.

Roos A and Boron WF. Intracellular pH. *Physiol Rev* 61: 296-434, 1981.

Rubio ME. Differential distribution of synaptic endings containing glutamate, glycine, and GABA in the rat dorsal cochlear nucleus. *J Comp Neurol* 477: 253-272, 2004.

Russell JM. Sodium-potassium-chloride cotransport. *Physiol Rev* 80: 211-276, 2000.

Saarikoski J, Ruusuvuori E, Koskelainen A, and Donner K. Regulation of intracellular pH in salamander retinal rods. *J Physiol* 498: 61-72, 1997.

Schmolesky MT, Weber JT, De Zeeuw CI, and Hansel C. The making of a complex spike: ionic composition and plasticity. *Ann N Y Acad Sci* 978: 359-390, 2002.

Schwiening C, Kennedy H, and Thomas R. Calcium-Hydrogen Exchange by the Plasma Membrane Ca-ATPase of Voltage-Clamped Snail Neurons. *Proceedings of the Royal Society B: Biological Sciences* 253: 285-289, 1993.

Schwiening CJ and Boron WF. Regulation of intracellular pH in pyramidal neurones from the rat hippocampus by Na(+)-dependent Cl(-)-HCO3- exchange. *J Physiol* 475: 59-67, 1994.

Schwiening CJ and Thomas RC. pH consequences of calcium regulation. In: *pH and Brain Function*, edited by Kaila K and Ransom BR. New York: Wiley-Liss, 1998, p. 277-288.

Slemmer JE, Matsushita S, De Zeeuw CI, Weber JT, and Knopfel T. Glutamate-induced elevations in intracellular chloride concentration in hippocampal cell cultures derived from EYFP-expressing mice. *Eur J Neurosci* 19: 2915-2922, 2004.

Staley KJ, Soldo BL, and Proctor WR. Ionic mechanisms of neuronal excitation by inhibitory GABAA receptors. *Science* 269: 977-981, 1995.

Taddese A and Bean BP. Subthreshold sodium current from rapidly inactivating sodium channels drives spontaneous firing of tuberomammillary neurons. *Neuron* 33: 587-600, 2002.

Thomas RC and Meech RW. Hydrogen ion currents and intracellular pH in depolarized voltage-clamped snail neurones. *Nature* 299: 826-828, 1982.

Thompson SM and Gahwiler BH. Activity-dependent disinhibition. I. Repetitive stimulation reduces IPSP driving force and conductance in the hippocampus in vitro. *J Neurophysiol* 61: 501-511, 1989.

Trapp S, Luckermann M, Brooks PA, and Ballanyi K. Acidosis of rat dorsal vagal neurons in situ during spontaneous and evoked activity. *J Physiol* 496: 695-710, 1996.

Trapp S, Luckermann M, Kaila K, and Ballanyi K. Acidosis of hippocampal neurones mediated by a plasmalemmal Ca2+/H+ pump. *Neuroreport* 7: 2000-2004, 1996.

Traub RD, Wong RK, Miles R, and Michelson H. A model of a CA3 hippocampal pyramidal neuron incorporating voltage-clamp data on intrinsic conductances. *J Neurophysiol* 66: 635-650, 1991.

Tzounopoulos T, Kim Y, Oertel D, and Trussell LO. Cell-specific, spike timing-dependent plasticities in the dorsal cochlear nucleus. *Nat Neurosci* 7: 719-725, 2004.

Vale C, Caminos E, Martinez-Galan JR, and Juiz JM. Expression and developmental regulation of the K+-Cl- cotransporter KCC2 in the cochlear nucleus. *Hear Res* 206: 107-115, 2005.

Vale-Gonzalez C, Alfonso A, Sunol C, Vieytes MR, and Botana LM. Role of the plasma membrane calcium adenosine triphosphatase on domoate-induced intracellular

acidification in primary cultures of cerebelar granule cells. *J Neurosci Res* 84: 326-337, 2006.

Van Damme P, Callewaert G, Eggermont J, Robberecht W, and Van Den Bosch L. Chloride influx aggravates Ca2+-dependent AMPA receptor-mediated motoneuron death. *J Neurosci* 23: 4942-4950, 2003.

Vaughan-Jones RD. An investigation of chloride-bicarbonate exchange in the sheep cardiac Purkinje fibre. *J Physiol* 379: 377-406, 1986.

Verkman AS. Development and biological applications of chloride-sensitive fluorescent indicators. *Am J Physiol Cell Physiol* 259: C375-388, 1990.

Voipio J and Ballanyi K. Interstitial PCO2 and pH, and their role as chemostimulants in the isolated respiratory network of neonatal rats. *J Physiol* 499: 527-542, 1997.

Voipio J and Kaila K. Interstitial PCO2 and pH in rat hippocampal slices measured by means of a novel fast CO2/H(+)-sensitive microelectrode based on a PVC-gelled membrane. *Pflugers Arch* 423: 193-201, 1993.

Wang L, Kitai ST, and Xiang Z. Activity-dependent bidirectional modification of inhibitory synaptic transmission in rat subthalamic neurons. *J Neurosci* 26: 7321-7327, 2006.

Wang SS, Denk W, and Hausser M. Coincidence detection in single dendritic spines mediated by calcium release. *Nat Neurosci* 3: 1266-1273, 2000.

Watanabe S, Takagi H, Miyasho T, Inoue M, Kirino Y, Kudo Y, and Miyakawa H. Differential roles of two types of voltage-gated Ca2+ channels in the dendrites of rat cerebellar Purkinje neurons. *Brain Res* 791: 43-55, 1998.

Weedman DL, Pongstaporn T, and Ryugo DK. Ultrastructural study of the granule cell domain of the cochlear nucleus in rats: mossy fiber endings and their targets. *J Comp Neurol* 369: 345-360, 1996.

White G, Lovinger DM, and Weight FF. Transient low-threshold Ca2+ current triggers burst firing through an afterdepolarizing potential in an adult mammalian neuron. *Proc Natl Acad Sci U S A* 86: 6802-6806, 1989.

Williams S, Toth T, Turner J, Hughes S, and Crunelli V. The 'window' component of the low threshold Ca2+ current produces input signal amplification and bistability in cat and rat thalamocortical neurones. *J Physiol (Lond)* 505: 689-705, 1997.

Williams SR and Stuart GJ. Mechanisms and consequences of action potential burst firing in rat neocortical pyramidal neurons. *J Physiol (Lond)* 521: 467-482, 1999.

Willoughby D and Schwiening CJ. Electrically evoked dendritic pH transients in rat cerebellar Purkinje cells. *J Physiol* 544: 487-499, 2002.

Wilson CJ. The mechanism of intrinsic amplification of hyperpolarizations and spontaneous bursting in striatal cholinergic interneurons. *Neuron* 45: 575-585, 2005.

Womack M and Khodakhah K. Active contribution of dendrites to the tonic and trimodal patterns of activity in cerebellar Purkinje neurons. *J Neurosci* 22: 10603-10612, 2002.

Wong RK and Prince DA. Afterpotential generation in hippocampal pyramidal cells. *J Neurophysiol* 45: 86-97, 1981.

Woodin MA, Ganguly K, and Poo MM. Coincident pre- and postsynaptic activity modifies GABAergic synapses by postsynaptic changes in Cl- transporter activity. *Neuron* 39: 807-820, 2003.

Wouterlood FG and Mugnaini E. Cartwheel neurons of the dorsal cochlear nucleus: a Golgi-electron microscopic study in rat. *J Comp Neurol* 227: 136-157, 1984.

Wright DD, Blackstone CD, Huganir RL, and Ryugo DK. Immunocytochemical localization of the mGluR1 alpha metabotropic glutamate receptor in the dorsal cochlear nucleus. *J Comp Neurol* 364: 729-745, 1996.

Wu M-L, Chen J-H, Chen W-H, Chen Y-J, and Chu K-C. Novel role of the Ca2+-ATPase in NMDA-induced intracellular acidification. *Am J Physiol Cell Physiol* 277: C717-727, 1999.

Xiong Z-Q, Saggau P, and Stringer JL. Activity-Dependent Intracellular Acidification Correlates with the Duration of Seizure Activity. *J Neurosci* 20: 1290-1296, 2000.

Yamada J, Okabe A, Toyoda H, Kilb W, Luhmann HJ, and Fukuda A. Cl- uptake promoting depolarizing GABA actions in immature rat neocortical neurones is mediated by NKCC1. *J Physiol* 557: 829-841, 2004.

Young ED and Davis KA. Circuitry and function of the dorsal cochlear nucleus. In: *Integrative Functions in the Mammalian Auditory Pathway*, edited by Oertel D, Popper AN and Fay RR. New York: Springer-Verlag, 2001.

Yue C, Remy S, Su H, Beck H, and Yaari Y. Proximal persistent Na+ channels drive spike afterdepolarizations and associated bursting in adult CA1 pyramidal cells. *J Neurosci* 25: 9704-9720, 2005.

Yue C and Yaari Y. KCNQ/M channels control spike afterdepolarization and burst generation in hippocampal neurons. *J Neurosci* 24: 4614-4624, 2004.

Zhan RZ, Fujiwara N, Tanaka E, and Shimoji K. Intracellular acidification induced by membrane depolarization in rat hippocampal slices: roles of intracellular Ca2+ and glycolysis. *Brain Res* 780: 86-94, 1998.

Zhang S and Oertel D. Cartwheel and superficial stellate cells of the dorsal cochlear nucleus of mice: intracellular recordings in slices. *J Neurophysiol* 69: 1384-1397, 1993a.

Zhang S and Oertel D. Giant cells of the dorsal cochlear nucleus of mice: intracellular recordings in slices. *J Neurophysiol* 69: 1398-1408, 1993b.

Zhang S and Oertel D. Tuberculoventral cells of the dorsal cochlear nucleus of mice: intracellular recordings in slices. *J Neurophysiol* 69: 1409-1421, 1993c.

Zhang S and Oertel D. Neuronal circuits associated with the output of the dorsal cochlear nucleus through fusiform cells. *J Neurophysiol* 71: 914-930, 1994.

ELSEVIER LICENSE
TERMS AND CONDITIONS

Dec 19, 2008

This is a License Agreement between Yuil Kim ("You") and Elsevier ("Elsevier"). The license consists of your order details, the terms and conditions provided by Elsevier, and the payment terms and conditions.

Supplier	Elsevier Limited The Boulevard,Langford Lane Kidlington,Oxford,OX5 1GB,UK
Registered Company Number	1982084
Customer name	Yuil Kim
Customer address	3181 sw Sam Jackson Park Rd L335A Portland, OR 97239
License Number	2092631338163
License date	Dec 19, 2008
Licensed content publisher	Elsevier
Licensed content publication	Trends in Neurosciences
Licensed content title	What's a cerebellar circuit doing in the auditory system?
Licensed content author	Donata Oertel and Eric D. Young
Licensed content date	February 2004
Volume number	
Issue number	
Pages	0
Type of Use	Thesis / Dissertation
Portion	Figures/table/illustration /abstracts
Portion Quantity	1
Format	Print
You are an author of the Elsevier article	No
Are you translating?	No
Purchase order number	
Expected publication date	Mar 2008
Elsevier VAT number	GB 494 6272 12
Permissions price	0.00 USD
Value added tax 0.0%	0.00 USD